Pre-meeting
Field Trip guide

PATA 2026

ANTIGUA, GUATEMALA

30 JANUARY – 6 FEBRUARY, 2026

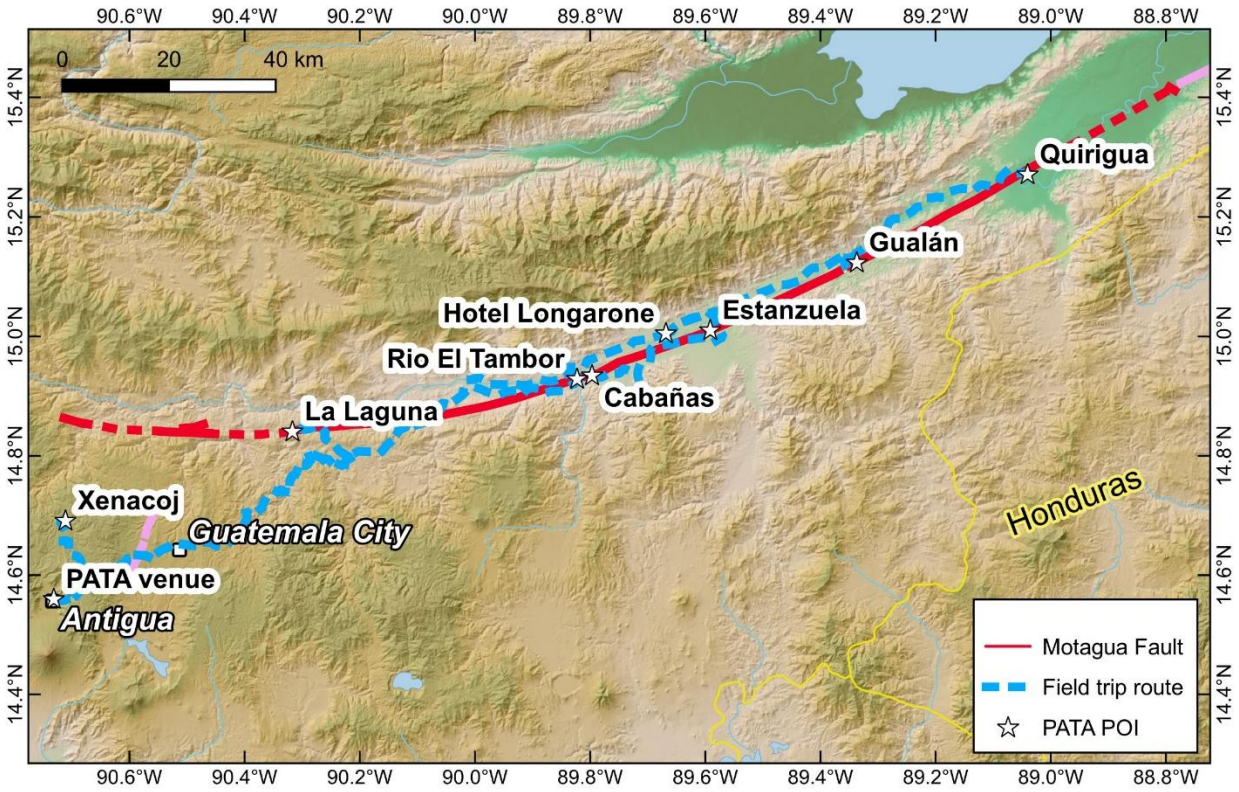

Field trip leaders:

Tina M. Niemi & Christoph Grützner

PATA Premeeting Field Trip Itinerary

DAY 1 – January 30, 2026

7:00 Pick up in Antigua: Tanque La Unión, corner 6a Calle Oriente/2a Avenida Sur, 14.5552°N 90.7311°W, https://maps.app.goo.gl/uPNC8Whv8RicUcYw7

- Leave for Rio El Tambor
- Restroom break at gas station
- Rio el Tambor Terrace Offsets
- Cabañas Lunch & Restrooms
- Zacapa road offset
- Trench site at Melon Plant
- Longarone Hotel, Poolside Party & Dinner Buffet at Longarone

Day 2 – January 31, 2026

6:00- 7:00 Longarone Breakfast Buffet

- Leave for Quirigua
- Quirigua (incl. Restrooms): Start tour of the archaeological site after an introduction; Divide into two groups; One goes clockwise with Aleigha and the other goes counter-clockwise with Tina
- Gualán: lunch at Martita's (Restrooms)
- Finca Los Limones trench site and offset canal
- Leave Gualán and drive back to Hotel Longarone
- Poolside Dinner with Pizza

Day 3 – February 1, 2026

6:00- 7:00 Longarone Breakfast Buffet

- Leave for Sanarate
- Restrooms at gas station
- La Laguna trench site
- Lunch at San Miguel mine
- Leave for Antigua
- Restroom stop
- Arrive at Antigua

Pre-meeting Field Trip Day 1 – Rio El Tambor slip rate site

Christoph Grützner, Hannes Ebell, Sumiko Tsukamoto, Tina Niemi, Jeremy Maurer, Paco Gomez, Omar Flores, Jonathan Obrist-Farner

Objectives

- Understand the Rio El Tambor terrace system
- Estimate a geological slip rate
- Explore challenges in OSL and ^{14}C dating

Introduction and Schwartz et al.'s (1979) data

Rio El Tambor is a southern tributary to the Motagua river. The confluence lies a few kilometers west of the town of Cabañas (Fig. 1).

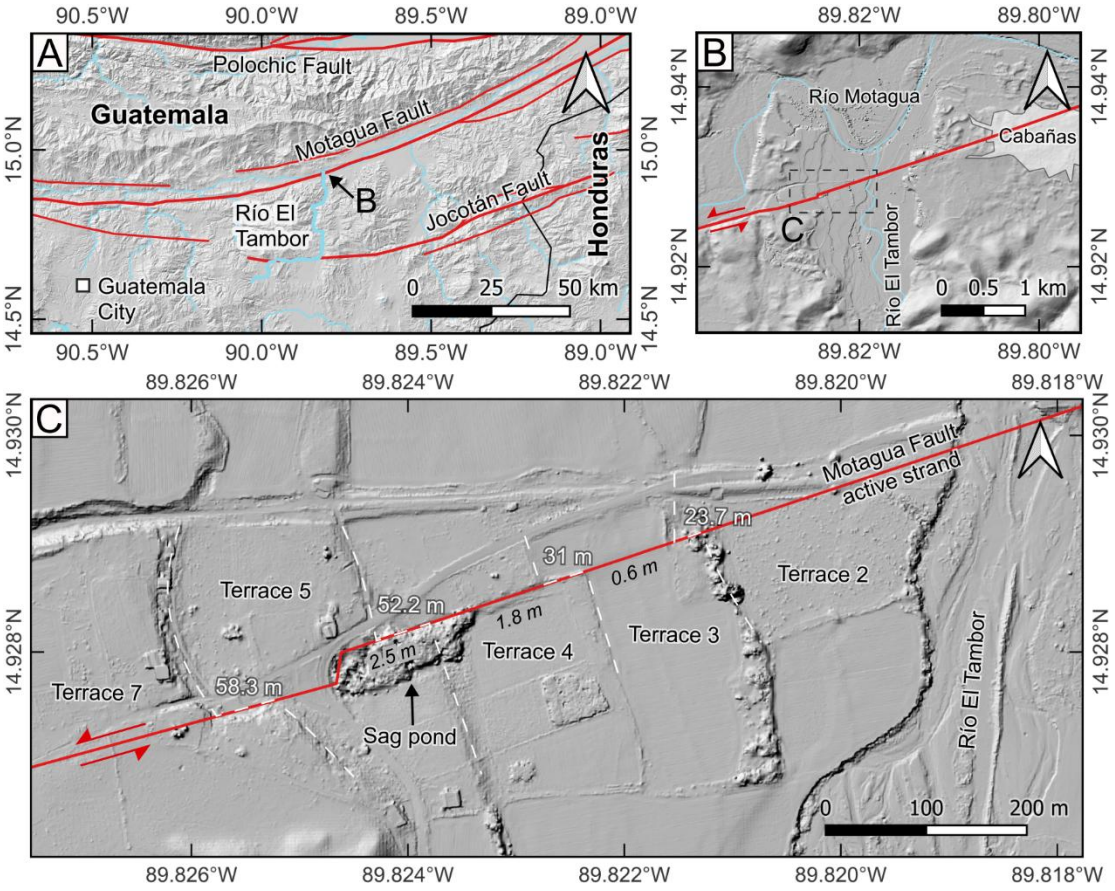

Figure 1: Offset river terraces at Río El Tambor. (A) Overview map showing the location within Guatemala. Red lines = faults (all left-lateral); black line = country border; topographic data are from the Copernicus WorldDEM-30 (ESA, 2024). (B) Confluence of the Río El Tambor and the Río Motagua west of the town Cabañas. (C) Zoom-in on the fluvial terraces crossed by the fault; note the progressive left-lateral offsets in the risers indicated by white dashed lines. Terraces are labeled following Schwartz et al. (1979); their measurements of the riser offsets (white numbers) and vertical scarp heights (black italic numbers) are given. A sag pond in terraces 5 and 4 is caused by a small releasing step in the fault. This is the trench site of Klinger et al. From Ebell (2025).

A flight of unpaired terraces T2-T7 (from youngest to oldest) is preserved on the western side of the river, and the terraces risers are offset by the Motagua Fault. Schwartz et al. (1979) described the site in detail and published a slip rate estimate (Fig. 2). They measured a lest lateral offset of 58.3 m in the riser of terrace T7, 52.2 m in T5, 31 m in T4, and 23.7 m in T3 (Fig. 1). Vertical offsets increase from 0.6 m across the fault on terrace 3 to 2.5 m across the fault on terrace 5. Schwartz et al. (1979) assume that the highest terrace T7 is older than 10 ka based on a well-developed soil profile, and younger than 40 ka, based on radiocarbon dating of volcanic tuffs exposed in the vicinity and their stratigraphic relation to the terraces. This results in a slip rate estimate of 1.5-6 mm/yr.

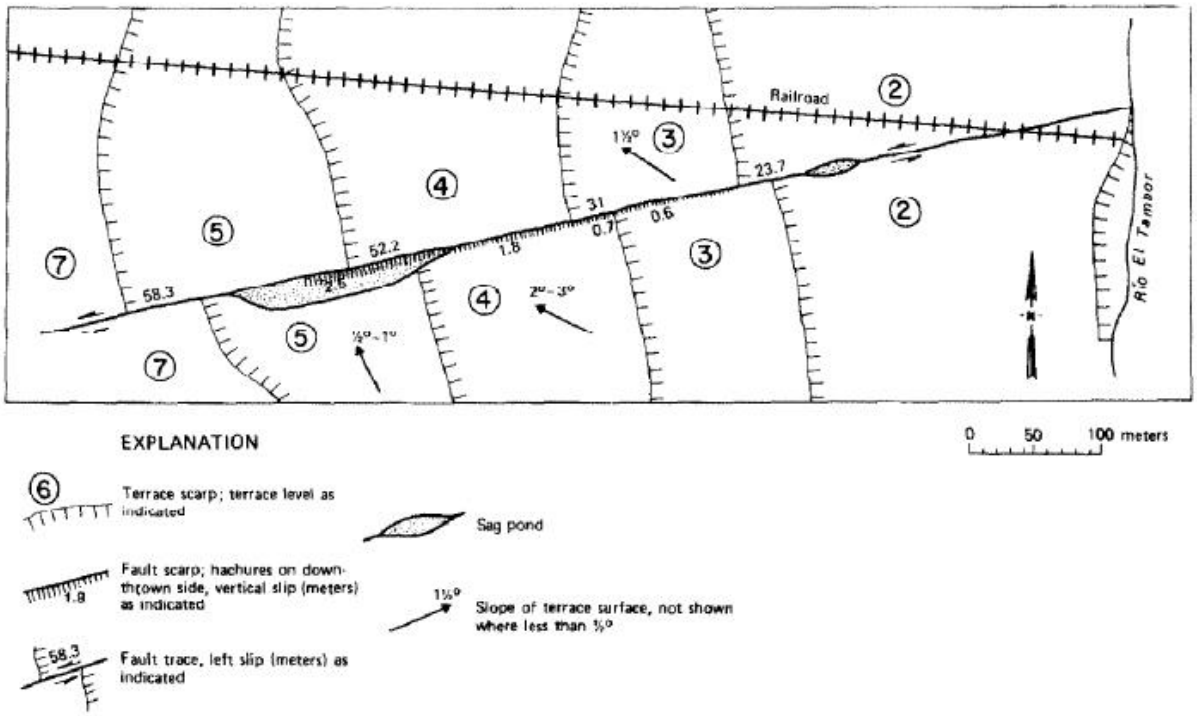

Figure 2: Original figure 4 from Schwartz et al. (1979).

New LiDAR data and terrace ages

Given the site's potential, we revisited the Rio El Tambor terraces. We used a fixed-wing drone with a laserscanner to create a new 0.5 m-resolution DEM. This allowed us to measure the terrace offsets even more precisely (Table 1, Fig. 3). Our new results are very close to those of Schwartz et al. (1979) except for terrace T4, which we think has a much larger offset than previously assumed. We also measure a much higher S-facing fault scarp across the faut in T5, although this measurement comes with significant uncertainty due to the sag pond present here.

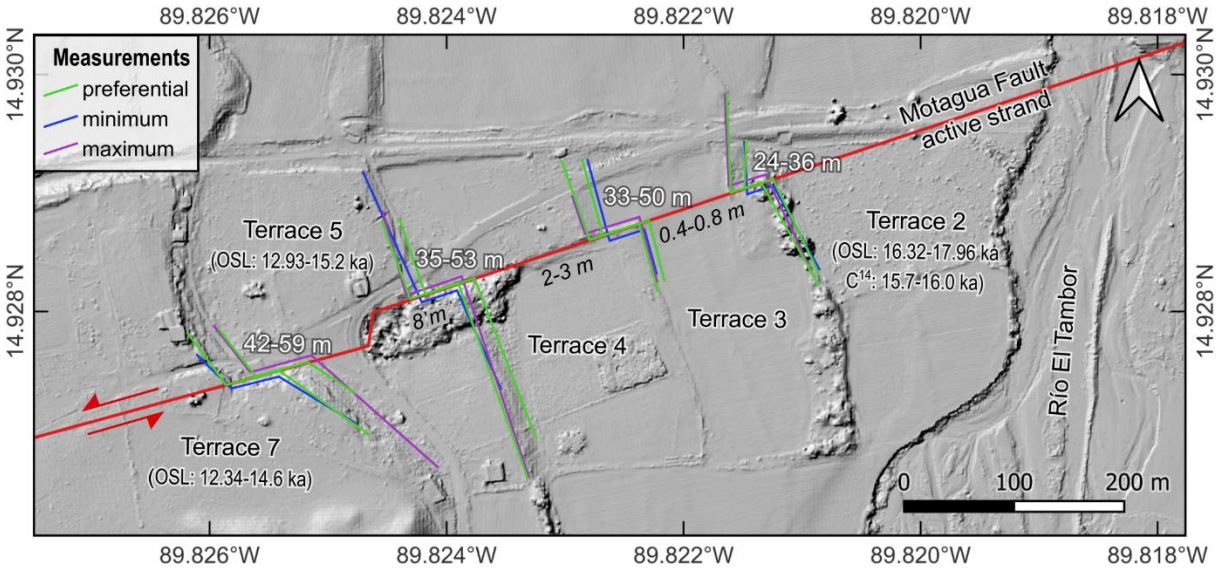

Figure 3: New data for the fluvial terraces at the Río El Tambor. Riser Offsets (white text), scarp heights (black italic text) and dating results. Preferential, minimum and maximum offset measurements are indicated with colored piercing lines.

Table 1: Displacements measured at the Río El Tambor terraces. The new measurements are based on the Río El Tambor LiDAR DEM with 0.5 m pixel resolution.

Terrace Number	Riser offsets [m]				Fault scarp heights [m]	
	Previous measurements by Schwartz et al. (1979)	New measurements			Previous measurements by Schwartz et al. (1979)	New measurements
		preferential	minimum	maximum		
7	58.3	50	42	59	no scarp	
5	52.2	47	35	53	2.5	8
4	31	46	33	50	1.8	2-3
3	23.7	28	24	36	0.6	0.4–0.8
2	no offset				no scarp	

In order to determine the ages of the terraces, we took optically stimulated luminescence (OSL) samples from terraces 7, 5, and 2 (Fig. 4). Terrace 2 was sampled at its riser which represents the current bank of the Río El Tambor. The sand lens was thin but mostly consisted of suitable grain sizes. From the riser of terrace 2 we also retrieved a charcoal for radiocarbon dating (Fig. 6). The samples from terrace 5 were taken from small road cuts at the southern and northern sides of a former railway line. The material came from very loose, small sandy lenses within coarse mixed gravels and therefore mostly consisted of grains > 1 mm. Both samples from terrace 5 can be assigned to approximately the same stratigraphic level (Fig. 7). Samples of terrace 7 were taken from within the terrace riser (Fig. 8), both from reasonably homogeneous sand layers at different stratigraphic levels.

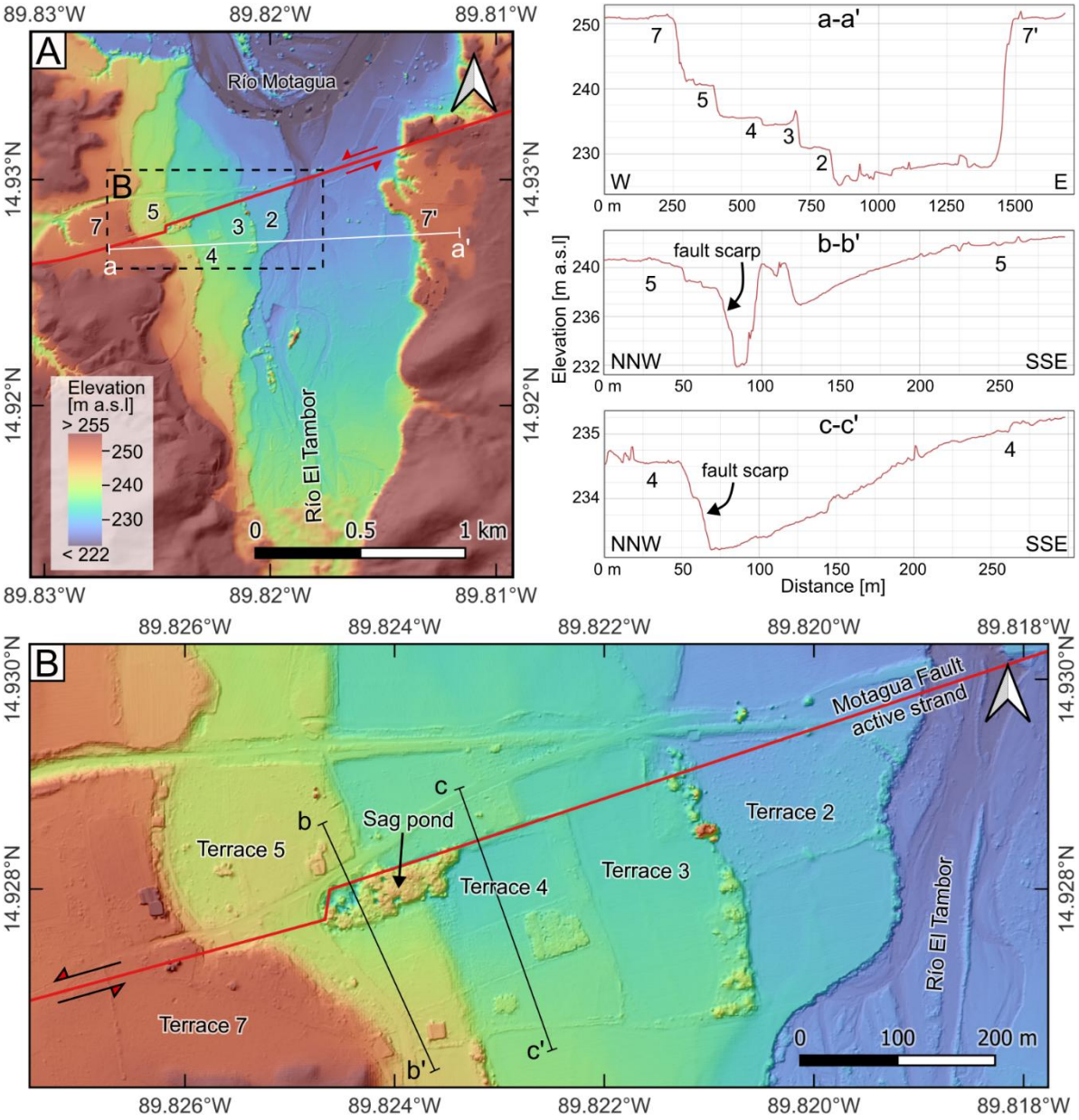

Figure 4: Morphology of the fluvial terraces based on the Río El Tambor 0.5 m LiDAR DEM. (A) Overview map showing the confluence of the Río El Tambor and the Río Motagua. Numbers 2–7 indicate the terrace levels as labeled by Schwartz et al. (1979). Note how multiple surfaces are only preserved on the western side while to the east only one terrace level exists. Lines show the trace of the active strand of the Motagua Fault (red), elevation profile a–a' (white) and the map extent of (B) (black dashed). Elevation profile a–a' shows the height differences between the terraces and the correlation of terrace 7 to the eastern side where a surface at the same elevation exists. (B) Detailed view of the offset terraces. From Ebell (2025).

The OSL samples were processed at the LIAG Institute for Applied Geophysics in the lab of Sumiko Tsukamoto. The charcoal was dated by BETA Analytics, Miami.

The OSL age of terrace T2 is 17.14 ± 0.82 ka and the radiocarbon age is 15.7–16 ka cal BP (table 2). Terrace 5 was dated to 11.02 ± 0.86 and 14.08 ± 1.15 ka, respectively, using two samples.

Two samples from the riser of terrace T7 yield OSL ages of 13.61 ± 0.84 and 13.47 ± 1.13 ka, respectively.

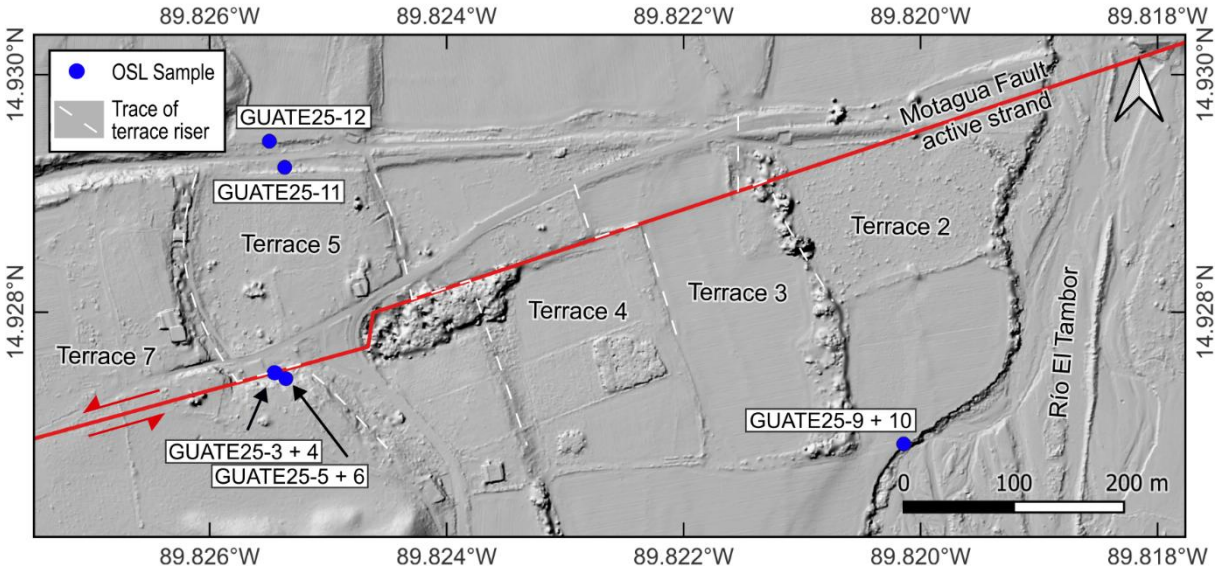

Figure 5: OSL sampling locations.

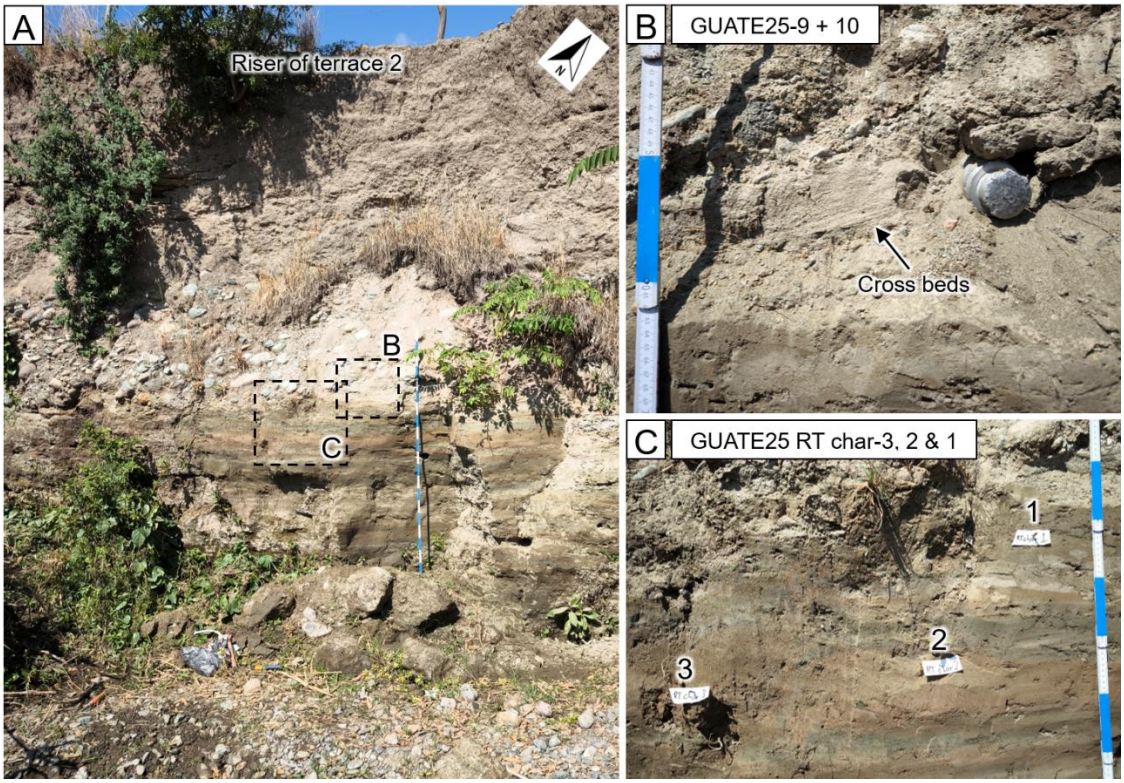

Figure 6: (A) Sampling site of terrace 2. The riser is the current bank of the Río El Tambor. Planar-bedded clayey-silty layers in the lower part of the outcrop are overlain by coarse, poorly sorted, imbricated gravels. The imbrications dip towards SSW indicating a flow direction towards NNE, similar to the river at present. (B) Zoom-in on the contact between the fine-grained layers and the gravels where sample GUATE25-9 + 10 was taken from a thin, cross-bedded lens of fine to coarse sand. The second tube was taken to the left where the cross beds are visible. (C) Locations of charcoal samples within the mud layers.

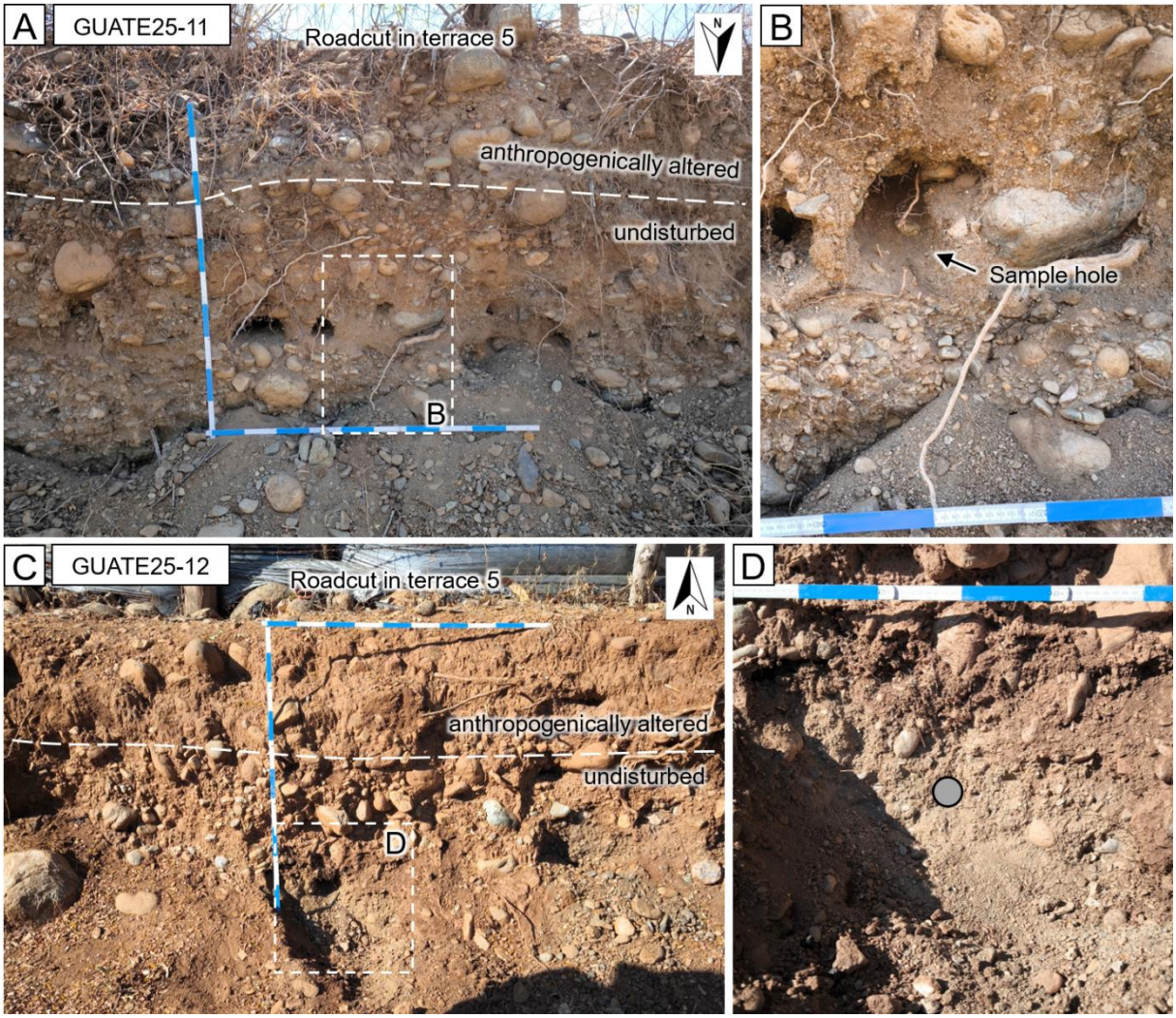

Figure 7: Sampling site of terrace 5. The outcrops are roadcuts on the S (A) and N (C) sides of an old railway line. The upper ca. 50 cm each consist of anthropogenically altered material, likely mixed by ploughing. The outcrops are made up of coarse, poorly sorted gravels mixed with sand. The samples, see zoom-ins (B) and (D), were taken from small, sand-rich lenses within the gravels. The material was very loose, which complicated sampling and may have led to partial bleaching in the case of GUATE25-11. Picture (D) was taken before sampling; the location of the tube is indicated with the grey circle.

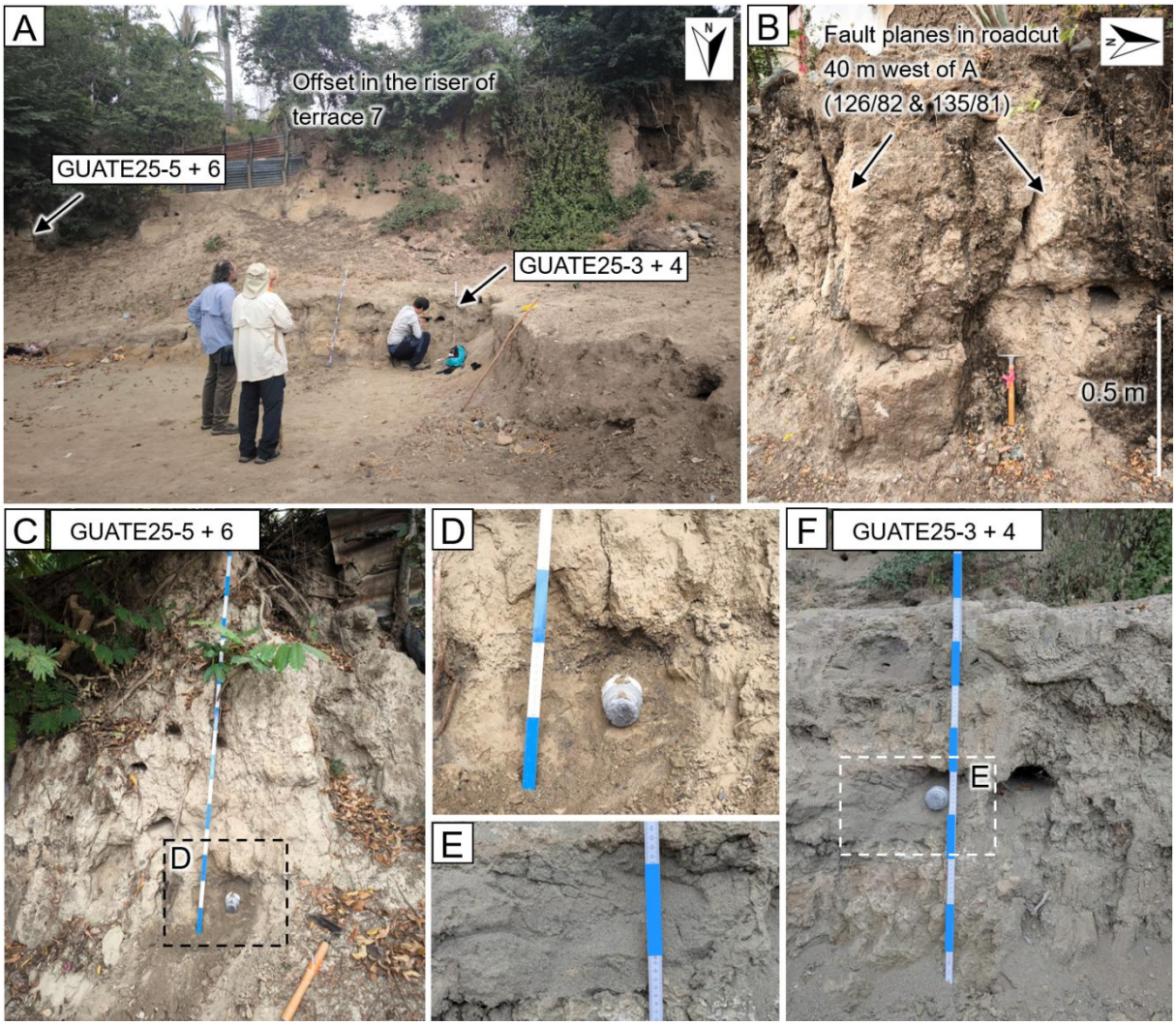

Figure 8: (A) Sampling site of terrace 7. Locations of samples are indicated, GUATE25-5 + 6 being stratigraphically higher than GUATE25-3 + 4. (B) Small roadcut west of the outcrop showing fault planes that are in line with the riser offset but strike a bit more SW instead of WSW. The values are in the format dip direction/dip. (C) Position of GUATE25-5 + 6 within the outcrop; zoom-in (D) shows one of the two tubes inserted in a fine sand layer below a lens of fine gravels. The second tube was taken a few centimeters to the left. (F) Position of GUATE25-3 + 4 within the outcrop; one of the two tubes is inserted in a ca. 15 cm thick fine to coarse sand layer, that is bracketed by silt horizons, the upper one containing gravel. The second tube was taken a few centimeters to the left. (E) Zoom-in on the sand layer in (F).

Using the offsets in terraces T7 and T5 with the respective dating results, we get **slip rates of 2.9-4.8 mm/ yr and 2.3-42 mm/yr**, respectively.

Table 2: Calculated OSL ages of the samples from the fluvial terraces at the Río El Tambor using different equivalent doses (D_es) with standard errors. Preferred values are marked in green. For comparison the radiocarbon age of the charcoal from terrace 2 is also shown.

Sample (terrace number)	Laboratory number	Age using mean D_e with outliers [ka]	Age using mean D_e without outliers [ka]	Age using finite mixture model D_e with outliers [Gy]
GUATE25-3 + 4 (7)	LUM5164	14.45 ± 1.01	13.61 ± 0.84	not calculated
GUATE25-5 + 6 (7)	LUM5165	13.47 ± 1.14	13.47 ± 1.13	not calculated
GUATE25-9 + 10 (2)	LUM5167	19.55 ± 1.59	17.14 ± 0.82	not calculated
GUATE25-11 (5)	LUM5168	11.13 ± 1.08	9.83 ± 0.82	11.02 ± 0.86
GUATE25-12 (5)	LUM5169	14.08 ± 1.15	14.08 ± 1.15	not calculated
GUATE25 RT char-2 (2)	Beta-740969 charcoal, radiocarbon dating*	**Age cal BP:** 15.697–15.995 ka		

Table 3: Slip rates calculated based on the terrace ages and riser offsets at the Río El Tambor.

Terrace Number	Riser offset range [m]	OSL age range [ka]	Slip rate [mm/a]
7	42–59	12.34–14.6	2.88–4.78
5	35–53	12.93–15.2	2.3–4.1

Discussion

Despite high overdispersions present in most of the samples the dating results are considered robust because the ages of both samples from terrace 7, LUM5164 and LUM5165, are very similar (13.61 ± 0.84 ka and 13.41 ± 1.13 ka, respectively). One sample from terrace 5 also has a comparable age (14.08 ± 1.15 ky), fitting well with both terrace risers showing about the same amount of offset. The second sample from terrace 5, LUM5168, yielded a lower age (11.02 ± 0.86 ky) but this is likely due to the effects of post-depositional bleaching; the sample is therefore considered unreliable.

The large overdispersions are most likely explained by heterogeneous dose rates. As the samples were taken from small lenses of sandy material next to highly heterogenous gravels, and in some cases the lenses themselves consisted of mixed material with varying grain types and sizes, grains from different positions within a sample might have received different amounts of radiation, leading to varying charges and ultimately different OSL signal intensities. The effect of nearby gravels on the dose rate is unknown; to test for this in situ dose rate measurements are needed in the future.

The higher age of LUM5167 compared to the other samples is surprising as terrace 2 was

initially thought to be the youngest, because it is the lowest and closest to the current river path, and does not appear to be offset by the fault. The OSL dating result seems to be valid however as the older age of terrace 2 was confirmed by radiocarbon dating (15.7–16 ka cal BP). This means that it consists of older material deposited before terraces 5 and 7 were created, refuting the initial idea of aggradational terraces whose sediments progressively get younger towards the river. All terraces are likely carved into an old valley fill or alluvial fan as suggested before by Schwartz et al. (1979). The OSL ages indicate that the downcutting was not interrupted by significant depositional phases, and therefore the terraces almost entirely consist of the old alluvium without larger amounts of new sediment placed on top. This means that they are degradational fill-cut terraces except for the uppermost one (7) which would be an aggradational fill terrace representing the initial top of the alluvium. However, it is possible that the samples of terrace 2 were just taken too far below the surface and missed the limited zone of newly deposited material.

If the western side of the Río El Tambor truly represents a set of degradational terraces cut into an older alluvial fill, only the sedimentary age of the uppermost level 7 would be suitable for slip rate estimation. The smaller offsets in the risers of the lower terraces would represent younger incision ages while the sediments themselves are much older as they are deeper within the stratigraphy of the fill. The OSL ages of the lower terraces would therefore lead to an underestimation of the slip rate. The sediments of terrace 7 are interpreted as the youngest part of the valley fill deposited right before incision started because no signs of a higher terrace level were found. The usefulness of terrace 7 for slip rate calculations may still be debatable because the timespan between deposition (= OSL age) and incision (= creation of the riser that was subsequently offset) is unknown. Nevertheless, given how dynamic the Río El Tambor is with ca. 20 m of sediments (height difference between terraces 2 and 7) being deposited and subsequently eroded in less than 20 ka it seems unlikely that the river stayed in equilibrium not changing its base level over a longer period of time. For that reason, the OSL ages of terrace 7 should be close to the timing of downcutting and the creation of the riser, providing a fairly accurate estimate for the slip rate. Still, the **slip rate represents a minimum estimate**, and the true value may be slightly higher.

The slip rate of 2.88–4.78 mm/a calculated from the offset in the riser and the OSL ages of terrace 7 **agrees well with the 1.5–6 mm/a originally estimated by Schwartz et al. (1979)**, but **is much lower than the 13 mm/a derived from GPS** studies (Ellis et al., 2019; Garnier et al., 2020). The 6-9 mm/a determined by Maurer et al. (2025) for the central part of the Motagua Fault using improved faulting models is closer to the new estimate but still significantly higher. The difference may be explained by additional deformation being distributed across minor strands within the Motagua FZ whereas the main active strand only takes up the biggest amount. Plafker (1976) did not find ruptures on parallel secondary stands after the 1976

earthquake but deformation in the rest of the fault zone might also happen via slow continuous creep.

Dividing the average 1.1 m offset of the 1976 earthquake (Bucknam et al., 1978) by the new slip rate of 2.88–4.78 mm/a gives an **approximate recurrence interval of 230–382 years for 1976-like earthquakes**. This calculation assumes that stress on the main active strand of the Motagua Fault is only released via such strong earthquakes without significant amounts of creep or smaller events. Therefore, 230–382 years can be seen as a minimum recurrence interval (i.e. it may be longer). Despite that, the numbers agree well with the average timespan of 250–340 years between the last 5 events found in the trenching study from La Laguna (Field trip day 3; Niemi et al., 2026), giving confidence to both results.

Pre-meeting Field Trip Day 1 – Estanzuela trench site

Christoph Grützner, Tina Niemi, Aleigha Dollens, Jeremy Maurer, Paco Gomez, Omar Flores, Carlos Perez, Jonathan Obrist-Farner

Objectives

- Examine field evidence for past earthquakes and creep
- Understand the fault geometry and the formation of the Estanzuela basin
- Explore how creep may manifest in trenches

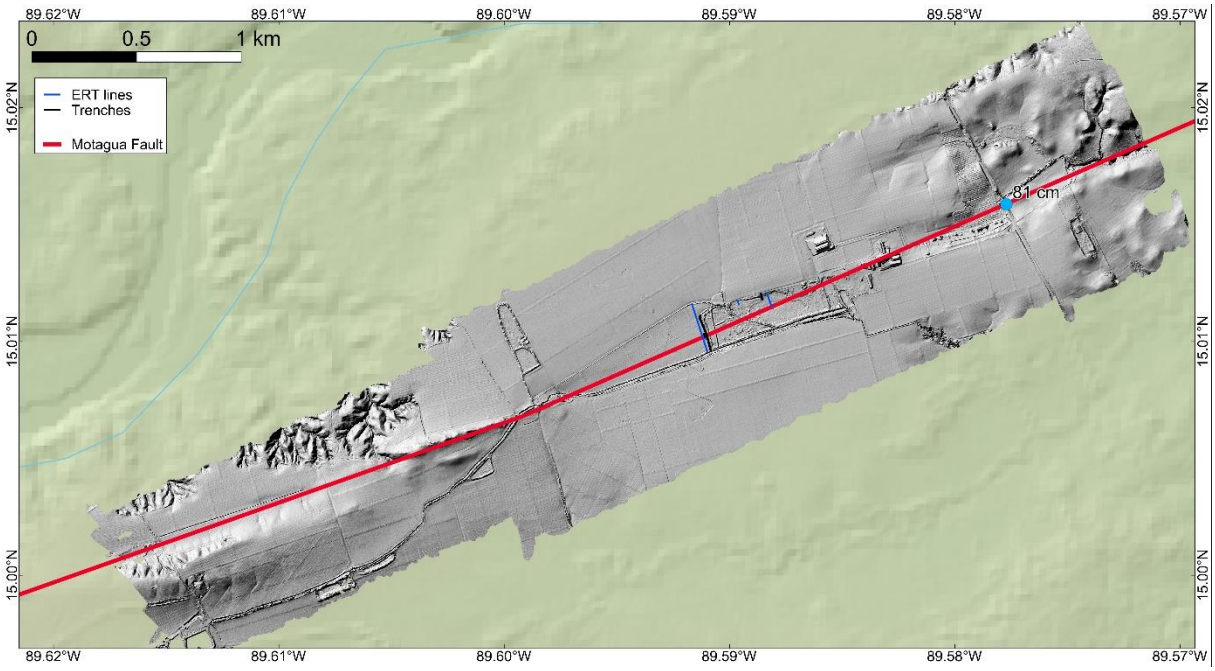

Figure 9: The Motagua Fault trace in the Estanzuela section. 1 m LiDAR DEM by Jeremy Maurer.

Local setting

In the Estanzuela section, the Motagua fault runs south of the Motagua River. Northeast of the highway offset in 1976, the fault trace manifests as a clear lineament in gentle hills (Fig. 9). Southwest of the highway, the fault crosses a topographic low, the Laguneta Los Yajes, and continues through agricultural fields, mostly melon and corn. Even further to the southwest, the fault trace is marked by elongated ridges. This topography indicates an alternation of push-up ridges and pull-apart basins, requiring either bends or stepovers (Fig. 10).

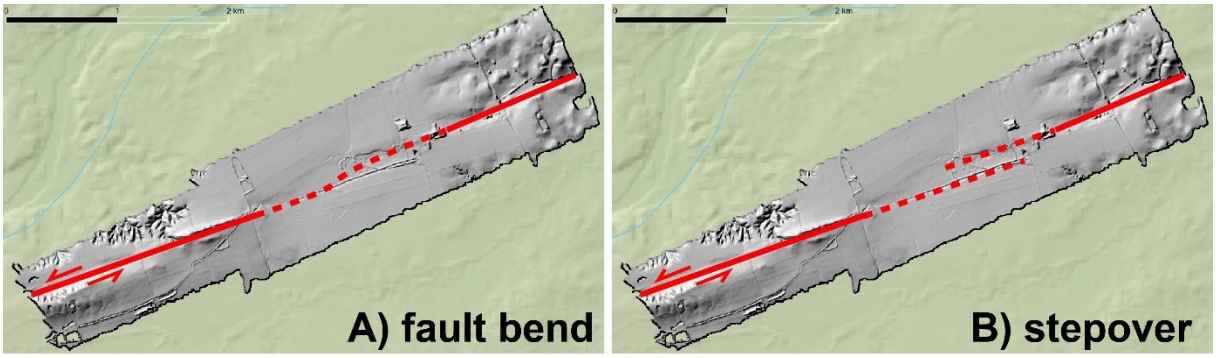

Figure 10: Possible fault geometries top produce the topographic low at Laguneta Los Yajes.

In 1976, the Laguneta Los Yajes was filled with water. Locals report that the water was up to 2 m deep in the rainy season and that fish were cultivated here. For this reason, the precise rupture trace could not be mapped in 1976 (Figs. 11-13).

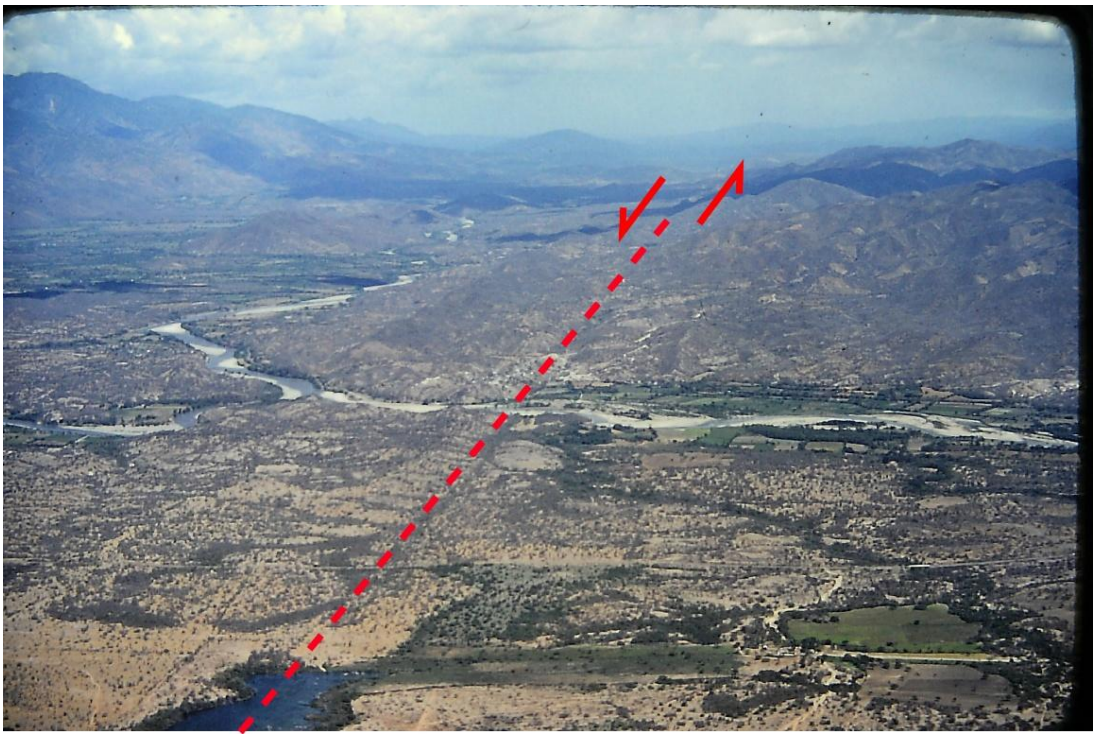

Figure 11: Oblique aerial photo of Laguneta Los Yajes in 1976 from the original 35 mm slide #71 (George Plafker USGS Archive). View is towards the NE.

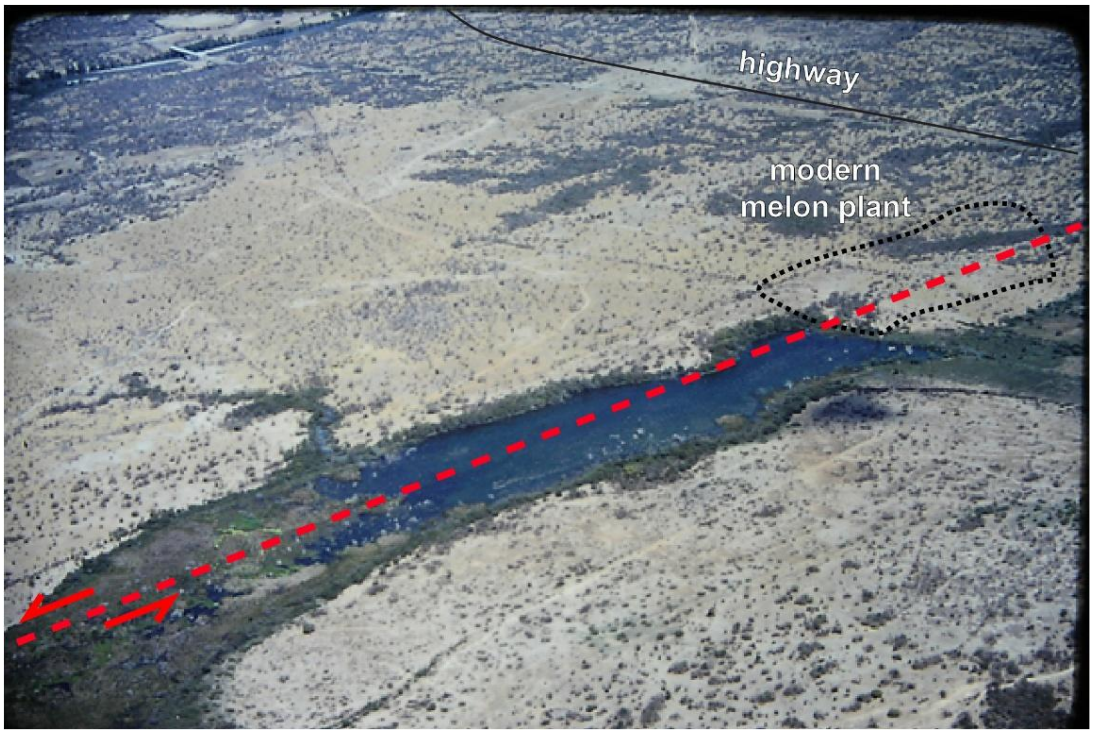

Figure 12: Oblique aerial photo of Laguneta Los Yajes in 1976 from the original 35 mm slide #70 (George Plafker USGS Archive).

Figure 13: Oblique aerial photo of Laguneta Los Yajes in 1976 from the original 35 mm slide #105 (George Plafker USGS Archive). View to the NE.

The 1976 Earthquake at Estanzuela

The 1976 offset measured in a drainage ditch along the highway was 60 cm left-lateral (Fig. 14). Similar values were recorded throughout the entire fault section (Plafker et al., 1976). There was almost no vertical slip. A moletrack was documented in the area on either side of the highway (Fig. 15).

Figure 14: Offset Highway CA-10 north of Zacapa in February, 1976. From Bucknam et al. (1978).

Figure 15: Installation of monitoring monuments across the mole track surface rupture for afterslip measurements. Plafker archive slide 1507

1976 Afterslip

In order to measure the afterslip of the 1976 earthquake, monitoring monuments were installed parallel to the highway across the fault, and the offset drainage ditch was re-measured several times (Figs. 16, 17). Bucknam et al. (1978) report a total of 31 cm of afterslip 610 days after the earthquake (Fig. 17), which is ~50% of the coseismic offset.

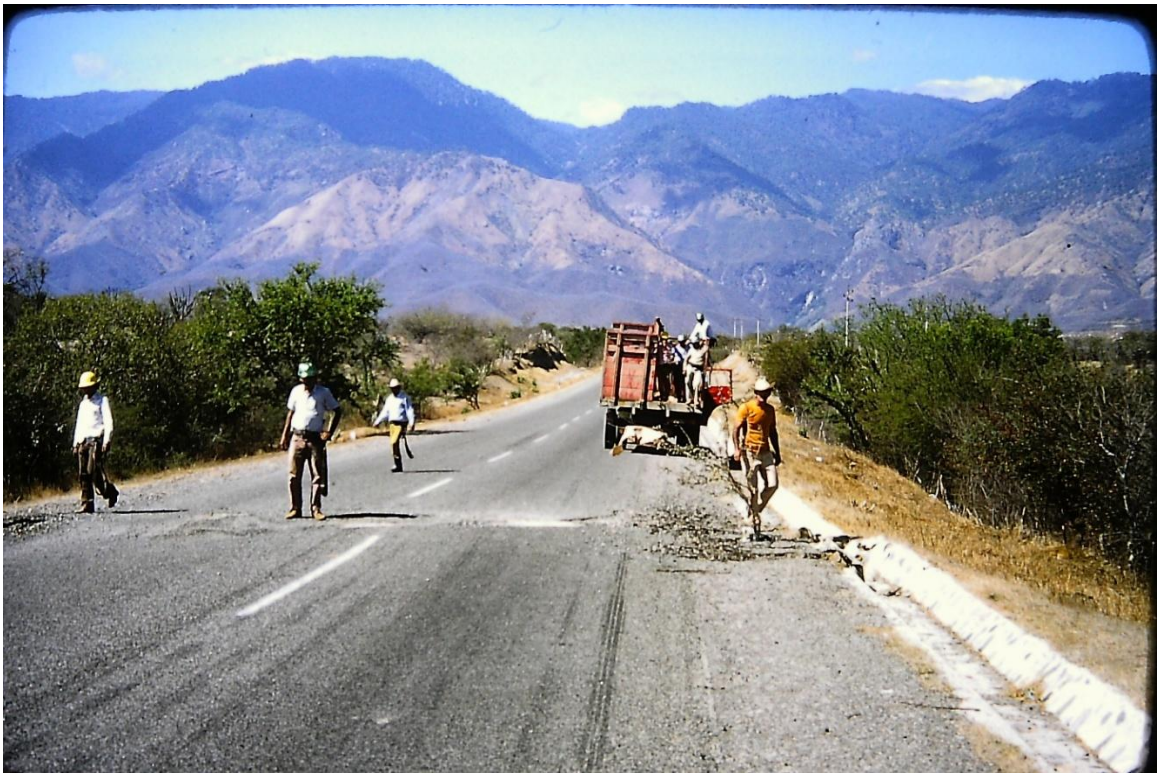

Figure 16: A total of 31 cm of left-lateral afterslip was recorded at the Estanzuela section 610 days after the earthquake (Bucknam et al., 1978).

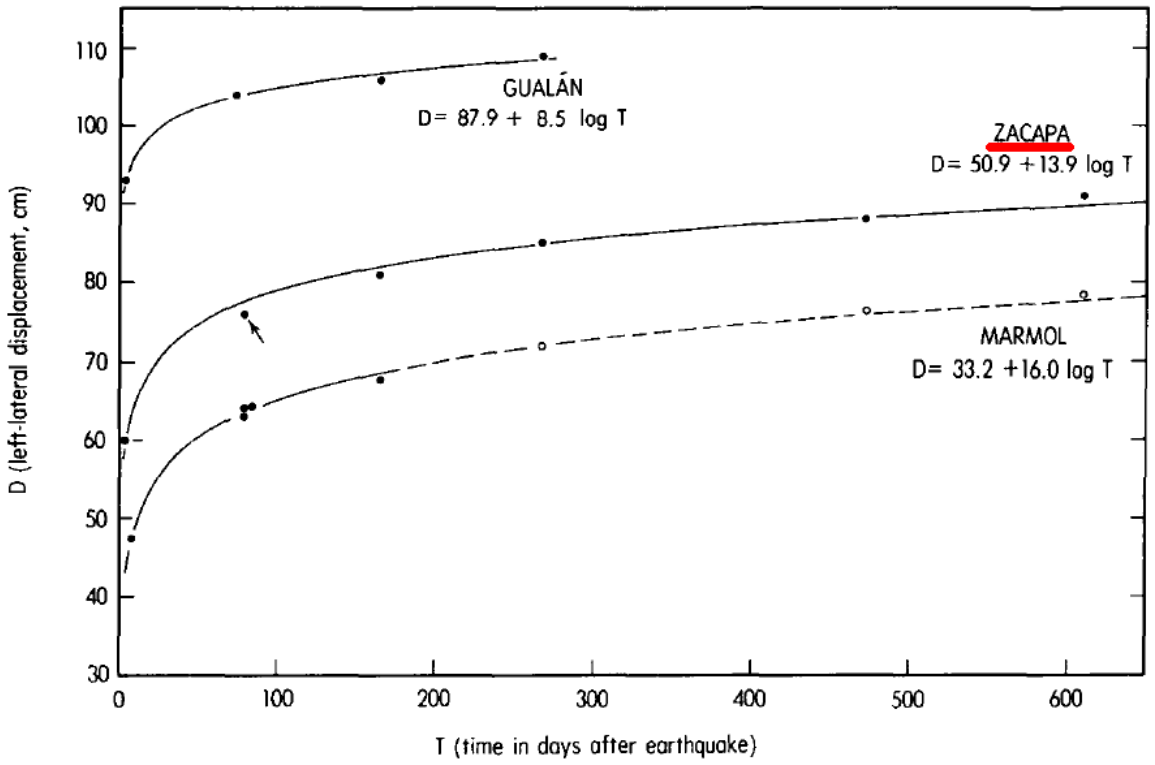

Figure 17: Measured afterslip at the Estanzuela (Zacapa) site by Bucknam et al. (1978).

Creep

In a certain section of the modern melon plant, floor tiles keep on cracking and had to be repaired several times. Cracks also appeared on the walls in the same place. The cracks are located on the projection of the fault trace, they are almost parallel to the strike of the Motagua Fault, and they show a right-stepping en-echelon geometry (Fig. 18). This indicates minor left-lateral creep, as we only observed millimeter-scale offsets in floor tiles several years old.

Figure 18: Cracked floor tiles show right-stepping en-echelon geometry and millimeter-scale offsets.

Geophysics

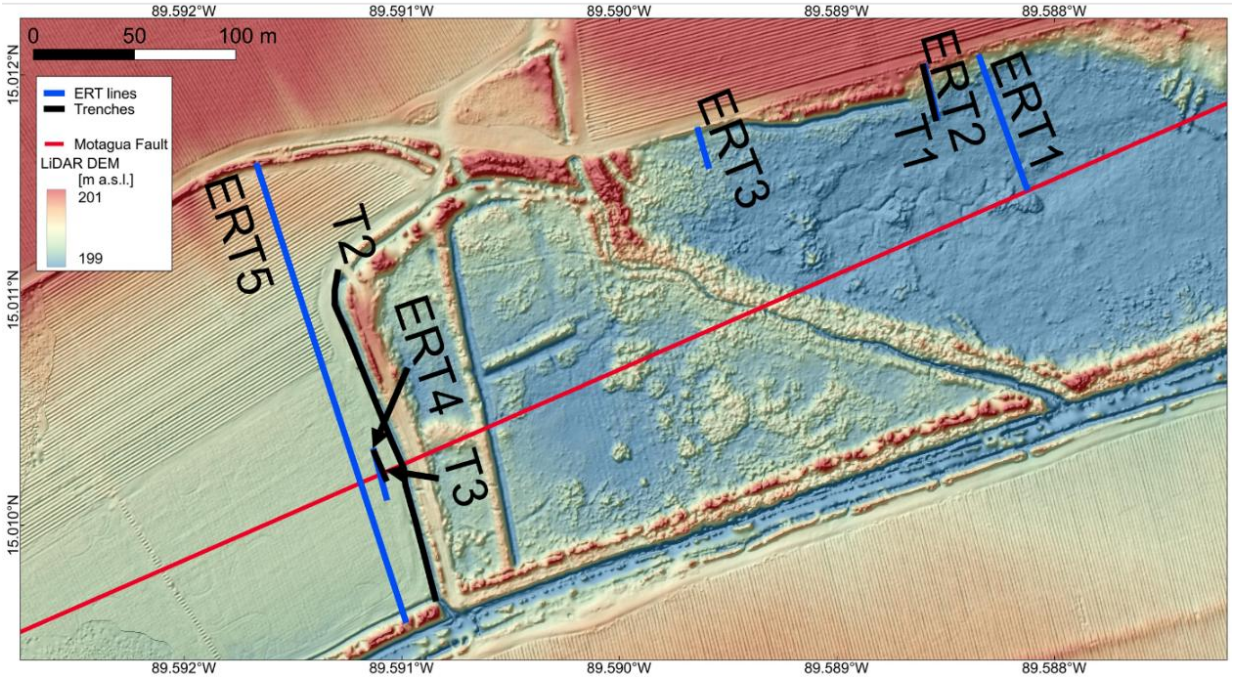

Figure 119: Location of the geoelectrics profiles (ERT) and the trenches.

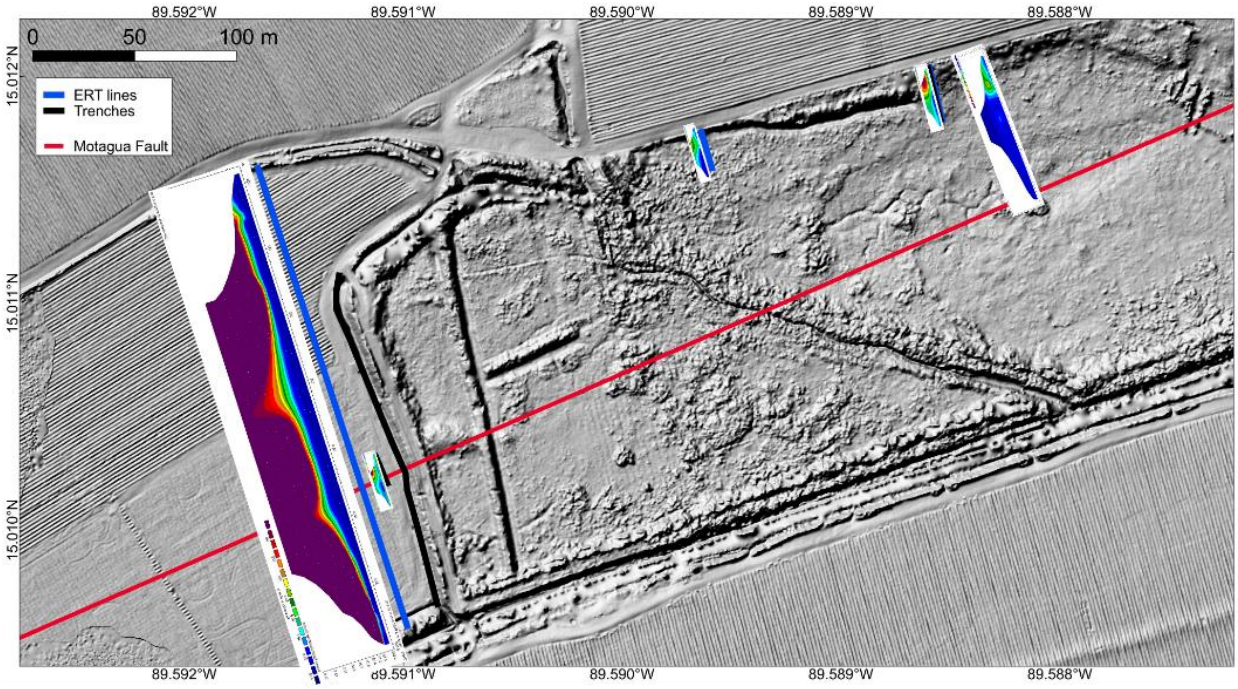

Figure 20: Geophysical surveys prior to trenching.

For trench site selection, we conducted electrical resistivity tomography surveys (ERT, geoelectrics) using a Ground Tester 6472 by AEMC (Figs. 19, 20). We first concentrated on the

northern edge of the depression, where a topographic step of ca. 2 m can be seen in the LiDAR DEM (Fig. 19). This part of the depression is not farmed but covered in bushes. We found a sharp contrast in resistivity values with higher values in the north and lower values south of the scarp in profiles ERT1-3 (Fig. 20). Here we opened trench T1 to check for a potential northern fault strand.

West of the depression we conducted a long ERT survey (ERT5) which showed hints for faulting in the central part of the section. A higher-resolution local survey (ERT 4) confirmed a sharp change in resistivities. Here we opened trenches T2 and T3.

Trench T1 – no northern boundary fault?

In contrast to what the geophysics implied, trench T1 did not reveal a sharp major fault zone (Fig. 21). Instead, we found a wide zone of distributed deformation.

The lowermost unit U1 is a sandstone made up of re-deposited volcanic material. Above that, units T2 and T3 are made up of weathered U1, forming sand- to siltstones. These first three units are found in the entire trench. They are locally topped by gravel layer U4 and by a clayey silt elsewhere in the trench. Above we found black clays related to the deposition of organic material in the laguneta and an organic top layer U7, including shells of freshwater bivalves. Units U1-3 show minor down-to-the-south faulting with total offsets of a few tens of cm only, and cracks and fractures are widespread all throughout the trench without clear localization of deformation.

We conclude that here there is plenty of evidence for secondary tectonic deformation, but our trench did not hit the main fault zone where most of the displacement is accommodated.

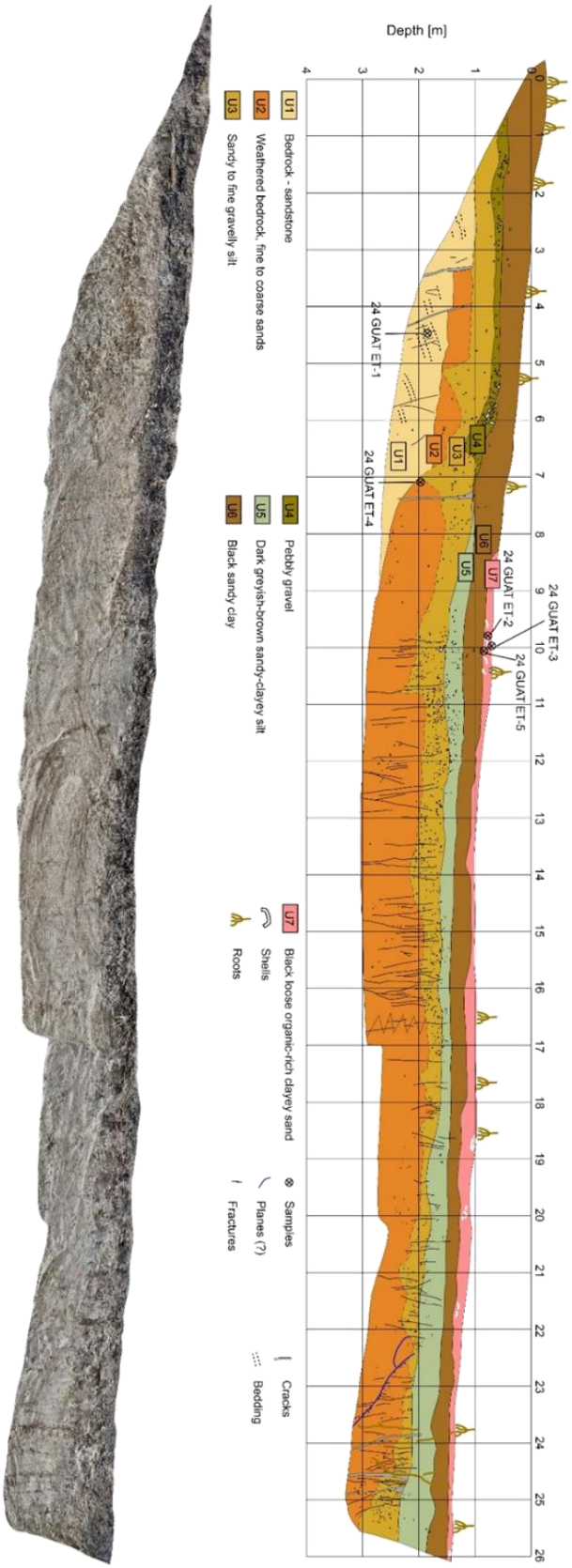

Figure 21: Trench T1 across the northern boundary scarp of the depression.

Trench T2 – Evidence of creep?

Figure 22: Trench T2 in the foreground, T3 in the background. Both show the main fault zone.

For trench T2 we took advantage of a north-south running, 140 m long drainage channel crossing the entire depression (Figs. 19, 22). According to the melon farm workers, this drainage channel is excavated and cleaned every two years.

We cleaned the western wall and excavated down to unit U1, a whitish-yellowish sandy clay to sandy, clayey silt with pumice, interpreted to be redeposited volcanic material. For most of the length of the trench, U1 is covered by unit U2, an organic-rich black clay and U4, the modern soil including the root zone and anthropogenic spoil from the excavation (Fig. 23). At ca. 90 m from the northern end, we encountered the main fault zone and here we excavated down to a depth of 4 m below surface (Fig. 23).

The fault zone is characterized by vertical planes with slickensides indicating normal motion. These planes separate greyish units that become darker the closer they are to the core of the fault. We interpret these greyish units as organic material from unit U2 that filled cracks which opened in surface-rupturing earthquakes, and that was subsequently sheared by later events (Fig. 23).

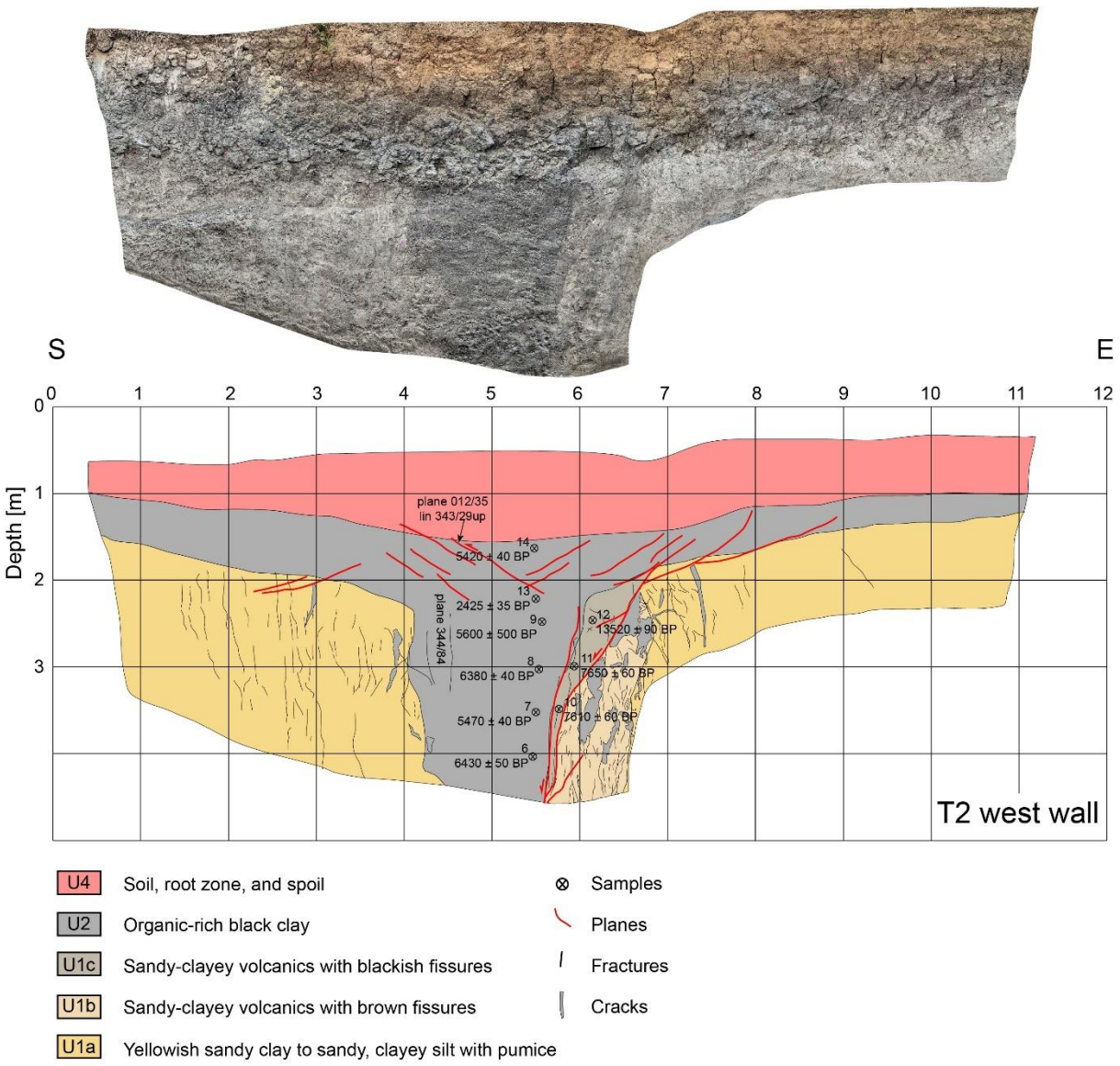

Figure 23: Trench log of the fault zone in T2.

Planes with hints for reverse motion and dips of around 30° were found on top of the fault zone. Most of these planes and fractures are restricted to units U2, but at least one of them reaches the modern soil, perhaps indicating the rupture of the 1976 earthquake.

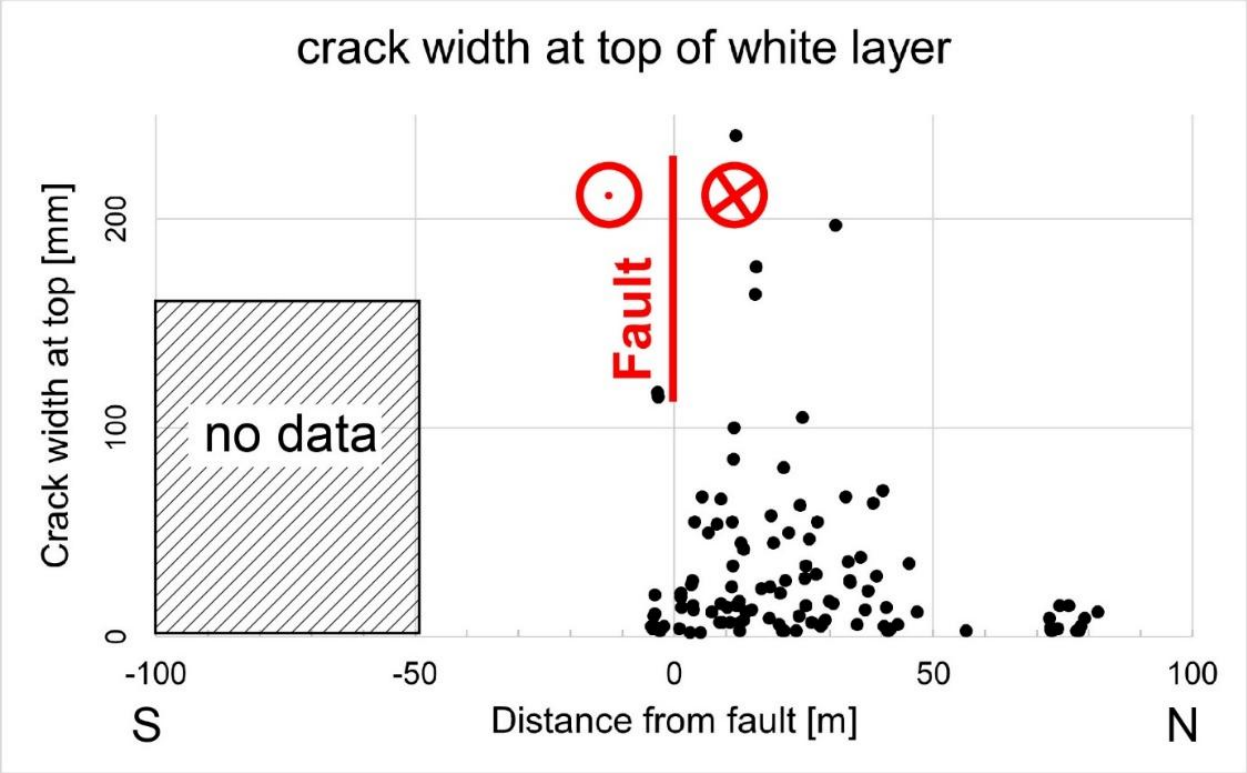

Figure 24: Width of cracks at the top of the whitish-yellowish layer U1 from trench T2.

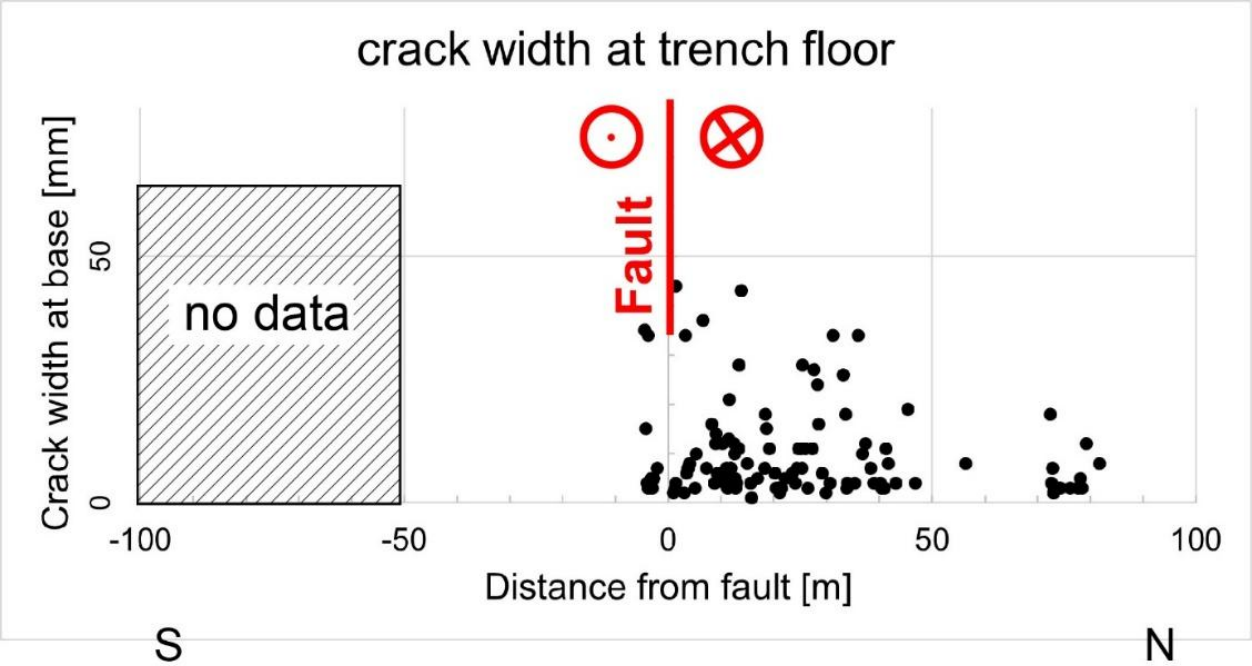

Figure 225: Width of cracks at the trench floor, T2.

Within unit 1a we found more than 100 cracks filled with material from units U1 and U2 that we systematically surveyed (Figs. 24-26). We recorded their location, their width at the top of the

white layer (Figs. 21, 23), and their width at the trench floor (Fig. 25). Interestingly, we found an increase in crack density from north to the fault zone, and almost no cracks south of the fault zone (Fig. 24). Their widths, both at the base and at the top, increases towards the fault zone.

Their average strike is slightly more towards the north than that of the main Motagua Fault (Fig. 26), and their dip is mainly vertical. This leads us to interpret them as en-echelon features that probably result from creep on the main fault of from off-fault deformation.

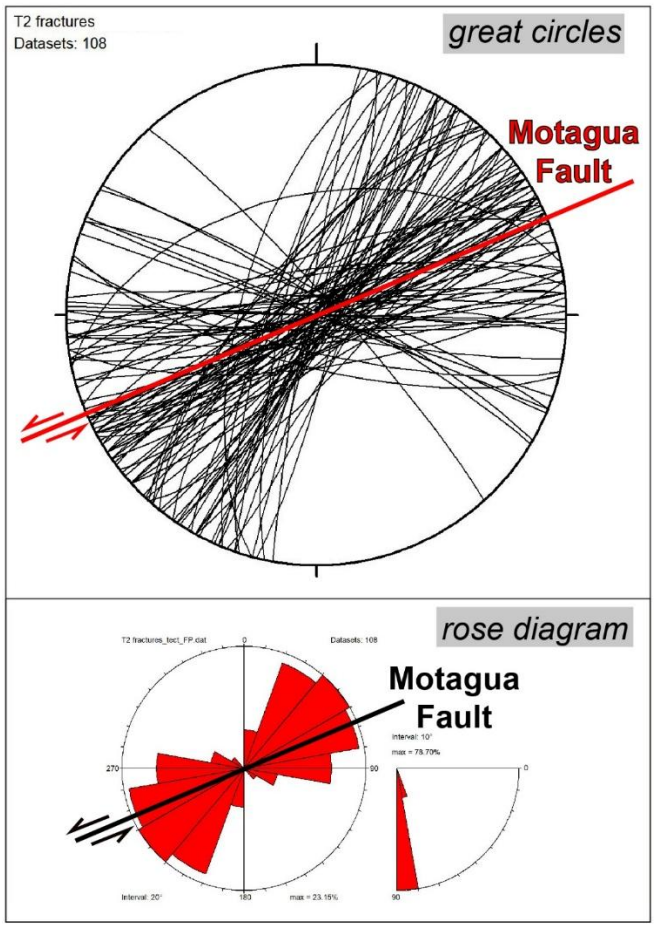

Figure 263: Strike and dip of the cracks found in T2 and comparison to the strike of the Motagua Fault.

In summary, T2 reveals distributed and off-fault deformation, but also the location of the main fault zone right in the center of the Laguneta Los Yajes depression.

Trench T3 – complicated fault networks in 3D

To better understand the fault zone, we opened trench T3 parallel to T2, guided by the location of the fault in T2 and the geophysics results (Figs. 20, 22). In contrast to T2, this 12 m-long trench enabled us to map both trench walls and the trench floor in detail (Figs. 27, 28). The general stratigraphy is the same as in the long trench T2, except for the additional unit U3, an organic-rich brown clay occurring as a pocket within unit 2 (Figs. 27-28).

The fault zone is about 3 m wide (as in T2) and has black organic clays all the way to the trench floor. Intense fracturing characterizes the entire trench. The complicated fracture network includes many structures parallel to the main fault trend, but also in all other directions. The larger fractures with up to several centimeters of opening width must have been open fissures filled with black organic, clayey material either from the top or from the sides. We speculate that the filling happened rapidly during or immediately after coseismic crack opening, perhaps eased by liquefaction during intense ground motion.

To conclude, we observe the main fault zone of about 3 m width in trenches T2 and T3. Intense fracturing indicates coseismic opening of fissures and immediate filling with the surrounding, perhaps liquefied material. The fact that the fault is located not on the edges of the laguneta depression implies that there is no fault stepover, but a fault bend causing the topographic low.

Figure 27: Trench T3 orthophoto.

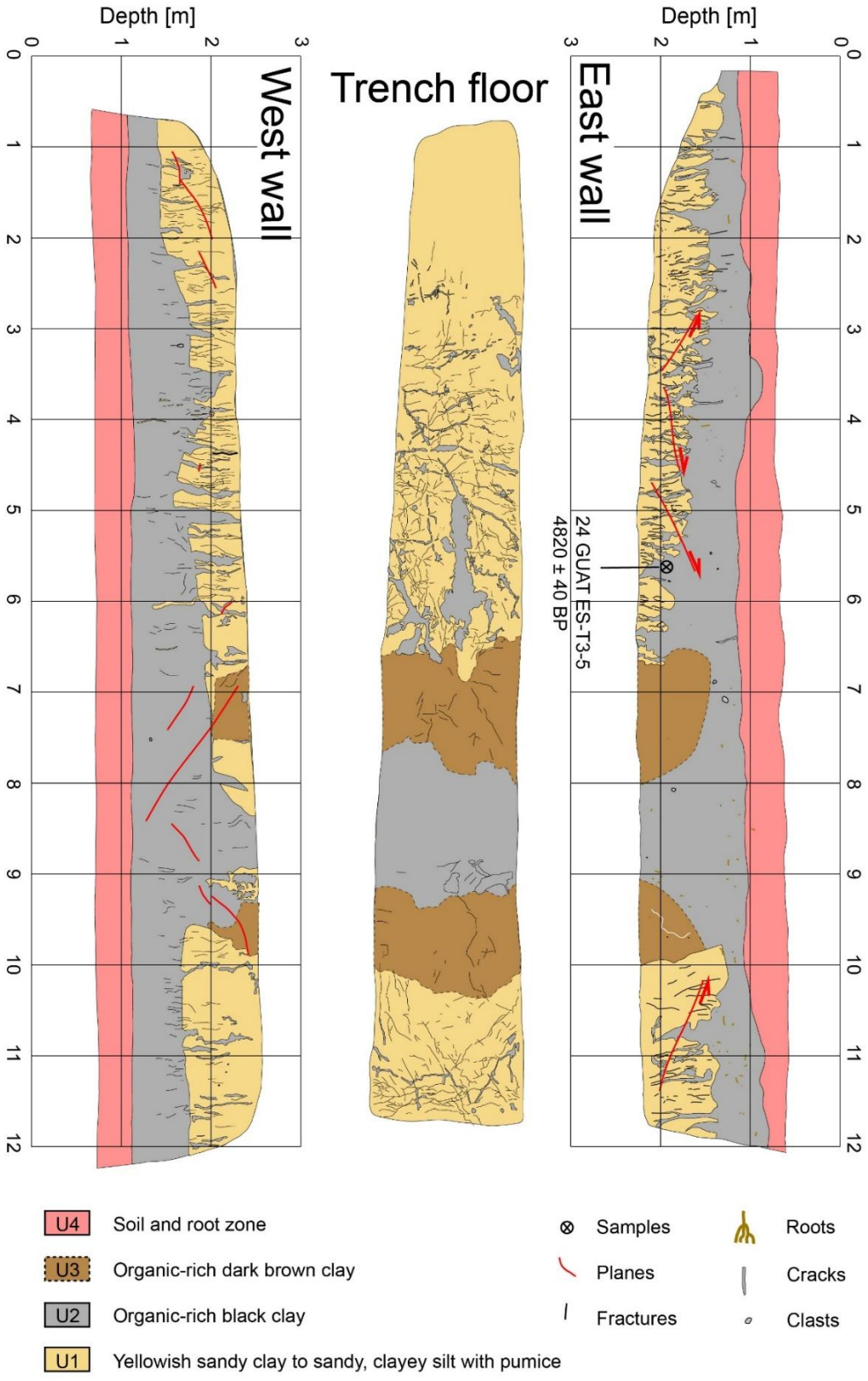

Figure 28: Trench log of T3.

Pre-meeting Field Trip Day 2 – Archaeoseismology of the Late Classic Maya Site of Quirigua, Guatemala

Tina Niemi

"Thus Quirigua was the first Old Empire city I ever saw and while I have visited it many times since, for me it has never lost its original romantic thrill or its absorbing human appeal."

– Sylvanus G. Morley (1935, p. 14)

Logistics

The epicenter of the 1976 earthquake was near Quirigua in Las Amates (Fig. 29) with the ground rupturing passing just north of the site. The purpose of the trip is not only to enjoy the remarkable Mayan ruins, but to point out evidence of past earthquakes at the site.

The tour usually lasts about an hour. There are restrooms at the park entrance. The site is located in a low-lying area just north of the Motagua River and is prone to mosquitoes, so it is advisable to use bug spray. Furthermore, the area is always hot and humid, so bring water. There are two recommended pathways through the Quirigua site (Fig. 30). The traditional route is to walk through the Great Plaza and Ballcourt to view all the monuments. Then, ascend the Acropolis steps and view the structures at the top. Alternatively, you can follow a route that does not require climbing up the platform steps to the top of the Acropolis. Follow the service road east of Stelae H-J to the central court of the Acropolis. Here, you can view all the structures and descend along a path on the west side of the Acropolis or the platform steps. When returning to the parking lot, be sure to observe the leaf-cutter ants on the large ceiba trees.

Introduction

Quirigua is best known for its spectacular and massive upright carved monuments that are the largest in the Maya World. The site of Quirigua is located along the lower Motagua River (Fig. 29), where the valley opens up into a vast floodplain about 100 km west of the Gulf of Honduras on the Caribbean Sea. As such, it was founded by 450 CE as a river port for the trade of cacao, jade, and obsidian from the Sierra de las Minas and the Guatemalan Highlands (Sharer and Traxler, 2012). The ruling dynasties of Quirigua, who were vassals of the much larger city of Copán, located about 50 km south in Honduras, appear to have originated from the expansive Mayan urban center of Tikal in the Petén region of northern Guatemala (Fig. 29; Sharer, 1990; Looper, 2007).

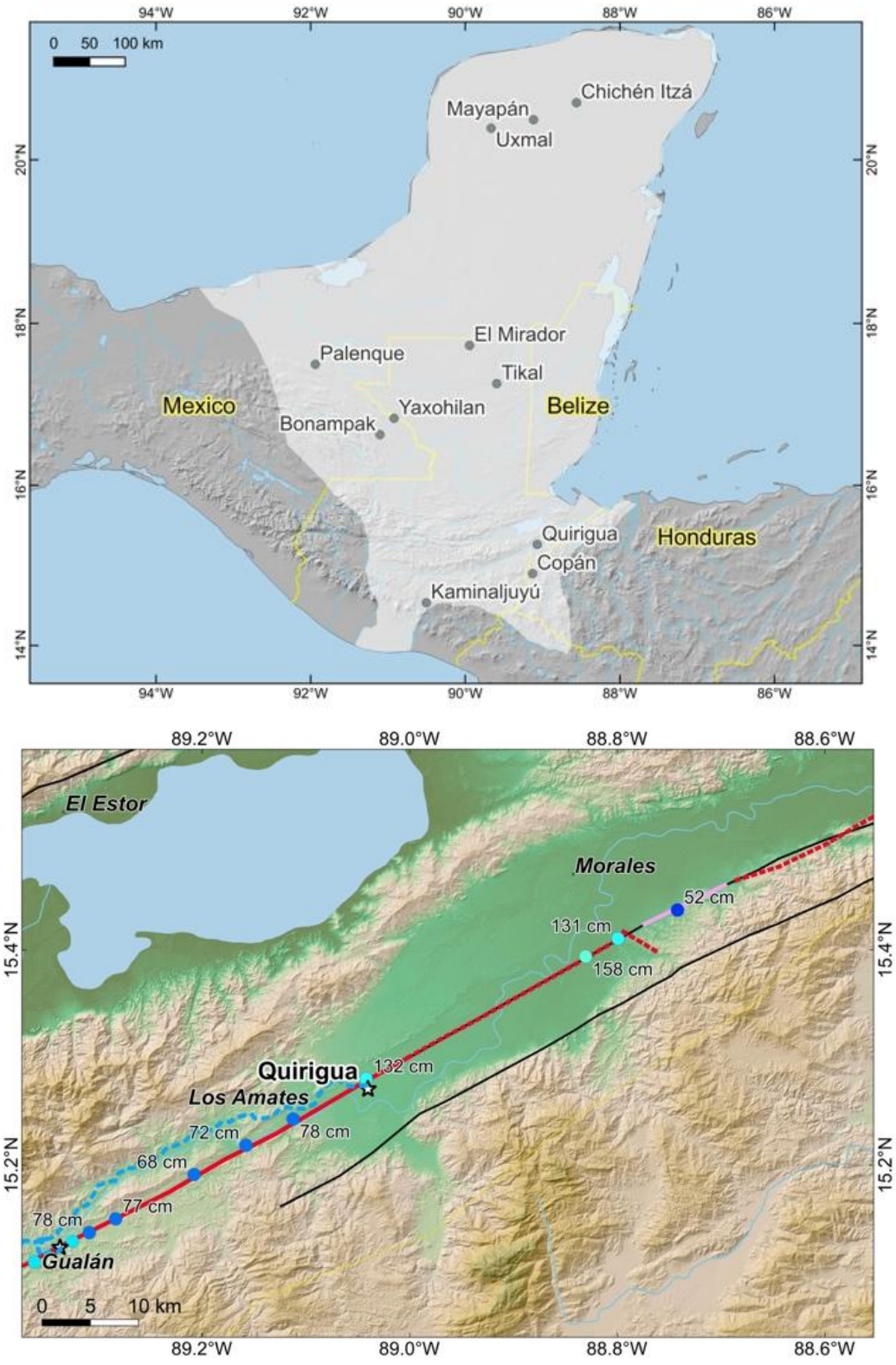

Figure 29: A) Map showing sites of the Maya world. B) Map of the lower Motagua River Valley showing the location of the Late Classic Period Maya site of Quirigua.

History of exploration

The property containing Quirigua was purchased by Juan Payes y Font, who guided Fredrick Catherwood by canoe and through thick jungle to the site in 1840. Drawings of two stelae at Quirigua (Fig. 30) and numerous drawings of Copán and other Maya sites by Catherwood are included in the book *Incidents of Travel in Central America, Chiapas, and Yucatan*, by John Lloyd Stephens (1841). The book became a Victorian-era classic. It transformed the Western World's perception of Central America, revealing the hidden secrets of the Maya World and its endemic growth from local populations. The book launched the field of Maya archaeology.

From 1882-1894, Alfred Percival Maudslay led expeditions that cleared the site of the giant ceiba and palm trees (Fig. 31) and excavated Structures 1 and 2. Maudslay photographed the stelae and acquired numerous molds to cast reproductions. Annie Hunter used the casts to create exquisite drawings of the Quirigua stelae. The "Maudslay casts" of Quirigua stelae are currently being 3D imaged at the British Museum (Joy and Elliott, 2018; Ward and Rice, 2022).

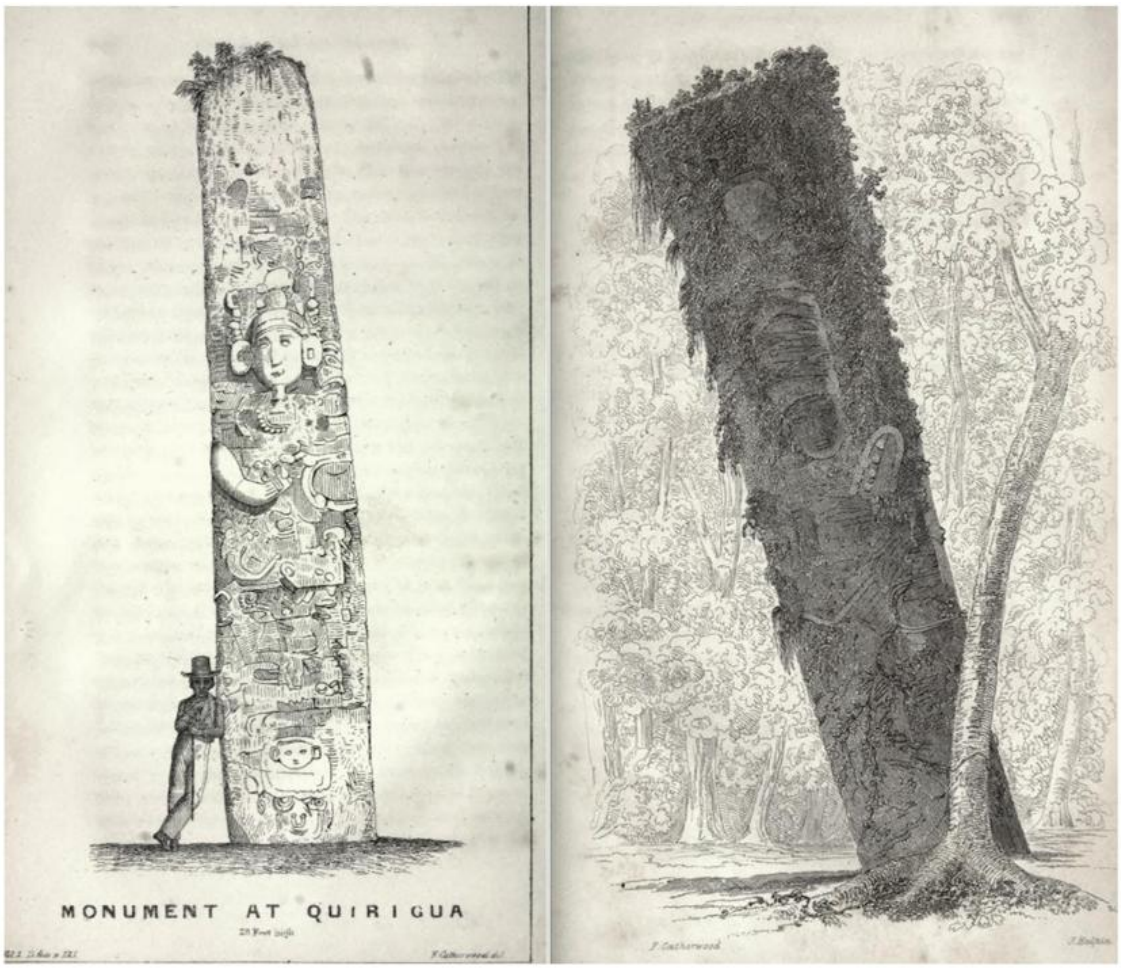

Figure 30: Catherwood made detailed drawings of various Maya ruins, including Stela F (left) and E (right) at Quirigua, aided by a camera lucida, which were published in Stevenson (1841) (Ward and Rice, 2022).

Figure 31: Structure IB-5 on the Acropolis after clearing enormous trees (Maudslay, 1889).

In 1910, the United Fruit Company purchased the land for a banana plantation and placed the core 75 acres of the Quirigua site into a preserve. Clearing, excavations, and restoration led by Edgar Lee Hewett (1911, 1912; Morley, 1913) and photographs by Jesse Nusbaum, (Fig. 32) provided documentary evidence of the site. In 1914, Hewett was commissioned to produce molds of Quirigua stelae to be displayed at the Panama-California Exposition commemorating the opening of the Panama Canal, which can still be viewed at the San Diego Museum of Man. Additional excavations of Structures 3 and 4 on the Acropolis were conducted in 1919 by Sylvanus Griswold Morley (Morley, 1935). The stelae were reset in concrete, straightened, and the foundation cache boxes under the monuments were excavated in 1934 by Gustav Stromsvik and Earl Morris (Ward and Rice, 2022).

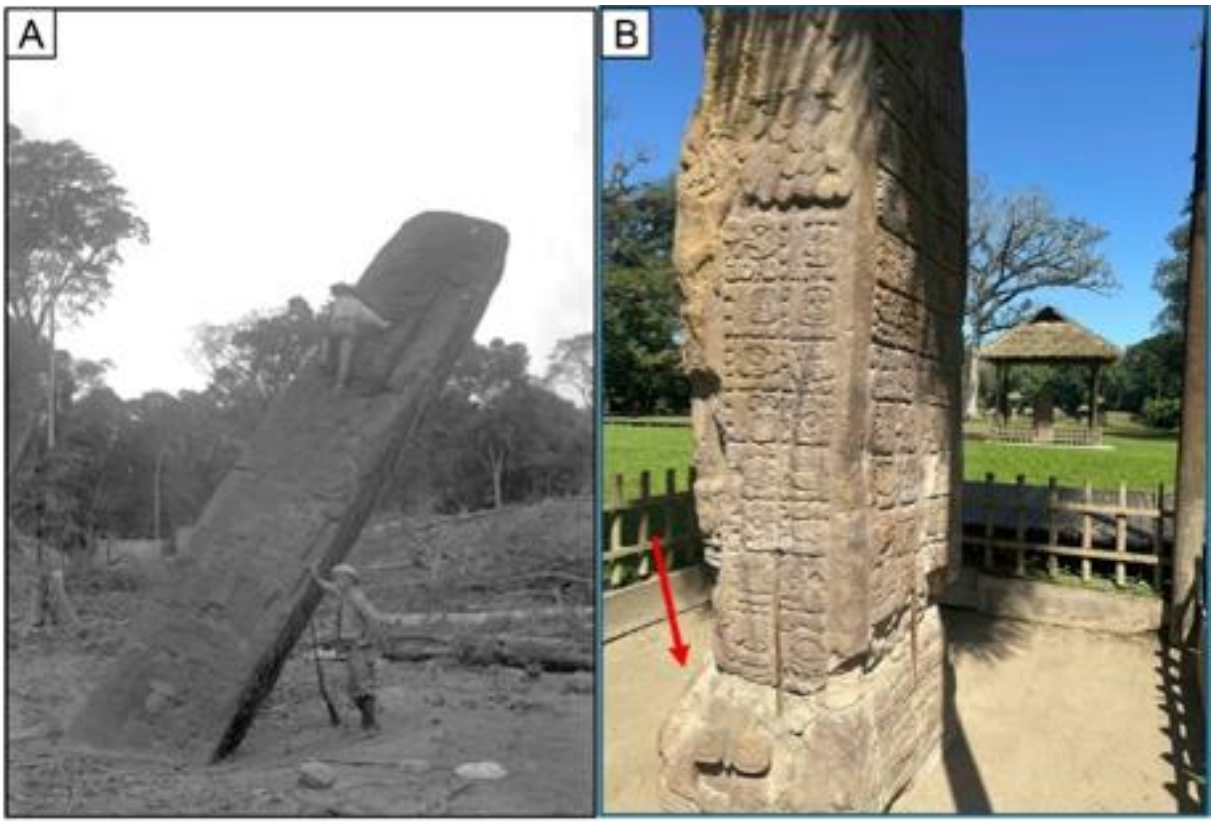

Figure 32: A) The tallest Stela E (771 CE) at 10.7 m was actively tilting until it fell in 1917. Photo by Jesse L. Nusbaum, Courtesy of the Palace of the Governors Photo Archives (NMHM/DCA B) 1976 EQ damage to the reset and rebar-reinforced Stela J (756 CE).

Robert Sharer, from the University of Pennsylvania (Penn) Museum, in conjunction with the Guatemalan Institute for Anthropology and History (IDAEH), led comprehensive modern excavations of the site and its periphery from 1975 to 1979 (e.g., Sharer, 1990). Epigraphic research of the hieroglyphs on the monuments has shed new light on the history of Quirigua (e.g. Looper, 2007). Quirigua was designated a UNESCO World Heritage site in 1981. Restorations to the site were conducted by IDEAH. The Instituto Guatemalteco de Turismo (INGUAT) helps manage the 48-hectare site.

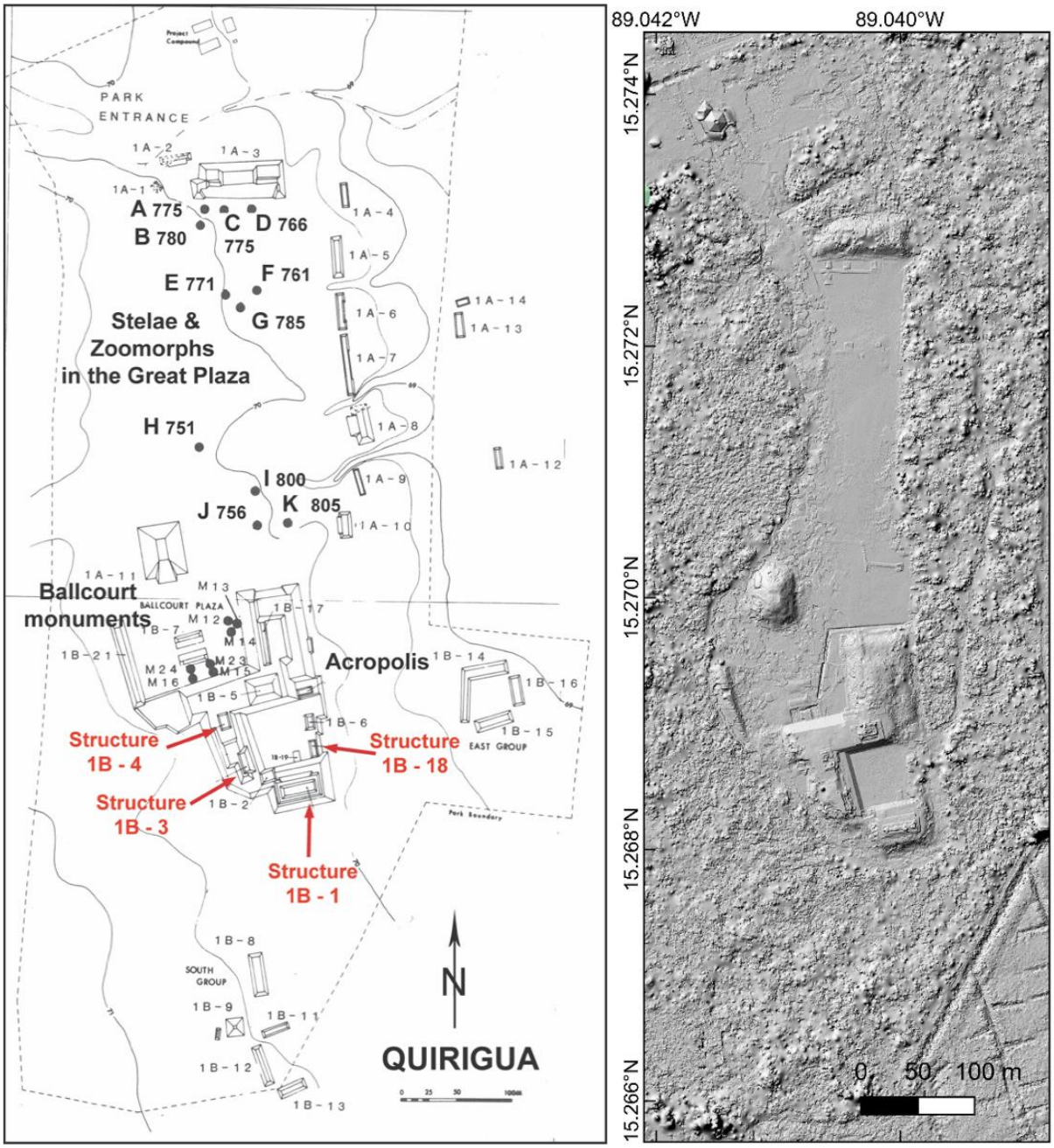

Figure 33: Left) Map of the Quirigua site core showing the location of structures on the stepped platform of the Acropolis, where evidence of past earthquakes has been documented. The stelae in the Great Plaza are identified with letters and their hieroglyphic age (Morley, 1935). (Map modified from Sharer, 1990, p.3). Right) LiDAR image in DEM shaded relief showing the Quirigua Archaeological Park. The fields to the southeast are part of a banana plantation.

Stelae of the Great Plaza

The ceremonial open space of the "Great Plaza" between the stepped Acropolis to the south and structure 1A-3 to the north (Fig. 33) features nine upright sculpted sandstone monoliths (stelae) and two rounded, boulder-like sculptures (zoomorphs). All but four of these were erected during the 61-year reign of *K'ak' Tiliw Chan Yopaat* (Cauac Sky, 724-785 CE), who conquered Copán in 738 CE and brought independence and prosperity to Quirigua. The large stelae display carved portraits of the ruler holding a scepter on the front and sometimes on the back, and hieroglyphs along the sides (Fig. 34). Mythical animal-human compositions and glyphs encircle the zoomorphs, and the disk-shaped altars are commemorative.

Figure 34: Photographs of Stela D (766 CE) showing the ruler K'ak' Tiliw Chan Yopaat (Cauac Sky)on the front and intricately carved glyphs on the side of the monument.

The sandstone monolithic stelae were quarried from the local Subinal Formation, which outcrops along most of the eastern Motagua River Valley. The Subinal Formation consists of interbedded siltstone, sandstone, and conglomerate that were deposited within a continental basin developed along the transform plate boundary. The age of the rocks is not well constrained, but is likely Eocene (e.g. Donnelly et al., 1990). The fracture and bedding planes within the Subinal Formation allow for quarrying of long slabs used to make the stelae. A geomorphic study by Ashmore (1987) indicates that the Motagua River once flowed closer to the west side of the site. Large monoliths were transported down the river and offloaded at a

dock, as confirmed by *in situ* large masonry blocks excavated along the west side of the Great Plaza.

The stelae and zoomorphs are labeled from the north end of the Great Plaza to the south, from A to P, and are not placed in chronological order (Morley, 1935; Sharer, 1990; Looper, 2007). Table 4 shows the age and a brief description of the eleven monuments in the Great Plaza. The stelae were hoisted up by some unknown method and set into a stone-lined foundation pit that was packed with river cobbles and mud (Fig. 35). The sides of the stelae contain hieroglyphics that occasionally show the Quirigua emblem glyph (Fig. 35)

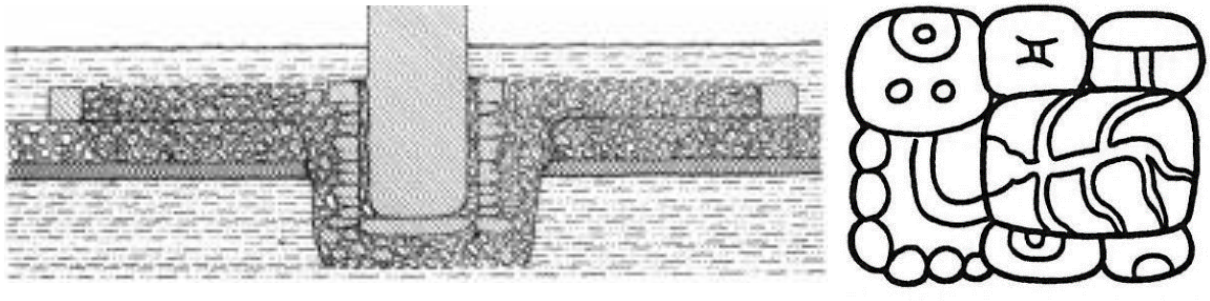

Figure 35: (Left) Example of stela foundation (Looper, 2007). (Right) Quirigua emblem glyph which appears to be a gourd (Ward and Rice, 2022).

Originally, three of the stelae (H, I, J) were discovered fallen (Fig. 32). Both stelae H and J were broken at the ground surface, but Stela I was uprooted and not broken. Three stelae (A, K, E) were tilted to the north or northwest. Stela A was shifted off its foundation, likely in response to ground motion during past earthquakes.

Table 4: List and brief description of the monuments along the Great Plaza at Quirigua

Monument	Date	Height	Description
A	775	Stela 4.3 m	It depicts Cauac Sky with a headdress on the south side and a masked Cauac Sky with jaguar paws on the north side.
B	780	Zoomorph 4 m by 2 m	This sculptured boulder depicts a crocodile with a human figure emerging from its open jaw. The text is in the rare full-figure glyph form. A 48-cm long, flint blade was found as a cache below the sculpture (Stromsvik, 1941).
C	775	Stela 4 m	This stela portrays Cauac Sky on both sides with a scepter in his hands. Hieroglyphs recount the "mythical creation date of the current Maya universe" (Sharer, 1990, p. 31) and an earlier Quirigua ruler from 455 CE.
D	766	6 m	It depicts the ruler Cauac Sky on both front and back, and intricately carved, full-figure glyphs.
E	771	8 m	It is the largest stela at the site. Cauac Sky is portrayed on both sides "wearing elaborate multi-masked headdress" (Sharer, 1990, p. 36). Copán is mentioned in the glyph.
F	761	7.3 m	The second largest stela at the site with portraits of a bearded Cauac Sky on both front and back is the earliest appearance of the goatee. Morley (1935, p. 71) believed Stela F to be the "most beautifully carved of any among the Maya inscriptions ".
G	785	Zoomorph 4.4 m by 1.2 m	A carved boulder that shows a composite mythological creature of a toad and female jaguar with part of a human in the jaws. Glyphs refer to the death of the ruler Cauac Sky.
H	751	5.2 m	It is located toward the north and west of the stelae cluster in the Great Plaza and is the earliest erected monolith. Cauac Sky is depicted on one side. Glyphs are in a diagonal pattern instead of the usual horizontal direction.
I	800	4.1 m	The ruler Jade Sky on the front and glyphs indicating he is the 16th ruler in the dynastic succession.
J	756	5 m	The ruler Cauac Sky on the front and glyphs indicating he is the 14th ruler in the dynastic succession. The glyphs also recount the sacrifice ot the Copán ruler in 738 CE.
K	805	3.5 m	The youngest stelae – tilted (photo). This one of Jade Sky

Stela E is the largest stela at the site and stands 8 m above ground level. The total length of the carved monolith is 10.6 m. When it was documented by Maudslay (1882), it was leaning ”12 feet out of vertical” (Morley, 1935, p. x). In 1883, during the creation of a mold, the nose broke off and was cemented back in place. In 1917, floodwaters ponded at the base of Stela E in the newly cleared site, causing the monument to topple and dislodging the repaired nose. In 1918, Morley rescued the nose and stored it. In 1934, Morris and Stromsvik reattached the nose. However, during the process of hoisting Stela E, it slipped, crashed, and cracked. The stela was set into a concrete base with rebar reinforcement. Stelae E, I, and J were damaged in the 1976 earthquake when rock around the metal reinforcement spalled off (Fig. 32).

Ballcourt Monuments

Two altars, M and N, and two zoomorphs, O and P, are found in the plaza of the ballcourt (Table 5). Two additional altars were found in front of O and P during excavations. Zoomorph P is of particular note as it describes the founding of Quirigua.

Table 5: List and brief description of the monuments along the Great Plaza at Quirigua

Monument	Date	Height	Description
M	734	Altar 2.25 m by 0.7 m	This round altar of carved rhyolite shows a jaguar head and the earliest use of the Quirigua emblem glyph.
N	NA	Altar 1.8 m by 1.2 m	Double-headed, four legged turtle curved out of rhyolite and broken in half.
O	790	Zoomorph 2.8 m by 1.4 m	Broken and weathered, this sculpted boulder likely “depict the cosmological reptilian monster” (Sharer, 1990, p.57). An intricately carved flint of a feathered serpent, a sculpted jadeite human head, jade pebble and a quartz crystal were cached beneath the monument. There is a flat carved altar in front of monument O.
P	795	Zoomorph 3 m by 2.2 m	Largest carved boulder at the site depicts the successor of Cauac Sky, the ruler Sky Xul sitting in the jaws of the cosmic reptile. The glyphs are Important as they recount the founding story. There is a flat carved altar in front of monument P

Buildings of the Acropolis

At the top of the raised, stepped platform of the Acropolis are six structures labelled IB-5, IB- 6, and IB1-4, in a clockwise direction viewed to the south (Fig. 36), surrounding a small courtyard plaza (Temple Plaza of Morley, 1935).

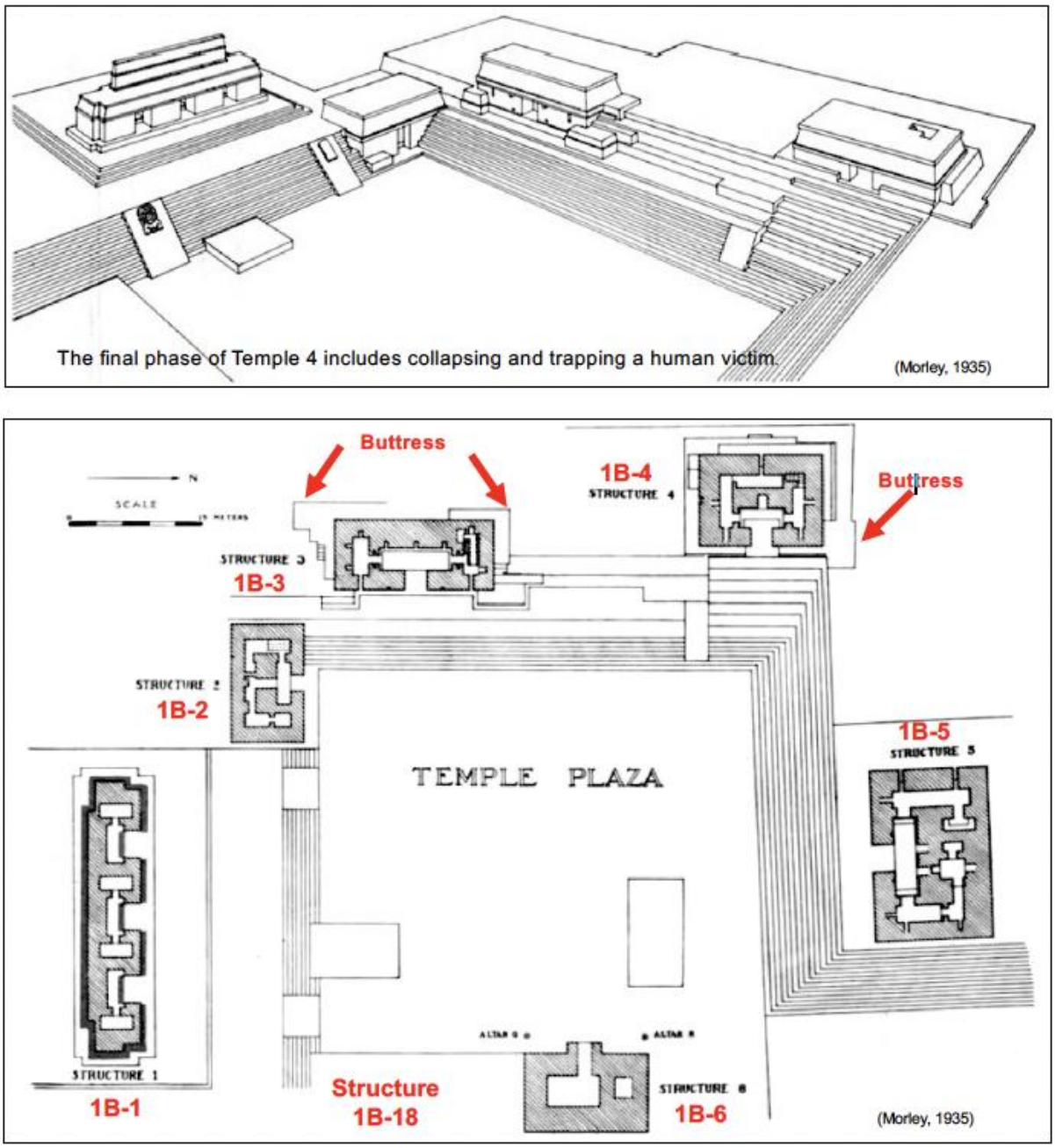

Figure 36: Perceptive drawing and map of the structures on the Quirigua Acropolis. The top drawing shows a perspective reconstruction of Structures 1B-1 to 1B-4 viewed toward the southwest. The bottom plan map shows locations of the earthquake buttressing and the site of the adobe Structure 1B-18 excavated by Jones et al. (1983). Both IB-4 and IB-18 collapsed in an earthquake in the latest phase of occupation.

The youngest structures of the Acropolis are Structures 1B-1 and 1B-5, both constructed by Jade Sky. Structure 1B-1 has a hieroglyph frieze on the stairs that dates to 810 CE (e.g. Sharer, 1990; Looper, 2007). Ward and Rice (2022, p. 39) suggest that, as "Structure 1B-1 (is) known to have post-dated other structures at the Acropolis, most of which have extensive earthquake retrofitting, (it) might have been built with thick walls because of seismic activity in the years immediately before its construction in AD 810".

Structure 1B-6 is the oldest building, and excavations into the lower levels revealed the founder's burial (426 CE), though the extant structure dates to 750 CE (Sharer, 1990). The remaining structures were built by Cauac Sky (724-785 CE) and modified during his reign and later. Ground motion in the 1976 earthquake caused portions of the reconstructed walls of structures 1B-1, IB-4, and IB-5 to collapse (Bevan and Sharer, 1983).

The Acropolis was built in six superimposing construction phases (1-5), with the final platform 3.5 m higher than the initial (Sharer and Traxler, 2012). Table 6 shows a summary of these data, which are annotated with the evidence for earthquake damage, repair, and collapse.

Table 6: List and brief description of the monuments

Phase 5	Reuse of the Acropolis as a domestic site >900 CE**, *Earthquake collapse horizon with human victims***
Phase 4	Ruler Jade Sky (800-810 CE). Acropolis was enlarged, 1B-1 and 1B-5 were built, and cut masonry blocks of rhyolite, sandstone, marble were used. **Walls are thicker as an anti-seismic design.**
Phase 3	Ruler Cauac Sky (724-785 CE), Ruler Sky Xul (785-800 CE). Acropolis was enlarged, 1B-2, IB-3, IB-4 were built. ***Buildings shored with buttresses after an earthquake late in the reign of Cauac Sky.***
Phase 2	Western wall reinforced. Enlarged Acropolis built with rounded cobbles and cut masonry facing (600 – 720 CE) Floodwater silt covers the site ca. 600 CE (Late Classic structures above this layer)
Phase 1	Earthen structure and founder's burial 426 CE (Zoomorph P)

Exterior buttress walls abutting many walls of the structures of the Quirigua Acropolis (Fig. 37) were likely built to reinforce the buildings after seismic shaking as recognized by Bevan and Sharer (1983). When describing the Structure 1B-3, Sharer (1990, p. 87) wrote: "The two front corners of the building are reinforced by secondary buttresses, presumably built in response to ancient earthquake activity that threatened the structure….Structure 1B-3 appears to have been built…probably during the last portion of Cauc Sky's reign" (Fig. 36). This places the construction of the buttresses based on dates of the stelae to after ca. 756-785 CE (Sharer, 1990, p. 88) but before the final construction phase starting at 810 CE. These buttresses appear to correlate to

our Event 5 at the La Laguna site with a radiocarbon age range of 672-987 CE, and likely constrain the range to 756-810 CE (late 8th century).

The best evidence for an earthquake at the Quirigua site is the data from the excavation of Structure 1B-18 on the Acropolis (Figs. 33, 36), where *in situ* vessels and human skeletal remains were discovered smashed on a floor (Jones et al., 1983). Figure 38 shows the plan map and a photograph of these deposits. Jones et al. (1983, p. 8) wrote: "…sixteen broken and complete storage jars, a censer and a curious duck-shaped pot, along with fragments of bone and a few teeth from a child's skeleton were found on the floor of the north room of Structure 1B-18 buried under the clay, burnt adobe fragments and stones of the collapsed adobe super-structure."

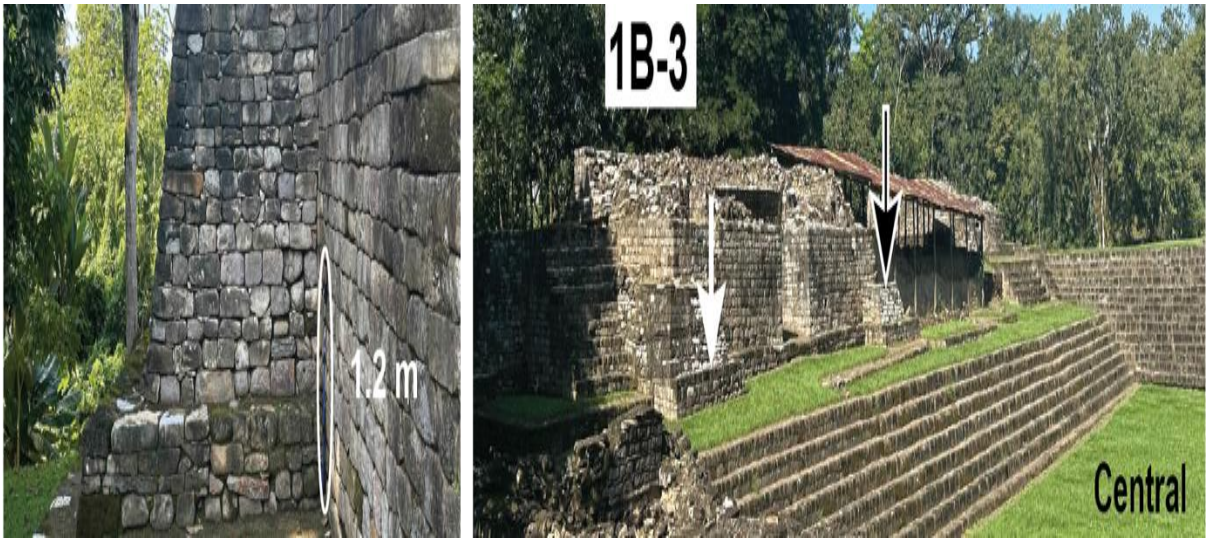

Figure 37: Examples of late 8th-century seismic retrofits. (A) Corner buttress marked by a black arrow to the Structure 1B-3 placed as reinforcement. Walking pole for scale circled in white (1.2 m). (B) Corner buttress (black arrow) and bench (white arrow) added to Structure 1B-3 along the east side of the building. The height of the bench is approximately 50 cm.

Cooking and storage ceramics, and the adobe construction, indicate that the Acropolis was no longer part of the dynastic control but was in domestic use. Artifacts recovered from the latest occupation phase at Quirigua suggest that a new and different population inhabited the site. These data are corroborated by the excavation of 1B-3 and 1B-4 (labelled Temples 3 and 4 by Morley in 1919; Morley, 1935). In his excavation diaries, Morley suggests that the structures were used for an industrial process using red paint (Ward and Rice, 2020). The final phase of Structure 1B-4 includes the collapse and entrapment of a human victim. These types of rapid collapse of a building with human victims and pottery on a living surface have been documented as evidence of an earthquake. The occurrence of copper, Plumbate pottery, and Chacmool effigies suggests that occupation at Quirigua extended into the Terminal or Early Post Classic Maya Period (Sharer and Traxler, 2012). We suggest that these data may corroborate our Event 4 (928-1126 CE) at the La Laguna site, and indicate an earthquake occurred in the earlier part of the age range in the 10th century. Quirigua was never reinhabited after this time period.

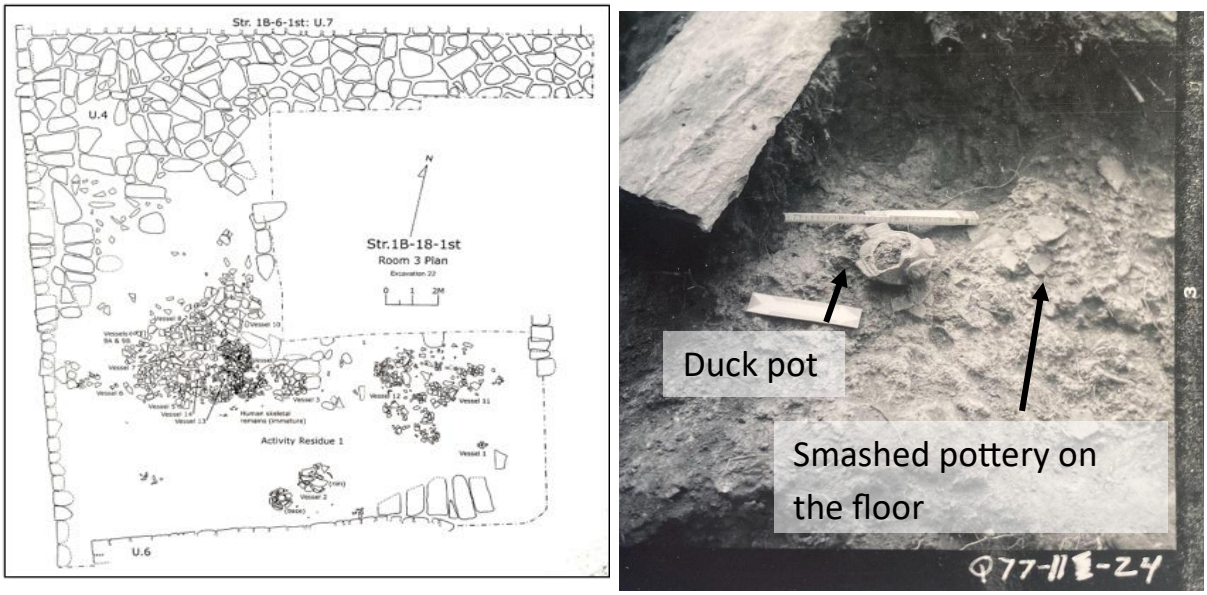

Figure 38: (Left) Plan map of excavation of Quirigua Structure 1B-18 showing the location of 16 vessels smashed in situ and human skeletal remains. [Courtesy of Penn Museum, Figure 6.18, Quirigua Reports Volume V (unpublished)]. (Right) Photograph of the unusual duck vessel and smashed in situ pottery of 16 vessels on a living surface of a domestic structure. The adobe construction and the household pottery indicate that the Acropolis was no longer in use as a dynastic administrative center. Ceramic vessels broken on a floor suggest instantaneous collapse and are evidence for an earthquake. A 20-cm folding scale is shown above the duck pot in the photo. (Courtesy of Penn Museum, Photo number Q77-11-24, Excavation at Quirigua, Guatemala, 1977).

Pre-meeting Field Trip Day 2 – 1976 Rupture in Gualán and Paleoseismology

Trenton McEnaney, Tina Niemi, Jonathan Obrist-Farner, Aleigha Dollens, Paco Gomez, Jeremy Mauer, Omar Flores, Carlos Perez

Objectives

- Discuss the 1976 earthquake rupture in Gualán
- Visit the offset canal and view the tectonic geomorphology of the trench site
- Review ERT and trench data along the Motagua fault at the site

Local setting

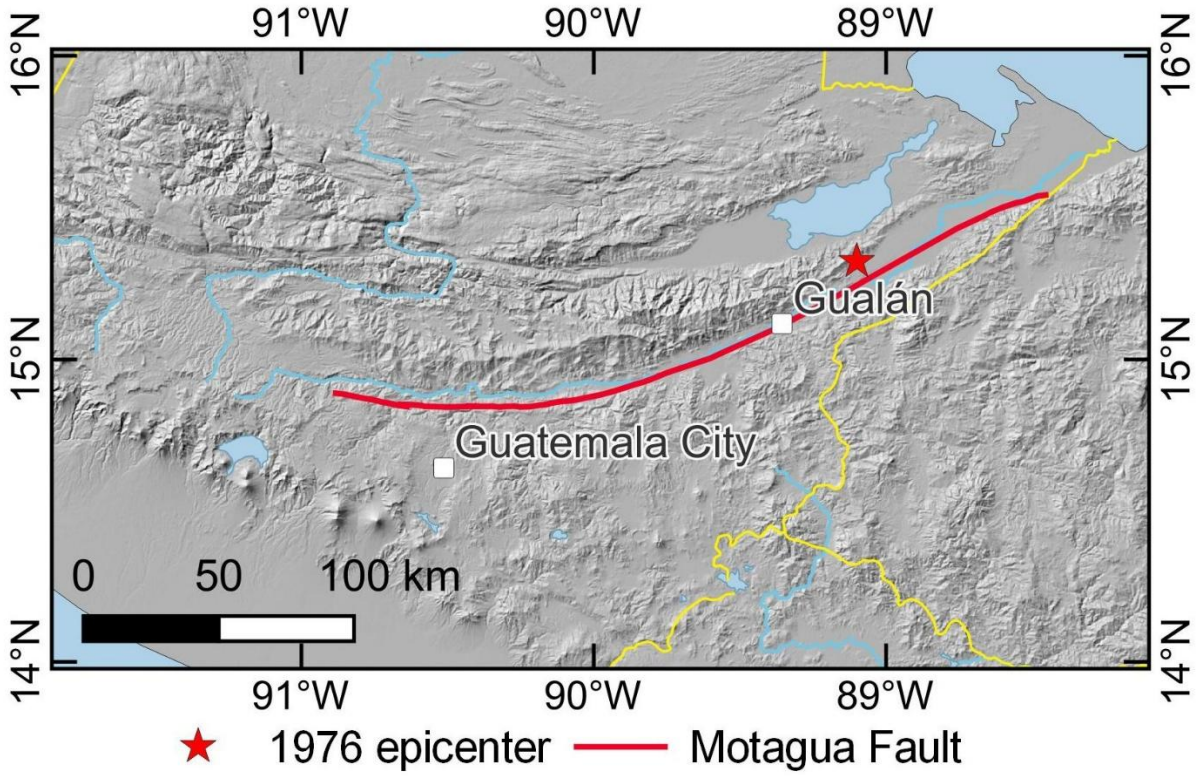

Figure 39: Location of the Gualán trench site.

The paleoseismic site is south of the Motagua River in the central Motagua Valley, approximately 35 km southwest of the 1976 earthquake epicenter. The regional LiDAR image (Fig. 39, 40) highlights the geomorphology of the Gualán area. The Motagua fault lies within lower hills and fluvial terraces that are bounded to the north and south by large mountain ranges. The fluvial terraces are composed predominantly of pumaceous alluvium that is reworked ignimbrites and tuff deposits interbedded with fluvial and alluvial fan deposits without primary ashfall tuffs (Johnson, 1984). The ridges within the Motagua valley are outcrops of the red sandstone and

conglomerates of the Subinal Formation that likely formed within pullapart basins in the early Tertiary (Donnely et al., 1990). The rocks of the mountains, both north and south of the Motagua valley, are schistose gneiss, mica schist, marble, and minor amphibolite that mark complex tectonic suturing events in the Paleozoic and the Cretaceous. Serpentinite within the fault zone (Bruekner et al., 2009; Harlow et al., 2004; 2025) may play a major in the Motagua Fault rupture history and seismic potential.

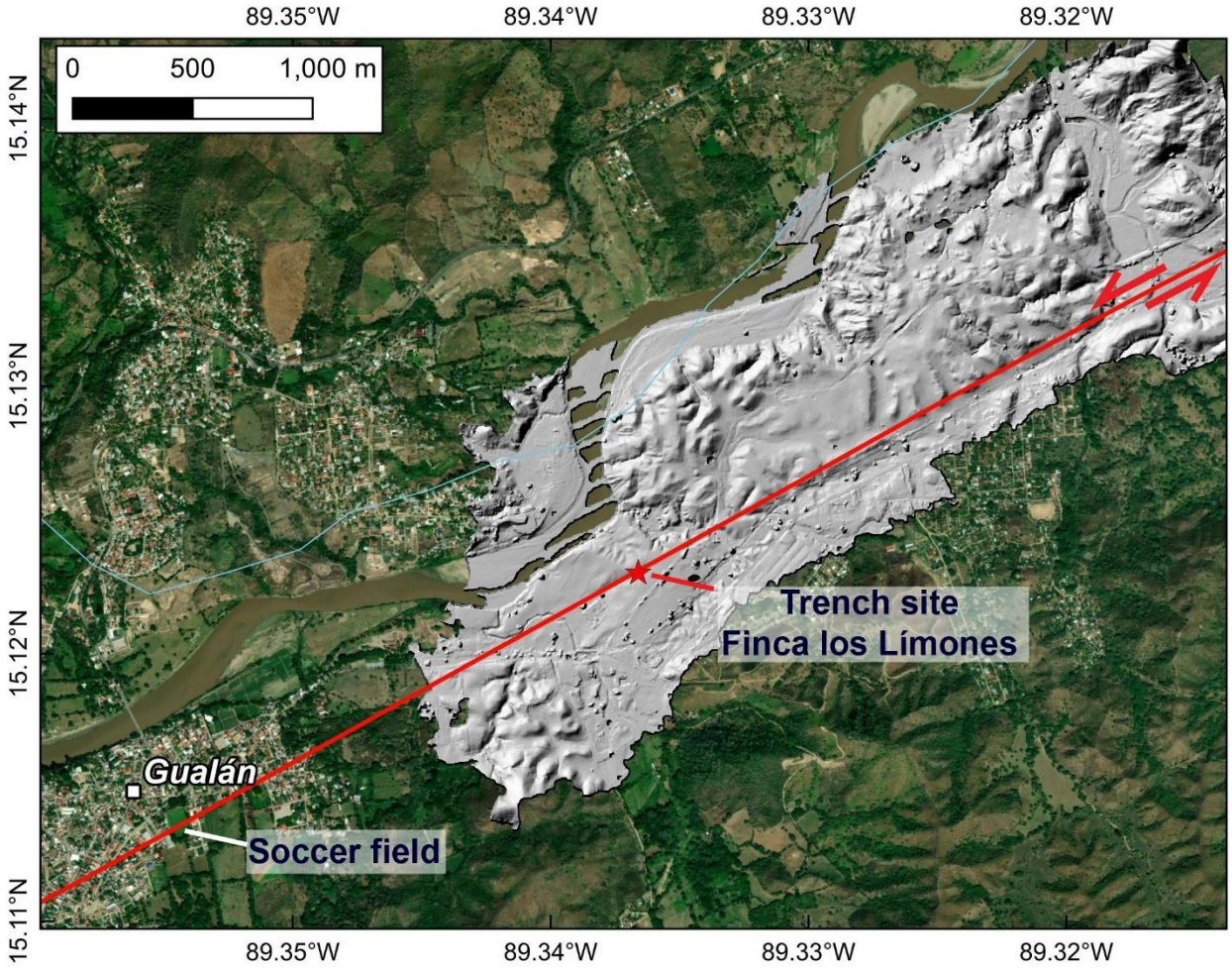

Figure 40: LiDAR DEM of the Gualán trench site.

The 1976 Earthquake at Gualán

The 1976 earthquake ruptured directly through the town of Gualán with a population, at the time, of nearly 23,500. Most of the buildings in Gualán sustained structural damage in the earthquake, and nearly 200 people died (Espinosa, 1976). The rupture crossed a soccer field, bent the railroad tracks, and crossed the cemetery to the west of town. Some of the most famous images of the earthquake are the fault rupture across the Gualán soccer field (Fig. 41). The moletrack formed *en echelon* fractures oriented 15° to 20° counterclockwise to the strike of the fault with small pressure ridges developed in between the right-stepping fissures. The width

of the zone of fracturing was 5 m or less. The sideline on the Gualán soccer field was offset by 89 cm (Plafker, 1976; Plafker et al., 1976). Only a gentle slope is still slightly visible along the fault trace (Figs. 41, 42).

Figure 41: (A) Scan of a 35 mm slide showing the en echelon pattern of the 1976 moletrack across the soccer field (Plafker USGS Archive). B) Photograph of the bent railroad tracks near the Gualán train station. C) Fault rupture through the soccer field in Gualán with photographs from 1976 shown above and from 2021 on the bottom. A slight slope marks the location of the rupture. D) Photograph of the ground rupture across the Gualán soccer field with a boy standing in the fissure (Marroquín & Gándara, 1982).

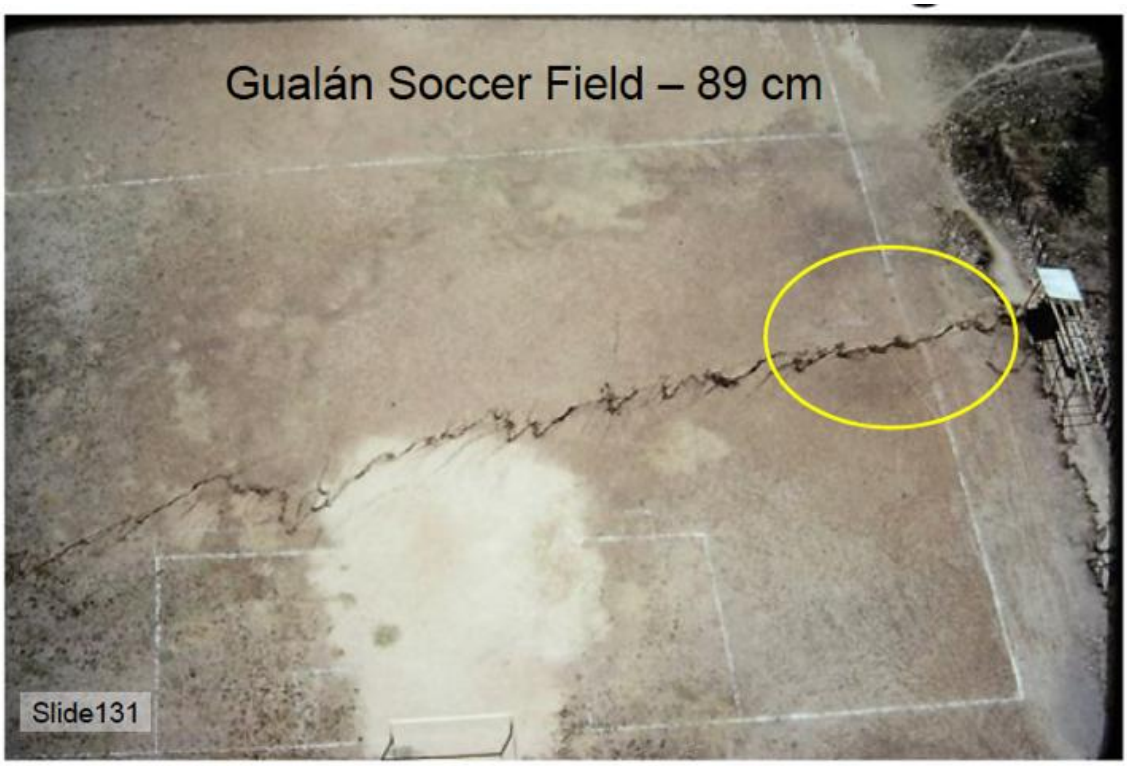

Figure 42: Oblique aerial photograph of the Gualán soccer field viewed northward showing the 1976 earthquake moletrack. A left-lateral offset of 89 cm was measured across the white sideline stripe (Plafker, 1977).

About 1.5 km east of the city at Finca Los Límones at our paleoseismic research site, the offset of the concrete-lined canal was measured as 93 cm (Plafker, 193). Figure 43 shows our relocation of the canal in 2021. In April 1976, a line of nail markers was placed as a reference along the canal, and new cracks developing along the ground rupture were documented. Bucknam et al. (1978) measured the offset of the Gualán canal and report three additional afterslip measurements approximately 100, 200, and 300 days after the earthquakes, with a maximum slip of 109 cm, including 16 cm of afterslip. Field notes from Plafker (USGS Archive) show an annotated sketch map of the canal from October 5, 1977, which states “could not re-locate all pins at canal. Measured offset ~30 cm…Canal last required patching about 6 months earlier…abundant new cracks visible with small sinistral offsets (~2 cm). Canal offset by alinement of edges is about 121 cm.” If this measurement is accurate, it represents an additional 12 cm of offfset more than reported in Bucknam et al. (1978).

Figure 43: Photograph of the concrete irrigation canal offset by slip of 93 cm of the Motagua fault in Finca Los Limones east of Gualán. Left, February 1976; Right, July 2021.

Using data from the 2023 RTK survey and orthophotos from UAS flights, we projected the straight edges of the canal to the 1976 fault rupture. Near the fault, the margins of the canal are rotated and dragged. From a straight projection 6 m from the fault, we measured 126-133 cm of total offset of the canal (Figure 44). Table 7 summarizes the offset measurements of the Gualán canal during various surveys in 1976 and 1977, and our new offset data. If we assume that afterslip is temporally constrained to a few years after the 1976 earthquake, then the additional 5-12 cm of slip may be attributed to creep. Given the 46 years between 1977 and 2023, the potential creep rate at this site ranges from 1.1 to 2.6 mm/yr.

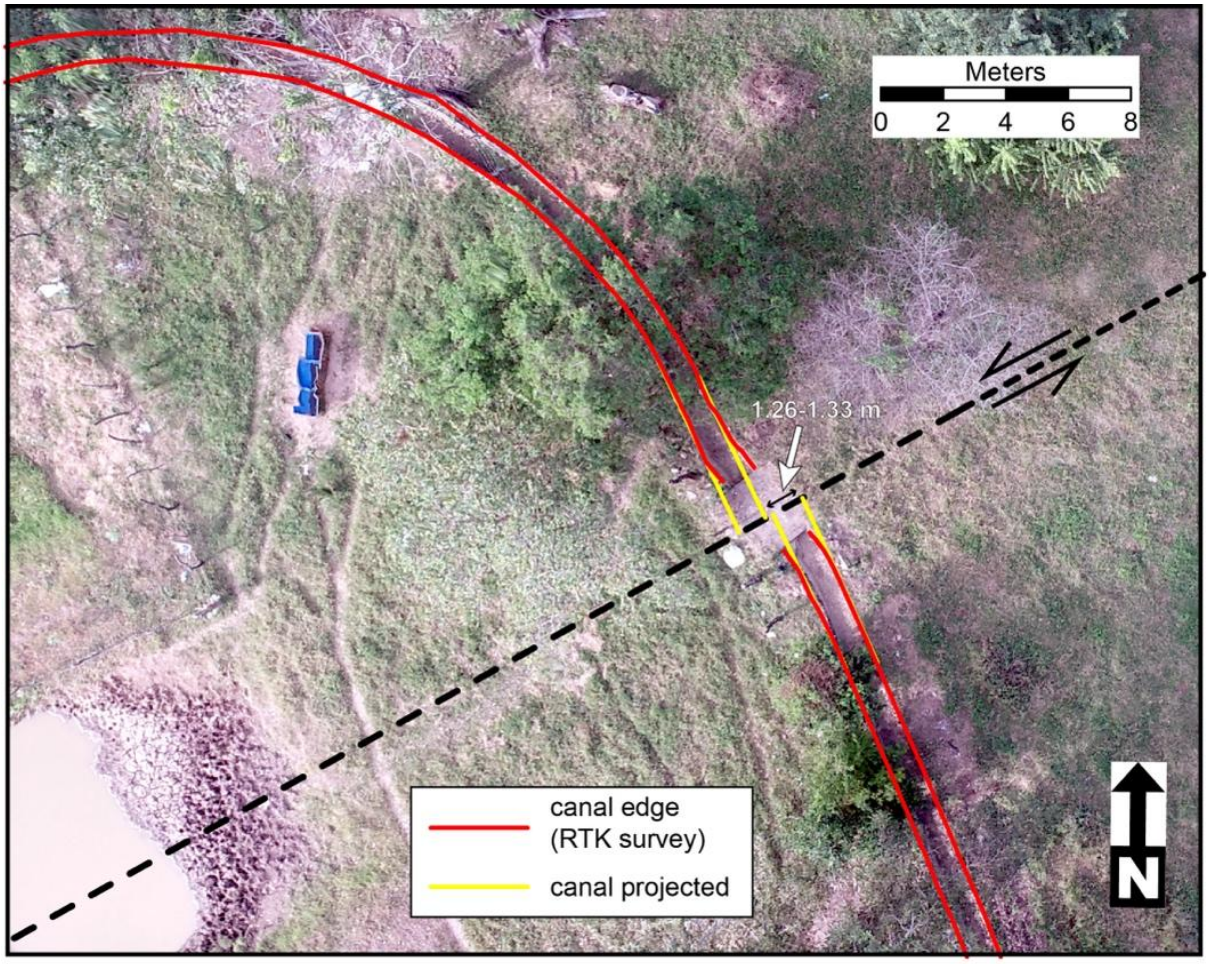

Figure 44: Orthophoto map and RTK survey along the concrete-lined canal with projections of the canal margins to the 1976 rupture trace of the Motagua fault and measured offsets.

Table 7: Offset measurements of the Gualán canal

Date	Days after EQ	Total offset (cm)	Slip Incr. (cm)	
Feb. 8, 1976	4	93		Afterslip
	74	104	11	Afterslip
	165	106	13	Afterslip
	268	109	16	Afterslip
Oct. 5, 1977	609	121	28	Afterslip
Jan. 8, 2023	17140	126	33	Creep?
	47 yrs	133	40	

Creep Rate?	Minimum	1.1 mm/yr
	Maximum	2.6 mm/yr

The Paleoseismic Data at Finca Los Límones (Gualán)

The Gualán paleoseismic research site is located 1.5 km east of the city at Finca Los Límones, south of the Motagua River, and just west of the offset canal (Fig. 45). The Motagua fault at the site crosses two fluvial terraces and recent alluvium. The upper, older terrace (Qft1) lies 3 m above the younger terrace (Qft2). The surface of Qft1 has cobbles and boulders. The stratigraphy of Qft1 is exposed in Trench 2 (T2) and Trench 3 (T3) and shows multiple cycles of graded sand-silt bedding with layers of carbonate nodules. The western margin of Qft1 has a curved erosional surface that marks the edge of the incised Qft2 terrace. This margin is offset by 42.3 m across the Motagua fault. The Qft2 terrace deposits were exposed in Trench 1 (T1) where the top of the section is silt that overlies a buried soil that contains cultural artefacts developed on a pebbly sand. A small modern drainage appears to be offset by 254 m. The age of the incision of Qft2 and the channel crossing should help determine slip rates at the site.

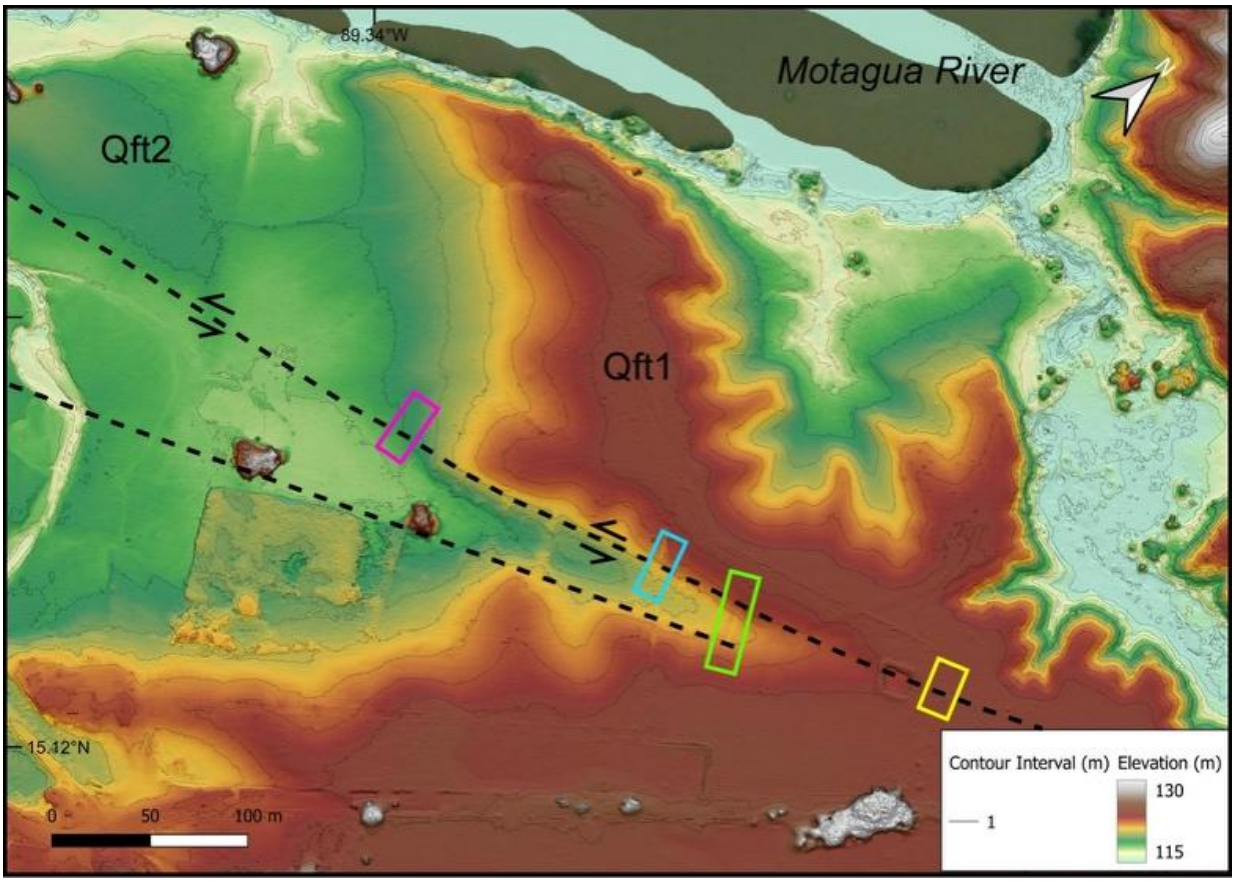

Figure 45: DEM map of the study site in Gualan based on LiDAR data collected in this study. The Motagua fault lies in a linear depression that offsets two fluvial terraces (Qft1 and Qft2). The paleoseismic trench sites are marked with rectangular boxes (T1=pink, T2=green, T3=blue). The location of the offset canal is marked by a yellow box.

The Motagua fault at the site is marked by a linear depression. A high, south-facing fault scarp is clearly marked across the site, but a more subtle north-facing scarp also lies along the depression, suggesting two strands of the fault. A 35 mm slide of the mole track at the site shows the *en echelon* right-stepping fractures of the rupture and upturned turf (Fig. 46). A seasonal natural sag

pond appears along the western end of the site. Cultural modifications include a dam across the sag and a recent (2022) pond on the fault, adjacent to the irrigation canal.

Figure 46: The ground rupture at the trench site photographed as a 35 mm slide on February 8, 1976 showing the location of the fault at the base of a south-facing scarp. View toward the west. (Plafker USGS Archive).

Electrical resistivity tomographic (ERT) data were collected along three lines across the 1976 earthquake rupture of the Motagua fault and parallel to two paleoseismic trenches (T1 and T2) at the Finca Los Limones site (Dollens, 2025). The ERT lines show a 20-m-wide zone of reduced electrical resistivity (10-50 Ωm) coinciding with the surface trace of the 1976 rupture (Fig. 9). This low-resistivity zone is interpreted as a structurally controlled topographic depression filled with water-saturated recently deposited sediments. Flanking regions exhibit higher resistivity (100-500 Ω m) characteristic of consolidated alluvial deposits. The fault zone displays asymmetric geometry with steeper southern margin and gentler northern slope, consistent with deformation along two strands of the fault and preferential erosion along the fault trace. Subsidiary fractures and secondary faulting extend 10-20 m from the principal displacement zone.

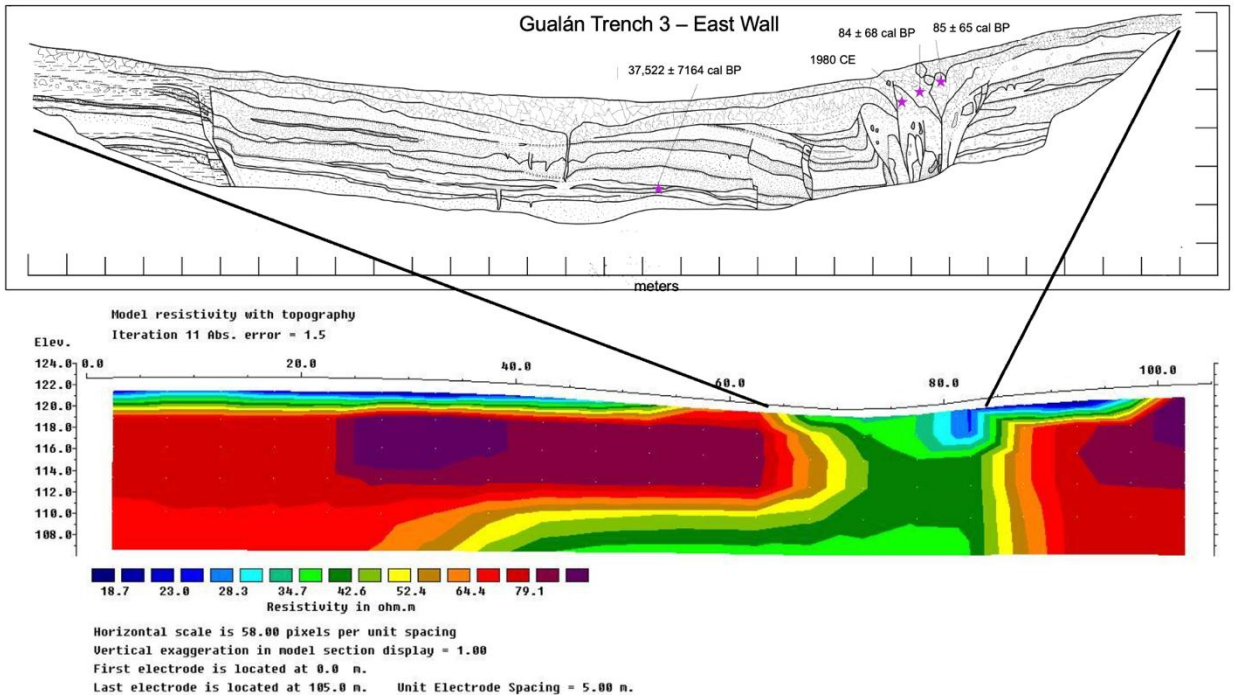

Figure 47: Trench log of the east wall of Trench 3 and ERT profile at the Finca Los Limones site in Gualán.

T2 and T3 (Figs. 45, 47), separated by only 21 m, both show the development of multiple inset large fissures filled with dark brown soil (Fig. 10). This area of distributed shear may be the manifestation of fault creep along *en echelon* fractures at the site.

Dating of the paleoseismic record at this site has been difficult due to a lack of radiocarbon samples. However, downwarping and folding of a buried soil surface, and the upward termination of faults and fissures suggest multiple pre-1976 earthquakes.

Figure 48: Photograph of the west wall of Trench 2 showing multiple, inset organic-rich fissures along the fault trace.

Summary

- Offset measurements of the straight margins of the concrete canal projected to the 1976 ground rupture of the Motagua fault at the Finca Los Limones site in Gualán show an additional 5-12 cm of offset since 1977. The additional slip may be evidence for fault creep along this segment of the fault.
- The Finca Los Limones site contains two fluvial terraces. A younger lower terrace (Qft2) is inset into the upper, older terrace (Qft1). The erosional west boundary of the Qft1 terrace is left-laterally offset by about 42 m. Furthermore, a channel incised into the Qft2 terrace surface appears to be offset by about 250 m. Determination of slip rate at the site may be possible with age modeling.
- ERT data across the Motagua fault at the site show a 20-m-wide low velocity zone that corresponds to a linear topographic valley marked by the 1976 earthquake ground rupture to the north and a subsidiary fault on the south.
- Paleoseismic trenching
- Character of the fault zone fissure may be evidence for fault creep.

Pre-meeting Field Trip Day 3 – La Laguna Quarry and Road Outcrop

Mario Sagüí, Tina Niemi, Sergio Moran-Ical, Christoph Grützner, Peter Frenzel

Objectives

- View the deformation within a bedrock ridge within the Motagua fault valley
- Examine faults and Quaternary sediments deposited in an inverted pull-apart basin

Local setting

The road to the La Laguna outcrop and trench site leads through the town of El Conacaste. West of the town, a concrete road built by Cementos Progresso leads to La Laguna. The Cementos Progresso San Miguel Mine, as well as Volcan de Agua, Fuego, and Acatenango (on a clear day), can be viewed from the high point of the road. The road then descends north and west into the La Laguna Valley. Cementos Progresso has limestone operations within the valley.

In the La Laguna valley, the bedrock exposed in outcrops is predominantly brecciated Early Cretaceous limestone with fault slices of coherent limestone. The bedrock is covered or abutted by volcanic tuff, colluvium, and alluvial deposits. The 1976 rupture of the Motagua fault is south of faults exposed in the roadcut and quarry (Fig. 49)

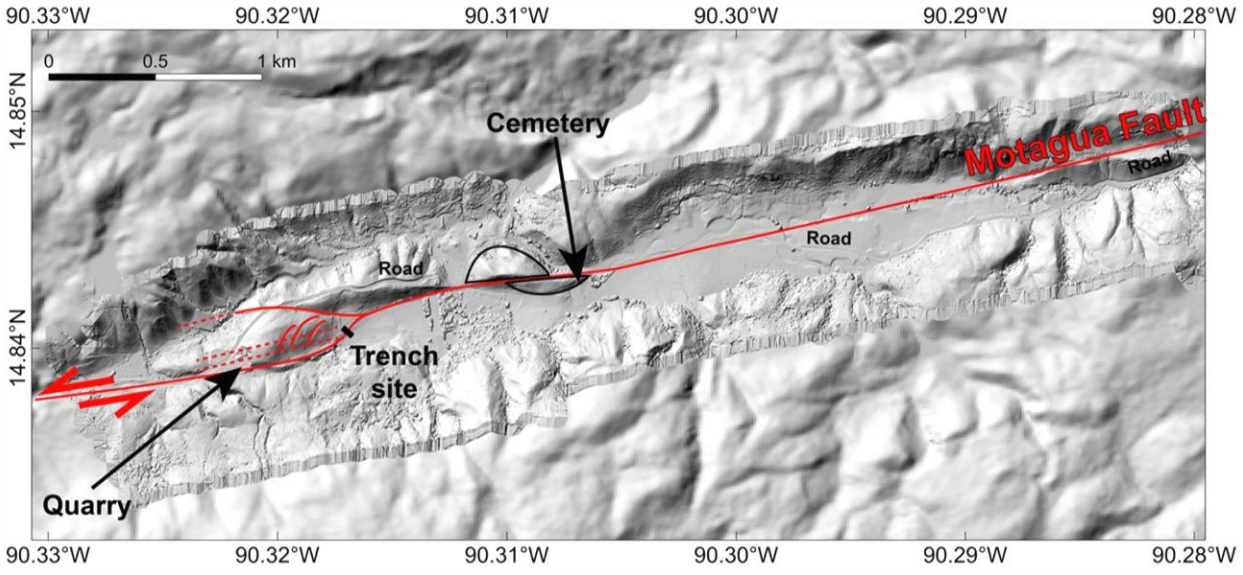

Figure 49: LiDAR map showing the location of the quarry and faults in the road outcrop.

Quarry

The limestone quarry exposes a complexly faulted and brecciated section (Fig. 50). The core of the ridge consists of a highly weathered, orange-stained, and fractured limestone bedrock, that is flanked by gray brecciated limestone and capped by a calcareous matrix-rich colluvium. Steeply dipping faults cut the outcrop. Along the southern margin, a series of faults appears to be younger as they cut to the top of the section and are filled with soil and breccia. These faults have apparent down-to-the-south separation, suggesting extension toward the location of the 1976 Motagua fault rupture.

The exposed Early Cretaceous limestones of the Cerro el Virgen Group have experienced multiple pulses of tectonism, including earlier convergence and translation along the Motagua fault zone. The ridge has been tectonically uplifted as seen by the basinal sediments in the adjacent road outcrops.

Figure 50: Highly brecciated and faulted exposure of Early Cretaceous Limestone.

Road outcrop

Outcrops along the road west of La Laguna expose a lower section of predominantly red conglomerates and paleosols and an upper section of brown muds, conglomerates, and white calcilutites. The lower clastic and upper calcareous sections are topographically separated by a saddle marking a fault zone. However, the lower red conglomerate section terminates in calcareous conglomerates, suggesting a stratigraphic connection as the base of the basinal deposits. The basinal sediments likely overlie brecciated limestone colluvium, although this contact is not clearly exposed in the roadcut.

The age of the basin fill sediments is not known, but is likely Quaternary or possibly Neogene. An OSL sample was collected from one of the only sandy layers at the base of the easternmost section, but the sample is still being processed.

The western end of the upper calcareous section exposes the continuation of brecciated limestone bedrock from the quarry face and is in fault contact with the upper calcareous section (Fig. 51). The upper calcareous section includes bioturbated brown muds interbedded with white calcilutite deposited in low-energy swamps. Ostracods from the calcilutite confirm standing

water in a low-lying basin. Layers of matrix-supported, boulders denote high-energy debris flows. These layers are interbedded in cycles with periods of paleosol development.

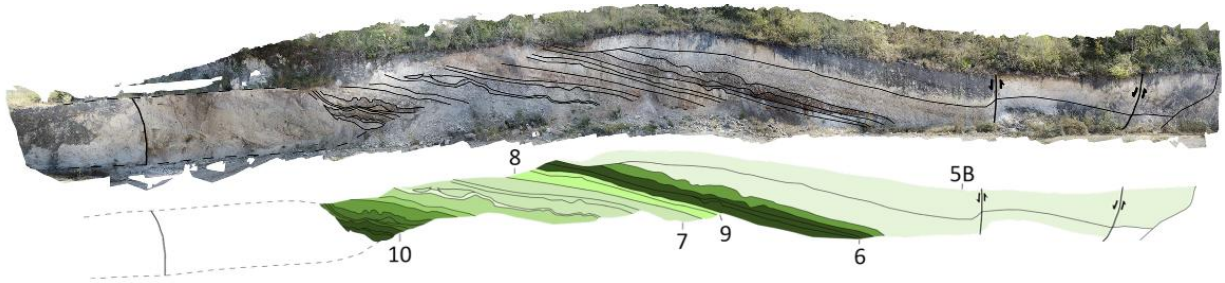

Figure 51: Stratigraphic section of the upper calcareous section.

Figure 52: Fault zone at the base of the upper calcareous section.

The base of the calcareous section is marked by a prominent strike-slip fault zone with several fault strands (Fig. 52). The fault is subparallel to the road and thus complicates the stratigraphic outcrop pattern. Horizontal to sub-horizontal slicken lines show that this is a strike-slip fault parallel to the recently active Motagua fault.

East of the calcareous section, the red conglomerates dip toward the west. The section includes interbedded horizontally bedded conglomerates and debris flows intercalated mud layers and red clay-rich paleosols with root casts penetrating downward (Fig. 53). At the western end of the outcrop and across the upper section, narrow channels incise several meters into the lower red conglomerates. The red conglomerates were deposited in an alluvial fan and braided stream environment with periods of landscape stability. The incised channels denote a period of uplift and incision as the basin changed from phases of aggradation to degradation. The base of the red conglomerates is marked by an anticline.

Figure 53: View east of the lower red conglomerates.

Summary

- A road outcrop west of the village of La Laguna exposes a sedimentary sequence deposited in a basin.
- The exposed stratigraphy includes a lower section of alluvial fan conglomerates intercalated with paleosols containing abundant rootcasts. The upper section consists of matrix-supported boulder debris flow conglomerates and brown mud intercalated with calcilute, which we interpret as the basin depocenter. Ostracods and rootcasts suggest swamps and shallow lakes. Both sequences denote pulses of rapid deposition and periods of quiescence, likely due to changes in the rate of fault motion in a subsiding (aggrading) basin.
- The basinal sediments have been uplifted as part of the margin of a ridge that is cored by Early Cretaceous brecciated limestone bedrock and overlying colluvium.
- Anticlinal and synclinal folding of the basinal sediment and strike-slip displacement indicate transpression.

Pre-meeting Field Trip Day 3 – La Laguna trench site

Christoph Grützner, Tina Niemi, Aleigha Dollens, Hannes Ebell, Jeremy Maurer, Paco Gomez, Omar Flores, Carlos Perez, Jonathan Obrist-Farner, Luis Romero

Objectives

- Examine field evidence for past earthquakes
- Visit the traces of the 1976 ruptures and offsets in both landscape and walls
- Understand the interaction between anthropogenic landscape use and trenches

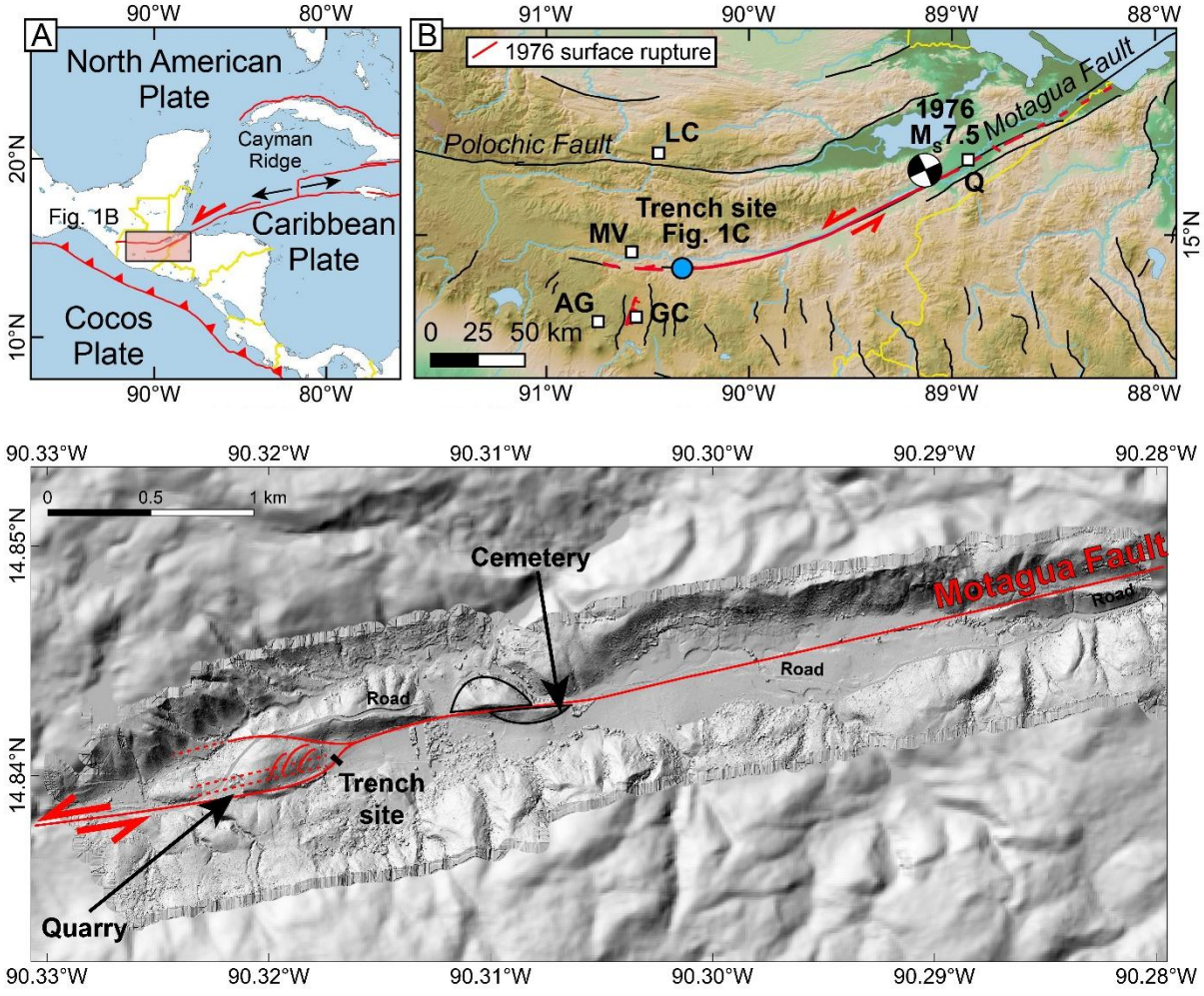

Fig. 54: Tectonic setting of the La Laguna Basin. (A) Tectonic setting of the North American-Caribbean-Cocos plate boundaries in Central America. (B) Motion of the North American-Caribbean transform plate boundary is accommodated on the Motagua and Polochic faults. The 1976 M 7.5 earthquake ruptured 240 km of the left-lateral, strike-slip Motagua fault and a portion of the N-S trending Mixco Fault (both marked with a red line). The location of the epicenter is shown with a moment-tensor solution. GC=Guatemala City, AG=Antigua Guatemala, MV=Mixco Viejo, Q=Quirigua, LC=Lake Chichój. The La Laguna Trench site is marked with a blue circle.

Local setting

The La Laguna Basin is a linear valley formed along the Motagua Fault approximately 150 km west of the 1976 earthquake epicenter (Fig. 54). The valley is bordered on the north and south by highly fractured Cretaceous limestone bedrock. Fluvial terraces, colluvial scree slopes, alluvial fans, and terraces of tuff from major volcanic eruptions, including the 79.5 ka supervolcanic event of Los Chocoyos, abut the bedrock within the La Laguna Basin.

The 1976 Earthquake at La Laguna

Aerial and ground photographs, 35 mm slides, and field notes from the collection of George Plafker (USGS Archive), who documented the La Laguna site on April 20, 1976, show the location and nature of the 1976 earthquake ground rupture (Fig. 55). On average, the horizontal surface slip in 1976 was only about 1 m. The largest horizontal offsets were found at La Laguna. Plafker's data show the offset of stone walls and a tree line that is offset by 3.25 m here (Figs. 56, 57). The vertical slip component of the offset in Wall 1 was measured as 83 cm in 1976 (Figs. 57, 58).

Fig. 55: Oblique aerial photo from the original 35 mm slide #648 (George Plafker USGS Archive) showing the surface rupture marked with red arrows at La Laguna. Our trench site is located within the area of trees. The view is toward the north.

Fig. 56: Ground photo from the original 35 mm slide #641 (George Plafker USGS Archive). The tree line is offset by 3.4 m.

Fig. 57: Field photo from the original 35 mm slide #646 (George Plafker USGS Archive) showing the offset wall 1 at La Laguna (red arrows). The view is toward the south.

Fig. 58: Field photo from the original 35 mm slide #644 (George Plafker USGS Archive) showing the surface rupture and offset of wall 1 measured on April 20, 1976 as 340 cm of left-lateral strike slip and 83 cm of vertical slip. The view is toward the north.

Pre-1976 earthquakes from preserved offsets

Our high-resolution digital elevation models of the La Laguna site, produced from two uncrewed aerial vehicle laser scanning campaigns, capture the location of Wall 1 (offset measured as 3.4 m in 1976) and Wall 2 (offset not measured in 1976). Measurements taken during our research (Fig. 59) indicate an offset of 4.8 m for Wall 2, which we interpret to be the cumulative offset from 1976 (3.4 m) and the penultimate event (1.4 m), see Figs. 59 and 60.

The present-day 120 cm-high fault scarp also records slip in a prior earthquake: 83 cm in 1976 plus another 37 cm prior to that (Fig. 59).

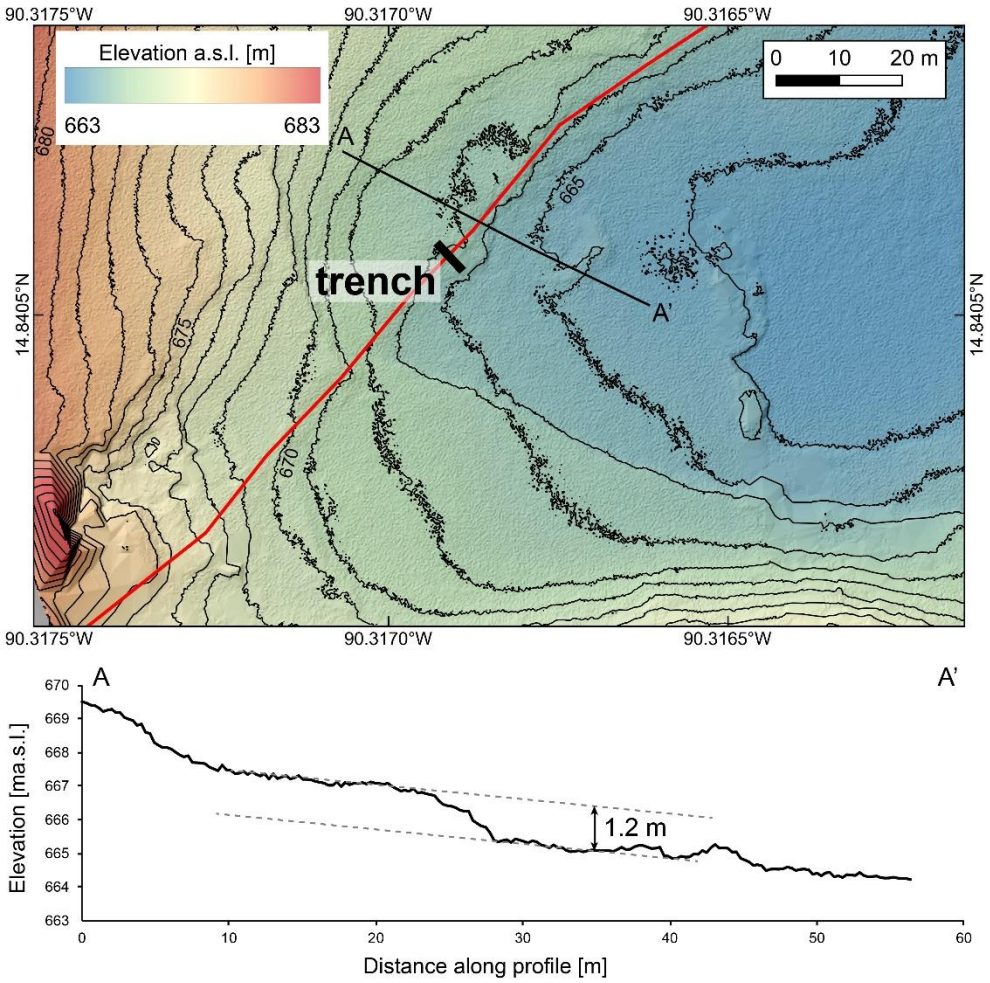

Fig. 59: Detailed topographic map of the trench site. The elevation model has a resolution of 25 cm and was produced using a drone with a mounted laser scanner. Vegetation was filtered out and the digital ground model is shown here. The contour interval is 1 m. The lower panel shows an elevation profile across the 1.2 m-high scarp.

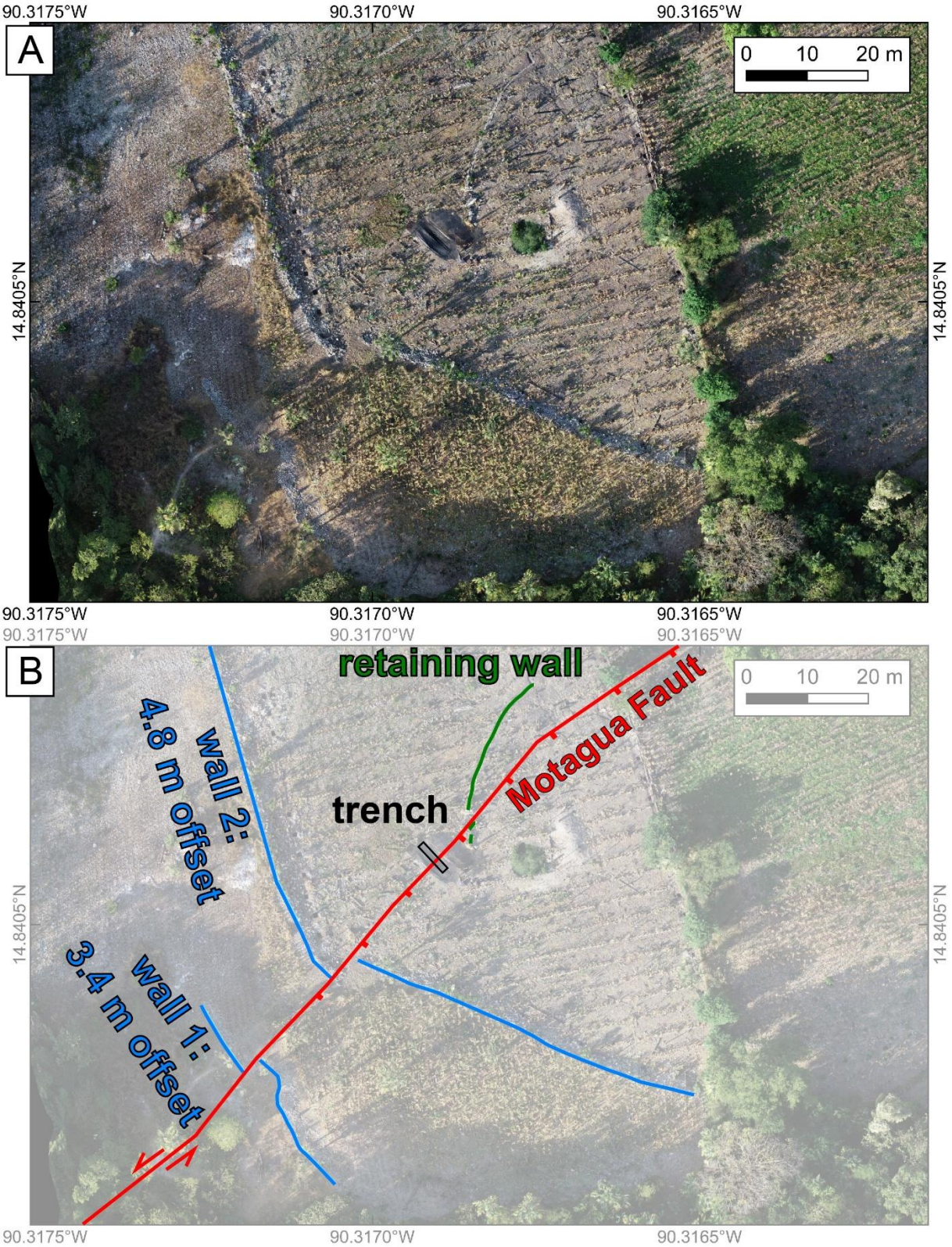

Fig. 60: (A) Drone orthophoto of the trench site. (B) Semi-transparent orthophoto of the trench site with the location of the fault (red), the two offset walls, and the deformed retaining wall. Red ticks mark the scarp with ticks on the downthrown side.

Paleoseismic trenching

The La Laguna paleoseismic trench was hand-dug adjacent to offset Walls 1 and 2 and across a ruptured segment of the 1976 Motagua Fault that bends toward the south across a terraced agricultural field (Figs. 54, 60). The left bend in this sinistral strike-slip fault creates a component of extension that, along with lateral slip, causes the southern block to subside during earthquakes. This creates a fault scarp where degradation of the upthrown side (footwall) provides sediment to the downthrown side (hanging wall), where it will form a colluvial wedge at the base of the newly formed fault scarp as shown in the trench log (Figs. 61, 62).

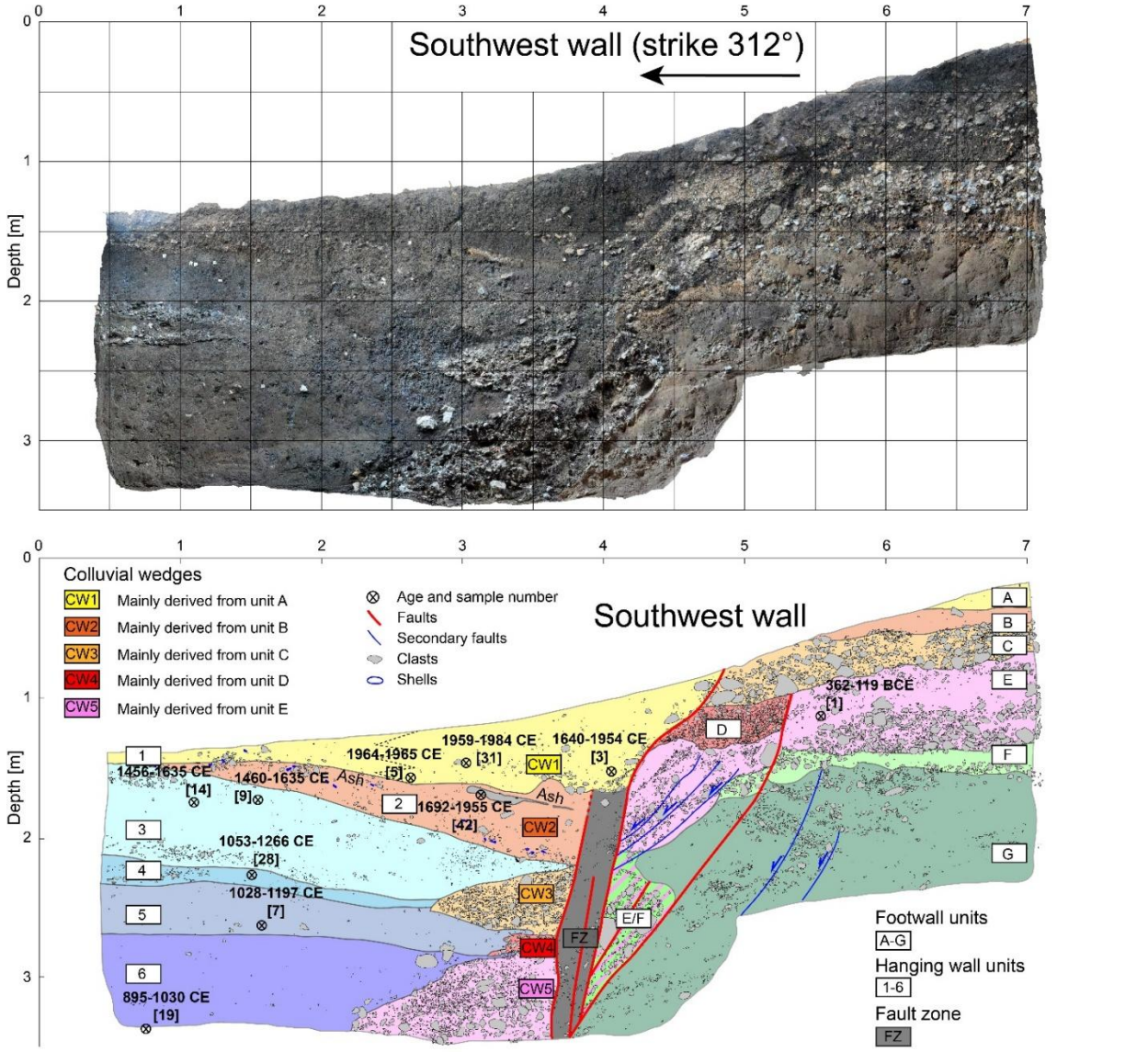

Fig. 61: Orthophoto and detailed log of the northeast and southwest walls of the trench with calibrated radiocarbon ages. Units A-G are on the footwall and Units 1-6 on the hanging wall across the active trace of the Motagua fault. Colluvial wedges (CW) on the hanging wall were deposited in five scarp-forming earthquakes. Numbers near sample locations indicate ages and sample numbers (in brackets) as shown in Fig. 63.

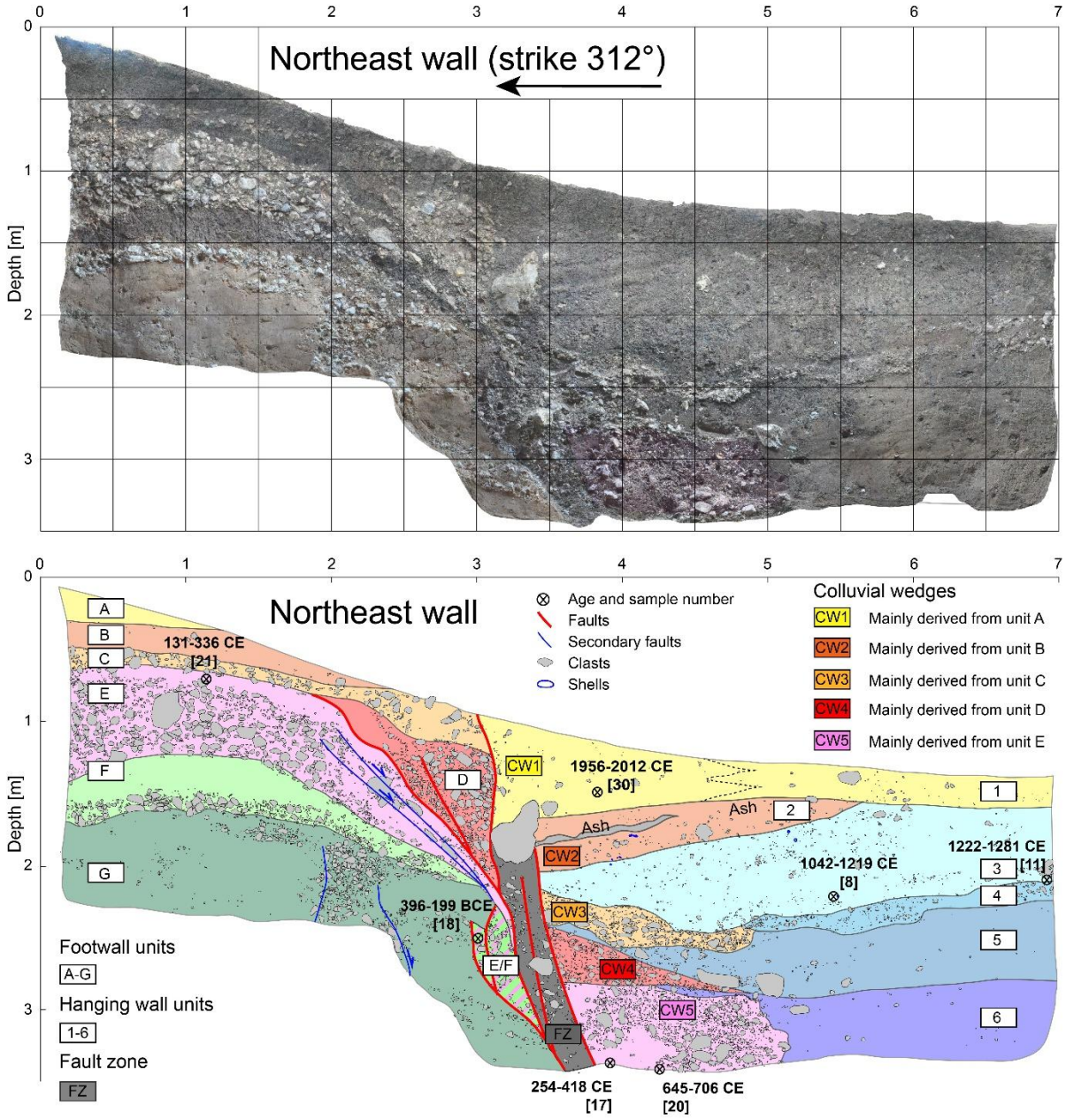

Fig. 62: Orthophoto and detailed log of the northeast and southwest walls of the trench with calibrated radiocarbon ages. Units A-G are on the footwall and Units 1-6 on the hanging wall across the active trace of the Motagua fault. Colluvial wedges (CW) on the hanging wall were deposited in five scarp-forming earthquakes. Numbers near sample locations indicate ages and sample numbers (in brackets) as shown in Fig. 63.

The oldest unit (Unit G), exposed exclusively in the footwall of the trench, is composed of yellowish brown, sandy silt with gravel interbeds and lenses deposited in the floodplain of an older fluvial terrace phase within the valley (Figs. 61, 62). Unit G is capped by a brown silty clay and cobble-sized gravel (Unit F) that is also only exposed on the north side of the trench. The upper stratigraphic units, Units A-E on the north side of the fault and Units 1-6 on the south side, all contain cultural debris, indicating that the valley had been converted to agricultural

fields and was inhabited and under cultivation. These anthropogenic units show evidence of five discrete earthquake ruptures and fault-scarp forming events.

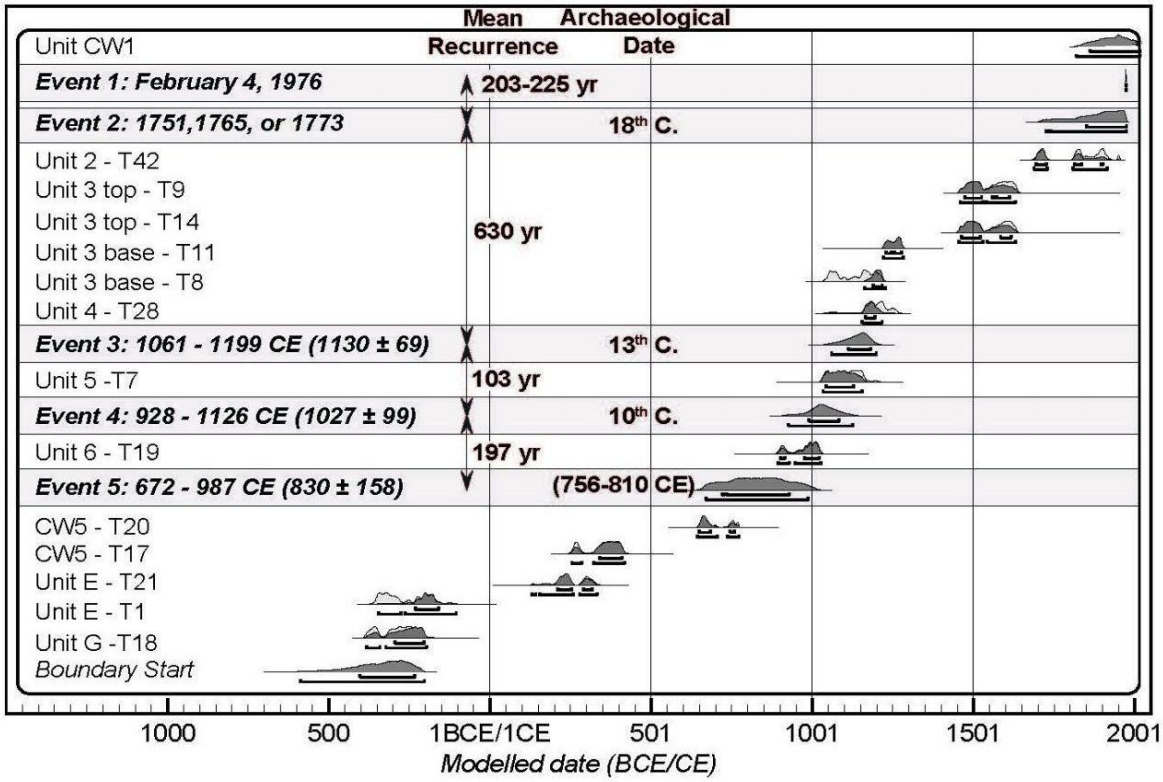

Fig. 63: OxCal age model and mean earthquake recurrence. In addition to the documented 1976 rupture, archaeological data indicate that earthquakes likely occurred on the Motagua Fault at the La Laguna site in the 8th, 10th, 12th, and 18th centuries.

The ground surface at the time of the oldest earthquake (Event 5) was a black anthropogenic, organic-rich soil overlying a cobble-sized gravel (Unit E). Unit E, containing obsidian flakes, projectile points, charcoal, and pottery sherds, is redeposited on the hanging wall at the base of a paleo-fault scarp in a colluvial wedge (CW5). Radiocarbon dating within Unit E and CW5 indicate that Unit E developed between the 3rd century BCE to the 7th century CE. Unit E is sheared by secondary faulting across the scarp. Given the long interval of human occupation indicated by Unit E and the very thick colluvial wedge, CW5 may represent deposition in more than one earthquake. Furthermore, mixing of Units E and F within a fault-bound fissure on the footwall suggests rupture in an earlier event. Given the limitation of trench depth, we can only constrain the latest scarp-forming earthquake involving colluvial wedge CW5. Pre-event ages are constrained by charcoals T17 and T20 from CW5 and by samples T1, T18, and T21 from the footwall unit E (Figs. 61, 62). The post-event age comes from charcoal T19 from the base of Unit 6, which is a fine-grained, brown silt and clay layer that overlies the CW5 scarp-derived colluvium. Thus, Event 5 occurred between 672-987 CE (830 ± 158 CE) (Fig. 63).

A unique clast-supported, well-sorted subangular to subrounded pebble- to small cobble-sized limestone gravel (Unit D) rests unconformably on the fault scarp of Unit E and is in contact with it at the fault. Unit D is not a natural deposit but anthropogenic in origin, likely the remnants of a stockpile of quarried limestone gravel used in lime production (Seligson et al., 2019). Unit D was faulted and dragged down across a scarp in Event 4 and then deposited at the base of the scarp in colluvial wedge CW4. The stratigraphic position of charcoal in Unit 5 overlying CW4 and the age model for older units suggests that Event 4 occurred between 928-1126 CE (1027 ± 99 CE).

Continued slope wash deposition or debris from additional construction of cobble terrace walls produced the silty gravel of Unit C that contains freshwater *Pachychilus* species gastropods. Unit C, which was the ground surface at the time of Event 3, thickens on the footwall and is redeposited as colluvial wedge CW3. Radiocarbon dates from within the dark brown clayey silt and pebbly gravel of Units 3-4 above CW3 constrain Event 3 to 1061-1199 CE (1130 ± 69 CE).

Evidence for the youngest two earthquakes (Event 1: 1976 and Event 2) exhibits a distinct sedimentologic pattern as compared to the fault scarp-derived colluvial wedge gravels of the older earthquakes. The relatively thin, clayey and silty layers in the footwall (Units A and B) are exposed and actively eroding across the degrading 1976 fault scarp. Layers in the hanging wall (Units 1 and 2) are predominantly fine-grained and are back-tilted toward the fault. The new style of sediment deposition denotes a change in landscape management or other environmental/climatic factors.

While gravel was present at the ground surface during older earthquakes, the penultimate earthquake (Event 2) occurred when fine-grained sediments of Units A and B in the footwall and Unit 2 in the hanging wall were at the land surface. Deposition below the fault scarp includes a northward thickening colluvial wedge CW2, which is composed of redeposited Unit A and B soil. Subsidence of the down-dropped block allows fine-grained sediments to fill a fissure along the fault, which contains Pachychilus gastropods from units A, B, and 2. The stratigraphic data for Event 2 show that sedimentary layers in Unit 2 were faulted in an earthquake that pre-dates 1976, as the faulted sediment underlies the colluvium formed by the 1976 earthquake. Age modelling of faulted Unit 3 and overlying ash from an anthropogenic burn in Unit 2/CW2 constrains Event 2 to 1728-1976 CE.

The 1976 fault cuts the full stratigraphic sequence in the trench and intersects the ground surface (Figs. 61, 62). The footwall units A, B, and C, which once formed a vertical, free-face scarp, have eroded and retreated northward to expose the units along a slope. A boulder sits upright within the 1976 fault fissure at the base of the fault scarp on the NE trench wall. A thick organic-rich, fine-grained sediment forms the colluvial wedge CW1 that developed above a pebble-sized gravel draping the base of the scarp on the SW wall. Radiocarbon analyses of

samples yield modern, post-bomb dates and mixed older carbon, placing the deposits as those after the 1976 earthquake.

Discussion – earthquake timing from archaeology

Yesterday, we have seen and discussed evidence for earthquakes at **Quirigua**. This included external buttresses and internal benches that were added as structural supports (Morley, 1935; Sharer, 1990). These data suggest an earthquake may be bracketed at Quirigua between 756 and 810 CE, when it was prospering. Our earthquake Event 5, with a modelled age interval of 672-987 CE, falls within this period, suggesting that Event 5 may have occurred during the late 8th or early 9th century CE.

The final occupation at Quirigua is marked by a sudden structural collapse that trapped two victims in rubble (Ward & Rice, 2022). These data corroborate the timing of an earthquake likely in the 10th century CE, which could correspond to Event 4 at La Laguna in the interval of 928-1126 CE.

Corroborative archaeological data from **Mixco Viejo** (*Chwa Nima Ab'äj)*, a highland Postclassic Maya site 35 km west of La Laguna, may further support the paleoseismic record. Excavation data (Lehmann, 1968; Fauvet-Berthelot, 1986) show three phases of the monumental platform construction with the first phase built of carved pumice blocks. It is not clear when the initial construction of Mixco Viejo began, but the first massive retaining wall was radiocarbon dated to the 13th century CE4. This construction may have been in response to a major earthquake on the Motagua Fault that likely correlates to our Event 3 (1060-1199 CE). Mixco Viejo was abandoned after it was conquered by the Spanish in the 1520s. In summary, earthquake Event 3 (1061-1199 CE) occurred when the Maya sought fortification in isolated hilltops for defensive purposes.

Discussion – earthquake timing from historical sources

Historical documents provide further constraints on the La Laguna paleoseismic record. The penultimate event is constrained by our paleoseismic data to later than 1728 CE (Fig. 64). As historical records of earthquakes since Guatemalan independence in 1821 CE are relatively complete, the penultimate earthquake is thus likely to have occurred sometime during the Colonial Period (White, 1984; Peraldo & Montero, 1999; White et al., 2004). We used the MARCA-GEHN v2.0 macroseismic database (Peruzza et al., 2021, 2023) to output macroseismic data point (MDP) maps for major earthquakes that may have ruptured the Motagua Fault in the Colonial Period (1717, 1733, 1751, 1765, and 1773 CE) and compare them to the intensity map for the 1976 earthquake (Fig. 64).

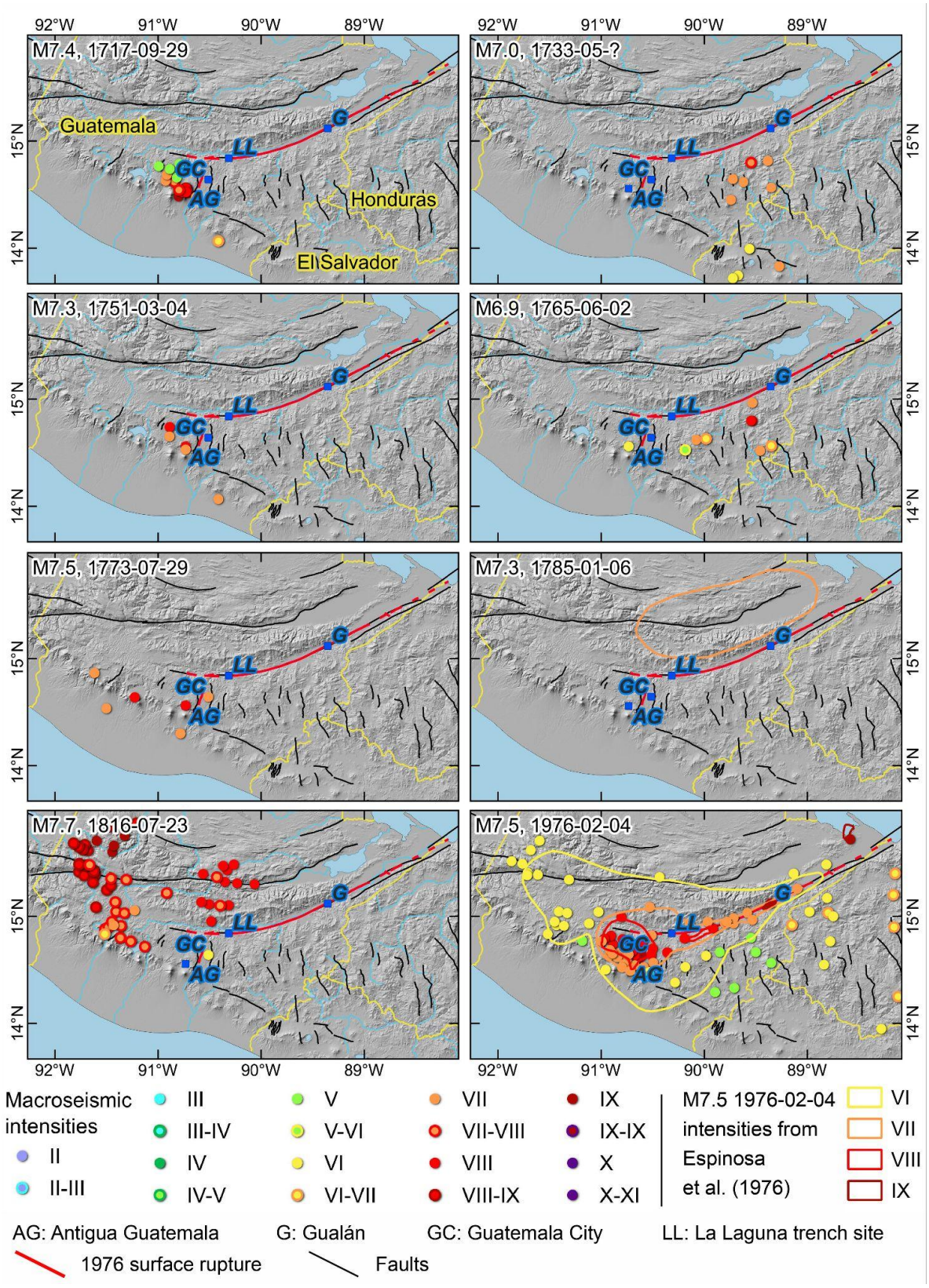

Fig. 64: Macroseismic intensities for historical earthquakes in Guatemala from the MARCA-GEHN V2.0 Database (Peruzza et al., 2021, 2023). Clear subduction events are excluded.

Maximum shaking intensity for the 1976 CE earthquake occurred along a narrow zone parallel to the Motagua Fault and in a broader region to the west of the rupture end. This demonstrates that the area of intensity for the 1976 Motagua Fault earthquake is similar in size to ruptures that White et al. (2004) assigned to subduction zone earthquakes. We suggest that a historical earthquake assigned to a subduction zone source may have actually originated on the Motagua Fault.

The MDP maps for the earthquakes of 1751 CE (M 7.3) and 1765 CE (M 6.9) are consistent with the isoseismal map (Fig. 64) of the 1976 CE event, although the 1765 CE earthquake has been assigned to a graben structure south of the Motagua Fault. We also consider 1773 CE as a candidate for rupture of the Motagua Fault. White et al. (2004) estimate the magnitude of the July 29, 1773 earthquake as M 7.5 and of the December 13, 1773 event as M 7.1. Either of these could be a candidate for Event 2. Very few macroseismic data points are available for all of these historical events, which leads to a large uncertainty in the epicentral locations and the potential magnitudes of the events. Also, the historical sources are very likely biased towards large cities and cities with colonial importance or Spanish population.

Discussion – earthquake timing from geological archives

Analyses of sediment cores from Lake Chichój near the Polochic Fault show that the 1976 earthquake shook the basin with great enough force to generate a seismically-triggered turbidite (Brocard et al., 2014). Nine additional seismically-induced turbidites were discovered in the lake cores (Brocard et al., 2016). Based on a published age model, four of the turbidites occurred between 750-900 CE in the Maya Late Classic Period, and five occurred between 1000-1450 CE during the Maya Postclassic Period. Our on-fault data for the Motagua Fault at the La Laguna site show clear evidence of three earthquakes during the 8th-12th centuries, which could have caused three of the older seismic turbidites in Lake Chichój, increasing confidence in both datasets. However, our Event 2 in the 18th century is not recorded as a seismoturbidite. Offset data at La Laguna indicate that Wall 2 was offset by a total of 4.8 m, suggesting that the penultimate earthquake (Event 2) had a lateral coseismic slip of 1.4 m, significantly less than the 3.4 m offset in 1976. Because of the lower coseismic slip documented for Event 2, it is likely that either the magnitude was lower or the rupture dynamics were different from the 1976 earthquake. For example, the 1733 earthquake likely had a magnitude of c. M 7.0, which means it released probably only ⅛ of the energy of the 1976 CE event. It is possible that the lower coseismic slip of 1.4 m resulted in less intense shaking in Lake Chichój compared to 1976, not exceeding the intensity threshold required to generate an event deposit. This also implies that caution is required when interpreting the archaeological records, because a smaller, but locally destructive earthquake may not have ruptured the whole fault. A recent study on lake

paleoseismology in Guatemala also sheds light on directivity effects in large earthquakes and their associated turbidites (Obrist-Farner et al., 2025).

Discussion – earthquake recurrence intervals

The average earthquake repeat time is 247-326 years (Fig. 63). However, the recurrence interval between two consecutive earthquakes is variable. The last two events happened ~100-225 years apart from each other, while more than 600 years lie between events E2 and E3. Looking at the entire plate boundary system, a complication with recurrence estimates is that the Motagua Fault is not the only structure accommodating the eastward motion of the Caribbean Plate. The Polochic Fault is seismogenic and lies parallel to the Motagua Fault, 40 km to the north (Fig. 59). White (1985) convincingly shows that the 1816 earthquake ruptured the western portion of the Polochic Fault. The earthquake damage zone of the 1785 earthquake also appears to suggest that this event ruptured the eastern Polochic Fault (Fig. 64). The long periods of seismic quiescence on the Motagua Fault could be the result of temporal switching of major seismic activity between major structures of the plate boundary or different segments of the Motagua Fault rupturing independently. This indicates that the plate boundary may not maintain constant behavior between earthquake cycles and that studying a single location on the complex Polochic-Motagua Fault System may not reveal overall system behavior.

References and further reading

- Bevan, B. & Sharer, R. J. (1983). Quirigua and the earthquake of February 4, 1976. In: Sharer, R. J., Schortman, E. M., & Urban, P. A. (Eds.) Quirigua Reports Volume II. University Museum Monograph 49, The University Museum, Museum of Pennsylvania, Philadelphia, 110-118.
- Brocard, G., et al. (2014). The recording of floods and earthquakes in Lake Chichój, Guatemala during the twentieth century. Journal of Paleolimnology, **52**, 155-169.
- Brocard, G., Anselmetti, F. S., & Teyssier, C. (2016). Guatemala paleoseismicity: from Late Classic Maya collapse to recent fault creep. *Scientific Reports*, **6**(1), 36976.
- Brueckner, H.K., et al. (2009). Metamorphic reworking of a high pressure-low temperature mélange along the Motagua fault, Guatemala: A record of Neocomian and Maastrichtian. EPSL 284, 228-235.
- Bucknam, R.C., G. Plafker, & R.V. Sharp, (1978). Fault movement (afterslip) following the Guatemala earthquake of February 4, 1976. Geology 6, 170-173.
- Cisneros de León, A*., et al*. (2025). Refining the eruption chronology of Atitlán caldera through zircon double-dating. *Geochemistry, Geophysics, Geosystems*, **26**, e2024GC011953.
- Dollens, A. (2025). Electrical resistivity tomography imaging of the Motagua Fault in Guatemala. Thesis. University of Missouri, Kansas City.
- Donnelly, T. W., Horne, G. S., Finch, R. C., and Lopez-Ramos, E., 1990, Northern Central America; the Maya and Chortis blocks, in Dengo, G., and Case, J. E., eds., The Caribbean region: Boulder, Colorado, Geological Society of America, The Geology of North America, v. H, p. 37-76.
- Ebell, H. (2025). Offsets and slip rate of the Motagua Fault, Guatemala. MSc thesis, Friedrich-Schiller University Jena.
- Ellis, A., DeMets, C., McCaffrey, R., Briole, P., Muralles, B. C., Flores, O., Guzmán-Speziale, M., Hernández, D., Kostoglodov, V., LaFemina, P., Lord, N., Lasserre, C., Lyon-Caen, H., Maradiaga, M. R., Molina, E., Rivera, J., Rogers, R., Staller, A., & Tikoff, B. (2019). GPS constraints on deformation in northern Central America from 1999 to 2017, Part 2: Block rotations and fault slip rates, fault locking and distributed deformation. Geophysical Journal International, 218(2), 729-754. https://doi.org/10.1093/gji/ggz173
- ESA (2024). Copernicus WorldDEM-30 (GLO-30) global digital elevation model. © DLR e.V. 2010-2014 and © Airbus Defence and Space GmbH 2014-2018 provided under COPERNICUS by the European Union and ESA. Retrieved from: https://browser.dataspace.copernicus.eu, last accessed 10.08.2025. https://doi.org/10.5270/ESA-c5d3d65.
- Espinosa, A. F., (1976). Editor. The Guatemalan Earthquake of February 4, 1976, A Preliminary Report, U.S. Geological Survey Professional Paper 1002, 90 p.
- Fauvet-Berthelot, M.F. (1986). Ethnopréhistoire de la Maison Maya (Guatemala 1250-1525). Etudes Mésoaméricaines, Vol. XIII. Centre d'Etudes Mexicaines et Centreaméricaines, Mexico, 296 p.
- Garnier, B., Tikoff, B., Flores, O., Jicha, B., DeMets, C., Cosenza-Muralles, B., Hernandez, D., Marroquin, G., Mixco, L., & Hernandez, W. (2020). An integrated structural and GPS study of the Jalpatagua fault, southeastern Guatemala. Geosphere, 17(1), 201-225.

- Innes, H. M., *et al*. (2025). Ice core evidence for the Los Chocoyos supereruption disputes millennial-scale climate impact. Commun Earth Environ 6, 137.
- Lehmann, H. (1968). Guide to the Ruins of Mixco Viejo Ceremonial Center and Fortified Town of the Maya Indians—Pokimam Group, Guatemala. English Translation by Andrew McIntyre and Edwin Kuh, Editorial Escolar "Pidera Santa," 53p.
- Johnson, K. R. (1984). Geology of the Gualán and southern Sierra de las Minas quadrangles, Guatemala. Dissertation, State University of New York at Binghamton.
- Jones, C., Ashmore, W., & Sharer, R. J. (1983). The Quirigua Project: 1977 Season. In: Sharer, R. J., Schortman, E. M., & Urban, P. A. (Eds.) Quirigua Reports, Volume II: Papers 6-15, University Museum Monograph 49, The University Museum, Museum of Pennsylvania, Philadelphia, 1-38.
- Joy, J., & Elliott, M. (2018). Chapter 1 - Cast aside or cast in a new light? The Maudslay replica Maya casts at the Museum of Archaeology and Anthropology, Cambridge (Authenticity and cultural heritage in the age of 3D digital reproductions). McDonald Institute for Archaeological Research. https://doi.org/10.17863/CAM.27034.
- Looper, M., 2007, Quiriguá: a guide to an ancient Maya city: Editorial Antigua, Guatemala City, Guatemala, 194 p. ISBN: 9789992272251
- Marroquín, H., & Gándara, J. L. (1982). La vivienda popular en Guatemala: antes y después del terremoto de 1976. Organización de los Estados Americanos [y] Comité de Reconstrucción Nacional [y] Universidad de San Carlos de Guatemala. Editorial Universitaria de Guatemala, Centro de Información a la Construcción.
- Maurer, J., Eckert, A., Sun, Q., & Obrist-Farner, J. (2025). Deformation and earthquake potential on the North America - Caribbean - Cocos triple junction in Guatemala (Manuscript submitted for publicatioan). ESS Open Archive. https://.doi.org/10.22541/essoar.175336982.28467707/v1
- Morley, S. G. (1935). Guide book to the ruins of Quirigua. Carnegie Institution of Washington, Supplementary Publication 16, 205p.
- Obrist-Farner, J., Maurer, J., Gibson, D., McEnaney, T., Eckert, A., Kenney, W. F., ... & Reyes, F. (2025). Paleoseismic evidence of directivity for the 1976 Mw 7.5 Motagua earthquake, Guatemala. Geology, 53(11), 971-976.
- Peraldo, G. H., & Montero P. W. (1999). Sismologia Historica de America Central. Instituto Panamericano de Geografia e Historia, Publication No. 513, Mexico, 347 p.
- Peruzza, L., et al. (2021). MARCA-GEHN, a prototype macroseismic archive of four Central America countries. *Bollettino di Geofisica Teorica ed Applicata*, **62**, 1-198.
- Peruzza, L., Esposito, E., Rodríguez García, F., & Giunta, G. (2023). A tool for archiving and updating knowledge about past earthquakes in Central America. In: Earthquake Ground Motion. IntechOpen. https://doi.org/10.5772/intechopen.1003080.
- Plafker, G. (1976). Tectonic aspects of the Guatemala earthquake of 4 February 1976. *Science*, **193**(4259), 1201-1208.
- Plafker, G. (1977). Color slides showing geologic effects and damage caused by the destructive Guatemala earthquake of February 4, 1976. U.S. Geological Survey Open-File Report 77-165.

- Plafker, G. (1978). A Guide to the Motagua Fault Field Trip: International Symposium on the February 4, 1976 Guatemala Earthquake and the Reconstruction Process, Guatemala City, May 15-19, 1978.
- Schwartz, D. P., Cluff, L. S., & Donnelly, T. W. (1979). Quaternary faulting along the Caribbean-North American plate boundary in Central America. Tectonophysics, 52(1-4), 431-445. https://doi.org/10.1016/0040-1951(79)90258-0.
- Seligson, K. E., Ortiz Ruiz, S., & Barba Pingarrón, L. (2019). Prehispanic Maya burnt lime industries: Previous studies and future directions. *Ancient Mesoamerica,* **30**(2):199-219.
- Sharer, R. J. (1990). Quirigua: A Classic Maya Center and Its Sculptures. Carolina Academic Press, Durham N. C., 124p.
- Sharer, R. J., & Traxler, L. P. (2012). Copan and Quirigua: Shifting destinies in the southeastern Maya lowlands: Contributions in New World Archaeology, v. 4, p. 141-158.
- Stevenson, J. L., 1843, Incidents of Travel in Central America, Chiapas, and Yucatan: Harper, New York.
- Ward, C., & Rice, P. M. (2022). The archaeological field diaries of Sylvanus Griswold Morley: Excavations at Quirigua, 1912 and 1919. The Morley Diary Project, Volume III. Published online at Mesoweb: www.mesoweb.com/publications/Morley/Morley_Diaries_Quirigua.pdf
- White, R. A. (1984). Catalog of historic seismicity in the vicinity of the Chixoy-Polochic and Motagua faults, Guatemala. US Geological Survey USGS-OFR-84-88.
- White, R. A. (1985). The Guatemala earthquake of 1816 on the Chixoy-Polochic fault. *Bulletin of the Seismological Society of America*, **75**(2), 455-473.
- White, R. A., Ligorría, J. P., & Cifuentes, I. L. (2004). Seismic history of the Middle America subduction zone along El Salvador, Guatemala, and Chiapas, Mexico: 1526–2000. *Geological Society of America Special Paper* **375**, 379-396.